Simulation of the Fatigue Performance of Spinal Vertebrae

Ruth Helen Coe

Submitted in Accordance with the requirements for the degree of Doctor of Philosophy

The University of Leeds

School of Mechanical Engineering

September 2018

The candidate confirms that the work submitted is her own, except where work which has formed part of jointly-authored publications has been included. The contribution of the candidate and the other authors to this work has been explicitly indicated below. The candidate confirms that appropriate credit has been given within the thesis where reference has been made to the work of others.

Chapters 5 and 7 of this thesis contain material published in a jointly authored paper:

Fernando Y. Zapata-CornelioEmail, Gavin A. Day, Ruth H. Coe, Sebastien N. F. Sikora, Vithanage N. Wijayathunga, Sami M. Tarsuslugil, Marlène Mengoni, Ruth K. Wilcox. (2018). Methodology to Produce Specimen-Specific Models of Vertebrae: Application to Different Species. *Annals of Biomedical Engineering*.

Dr Fernando Zapata-Cornelio authored the paper, and all authors contributed to either experimental testing or computational modelling of vertebrae compared in this study. The candidate contributed experimental testing and computational modelling for one species of bone presented in the paper, and contributed to discussion of the presented results.

Acknowledgements

Abstract

Over 25% of the population are expected to suffer a vertebral fracture over the course of their lifetime (Palastanga and Soames, 2011). This can lead to severe pain and a dramatically reduced quality of life for the patient. Vertebroplasty is a surgical intervention for the treatment of osteoporotic vertebral compression fractures, and there is contradictory evidence as to the efficacy of the procedure. Experimental and finite element (FE) investigations have been undertaken to evaluate the mechanical behaviour of damaged vertebrae, and the effects of vertebroplasty immediately after cement injection. However further work is required to investigate the longer-term behaviour of damaged and treated vertebrae. The aim of this research was to develop experimental and FE fatigue simulation techniques suitable for investigating the longer-term mechanical behaviour of fractured vertebrae, both when left untreated and following vertebroplasty.

A combined experimental and FE approach was adopted for this study. Experimental fatigue methods were established by first developing a damage model and vertebroplasty repair techniques in bovine tail vertebrae. Fatigue testing was then carried out on both cement augmented and untreated specimens, and quantified for different levels of loading. Subsequently specimen-specific FE models were created and used to optimise a density to Young's modulus conversion parameter, where density was found from micro CT images, allowing for variation in bone stiffness to be captured in the models. Yield properties were then determined, also using optimisation, to capture varying yield behaviour across the bone in an elastic perfectly-plastic FE model. Models were compared against experimental data and shown to predict stiffness well and adequately predict yield. A fatigue simulation method was then developed by creating an automated script to implement material property changes in the models on an iterative basis. These models were then directly compared to experimental fatigue displacement data, and microCT images of fatigue failure, in the untreated vertebrae.

The experimental fatigue testing showed no significant difference in the number of cycles withstood before failure occurred for the un-treated and cement augmented groups. Differences were difficult to identify between groups due to large variations in fatigue response between specimens. However, there was some evidence to suggest that augmented vertebrae retain mechanical stiffness through fatigue testing to a greater degree than un-treated vertebrae.

It was found that the fatigue simulation methods showed a good correlation between predicted displacements after large numbers of cycles and experimental displacements at failure, in cases where the plastic strain response in the FE model was not affected by the assumed boundary conditions. However, in some cases, the boundary conditions resulted in a poor distribution of plastic strain, and poor correlation. Additionally, the models showed the potential to give a reasonable indication of fracture locations in some cases. Further work is required to improve the representation of experimental boundary conditions in the models. Although further work is needed to simulate the vertebroplasty procedure in the FE models, the methods developed have the potential to be applied to examine the fatigue behaviour of human vertebrae and a range of different treatment scenarios.

Table of Contents

List of Figures

List of Tables

1. Introduction

1.1. Introduction

The study of spinal biomechanics has grown rapidly in recent decades, facilitated by advances in imaging and simulation techniques and an increase in the spinal treatments and instrumentation available. Spinal biomechanics encompasses the study of loading and motion of the spinal column and is essential in the understanding and improvement of all spinal pathologies and the optimisation of therapies and interventions (Kowalski et al., 2005).

Over 25% of the population are expected to suffer a vertebral fracture over the course of their lifetime (Palastanga and Soames, 2011). This can lead to severe pain and a dramatically reduced quality of life for the patient. Osteoporotic compression fractures are the most numerous type of vertebral fracture, and are thought to affect over 27% of women over 70 (Melton et al., 1997; Cummings and Melton, 2002). The social burden of such fractures will only increase with the aging population (Cummings and Melton, 2002), therefore it is of great importance that fractures are diagnosed and treated in the most effective, reliable way.

Osteoporosis is a decrease in bone mass caused by excessive bone resorption and insufficient bone formation, resulting in bone fragility and a high risk of fracture (Riggs et al., 1998). Osteoporotic vertebral fractures can be treated non-surgically through analgesics and physical therapy, or through surgical intervention when non-surgical options are insufficient. Longer-term biomechanical investigation of osteoporotic and fractured vertebrae, that includes the structural changes over time, can be investigated through *in vitro* testing and computational simulation. Currently there is little evidence describing validated methods for the simulation of long term behaviour of vertebrae, therefore the main aims of this research were to develop experimental and computational methodologies to investigate the fatigue properties of vertebrae. Up to half of all vertebral fractures are a result of

multiple loading events occurring over a period of time rather than a single known event (Lambers et al., 2013), meaning fatigue and fracture progression in vertebrae are important issues that need to be considered (Wilcox, 2006; Wilke et al., 2006).

Vertebroplasty is a technique that involves the injection of bone cement into the fracture to restore the mechanical properties of the vertebrae and reduce pain by stabilising the fracture (Garfin et al., 2001). However, there is still debate over the suitability and efficacy of vertebroplasty, with contradictory studies reporting excellent outcomes and others reporting no improvement over a control group (Buchbinder et al., 2009; Garfin et al., 2001; Kallmes et al., 2009). Subsequently this work aims to adapt methods developed for fatigue investigation of vertebrae to investigate the mechanical effect of the cement augmentation of vertebrae on fatigue outcome.

Further investigation into the long-term mechanical properties of pathological vertebrae is essential to understand the overall efficacy of spinal treatments, and providing a platform with which to do this can enable such investigations for a number of treatments. Specifically, investigation into the longer term outcomes are necessary as current literature focusses on short term, or instantaneous, changes in the spine (Wilcox, 2004). An overview of the contents of this thesis is shown below.

1.2. Thesis Overview

Chapter 2 covers a review of current literature, starting with a background to the human spine, vertebral fracture and vertebroplasty treatment. A review of the use of animal models for *in vitro* testing, and relevant literature discussing the mechanical testing and finite element modelling of vertebrae is provided. The study focusses on existing methods for fatigue modelling treated and un-treated vertebrae and finite element studies modelling damage in vertebrae.

Chapter 3 covers the development of an *in vitro* fracture model and the methods adopted for the static and fatigue testing of vertebrae. Chapter 4 presents the results from these

experimental studies, including the mechanical fatigue response in terms of cycles to failure and change in stiffness, and microCT images of fatigue fractures for un-treated vertebrae.

Chapter 5 covers the computational methods used to create and validate specimen-specific FE models, for both linear elastic models and models with yield behaviour, including the optimisation of material properties. The development process for the methods used to simulate fatigue in the validated FE models is shown here. Chapter 6 shows the results for the validation of models in a static loading case, then covers sensitivity studies run on the developed fatigue simulation script. Results from cyclic loading cases are shown, and compared back to experimental data.

Chapter 7 covers the methods and results for the fatigue testing of augmented vertebrae. Additionally FE modelling of augmented specimens is discussed.

Finally, Chapter 8 reviews the work carried out for this research, with a discussion of achievements and novelty of the work and suggestions for future studies.

2. Literature Review

2.1. Anatomy of the Spine

The human spinal column is made up of 33 individual vertebrae connected and supported by ligaments and muscles. The column can be divided into five sections: cervical, thoracic, lumbar, sacrum and coccyx, as seen in Figure 2-1. The vertebrae in each section are numbered from the cranial to the caudal location, with the exception of the sacrum and coccyx which consist of five and four fused vertebrae respectively. The vertebrae differ in morphology in each section, and increase in size from cranial to caudal position, to withstand the greater loads seen in the more caudal spine, Figure 2-2. The curvatures of the spine allow the structure to be flexible whilst providing support for axial forces, Figure 2-1. Between each pair of vertebrae are intervertebral discs, which provide flexibility and transfer loads along the column.
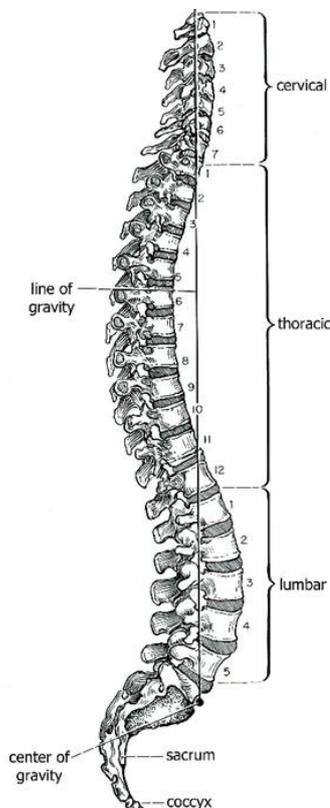
Figure 2-1, Anatomy of the adult spinal column (Woodburne and Burkel, 1988).
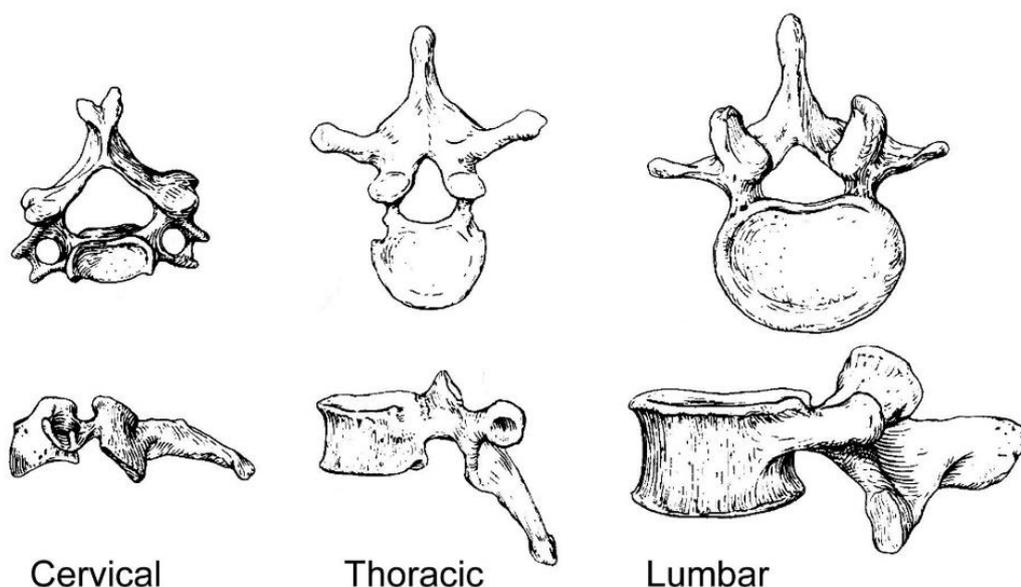
Figure 2-2, Anatomical differences in cervical, thoracic and lumbar vertebrae showing superior and left lateral views (Abeloff, 1982).

The spinal column is a complex mechanical structure required to deal with high dynamic demands. For the most part it is adapted to deal with these demands, however it is not uncommon for the spinal column to suffer from a number of different pathological conditions, often associated with age and disease related degeneration. This study will focus on vertebral fracture and its treatment, therefore the structure of the vertebrae will be investigated in more detail. As vertebral compression fractures typically occur in the thoracolumbar region of the spine, the thoracic and lumbar regions will be in the focus of this review.

2.1.1. Structure of the Vertebrae

The vertebrae consist of the main weight bearing centrum and a series of posterior elements, or processes, rising from the vertebral arch. This arch, which consists of the pedicles and laminae, forms the vertebral canal which protects the spinal cord. The processes in adjacent vertebrae are in contact, forming a pair of articulating zygapophyseal joints (or facet) joints, the shape of which varies through the different spinal sections. Details of the anatomical features of the lumbar vertebrae are shown in Figure 2-3. Anatomical shape of the vertebrae

in different spinal sections correlates with the function of that region. Lumbar vertebrae are larger to support the higher loads seen in this region; thoracic vertebrae support the ribcage and have limited range of motion, cervical vertebrae support the weight of the head and have

Superior View
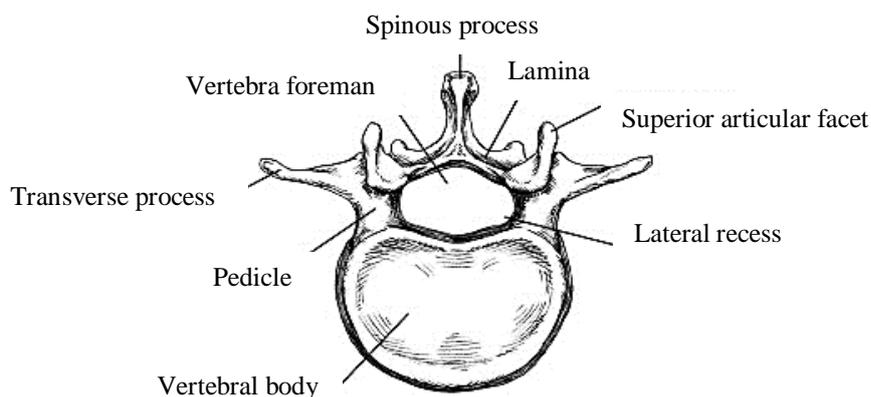
Lateral View
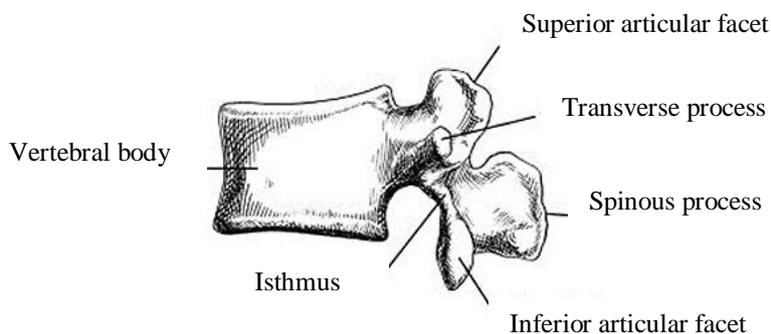
the greatest range of motion of the vertebrae (Betts, 2013).

Figure 2-3, Anatomy of the lumbar vertebrae, showing superior and lateral views (Ebraheim et al., 2004).

2.1.1.1. Trabecular Structure

The vertebral body predominantly consists of trabecular bone, with trabecular strut thickness typically in the range of 100-150μm, with a much denser vertebral shell. The principal trabecular structure is arranged in a vertical orientation in order to sustain body weight and typical loading patterns, providing the most mechanical stiffness and strength in this axial

direction. Secondary, oblique trabecular systems form horizontal struts thinner those in the axial direction and resist torsion, bending and shear. The trabecular structure is denser towards the posterior vertebral body, and is thought to be one of the reasons that anterior wedge-shaped vertebral fractures are common (Mosekilde, 1988; Palastanga and Soames, 2011).

Bone consists of approximately 30% organic components, mainly collagen fibres, and approximately 70% inorganic material, or mineral content, predominantly hydroxyapatite (HA), a calcium phosphate. The mineral provides bone with strength and structure, whilst the collagen content makes the bone less brittle, providing fracture resistance. Bone has a hierarchical structure such that the collagen forms fibres, which in turn form a lamella structure. In cortical bone the lamellae are arranged cylindrically to form osteons, or concentric lamellae structures with a central canal containing blood vessels; whereas in trabeculae bone the lamellae arrange similarly concentric cylindrical structures however without a central canal and the space between the structures contains bone marrow (Rho et al., 1998).

2.1.2. Intervertebral Discs and Facet Joints

The soft tissues of the spine play an essential role in the load transfer and kinematics of the vertebral column. Whilst ligaments and musculature are essential for support and locomotion, the intervertebral discs and facet joints are crucial to the load transfer and mechanics of the spine.

2.1.2.1. Intervertebral Disc

The intervertebral disc is the cartilaginous structure connecting the vertebrae, consisting of a fibrous annulus fibrosis (AF) and inner more gel-like nucleus pulposus (NP), Figure 2-4. In addition to transferring loads arising from body weight and muscle activity, the intervertebral discs allow for flexion, bending and torsion of the spine. The NP consists of randomly organised collagen and radially aligned elastin. It is a highly hydrated structure,

containing a high proportion of the macromolecule proteoglycan and glycosaminoglycans, which provide water retention and cause a swelling pressure in the NP. This allows for load to be distributed evenly through the disc and adjacent vertebrae. The AF is comprised of concentric lamellae of collagen fibres, interspersed with elastin fibres, giving the disc strength and resistance to compressive forces. At either side of the intervertebral disc, adjacent to the vertebral body, are cartilaginous endplates; these are thin layers of hyaline cartilage (Urban and Roberts, 2003). Degeneration of the intervertebral discs is incredibly common, and can be characterised by a loss of hydration and swelling pressure, a reduction in disc height and a change in disc mechanics and loading through the disc (Rohlmann et al., 2006).

Vertebral body
Intervertebral foramen
Anulus fibrosus
Nucleus pulposus

Lateral view   Superior view
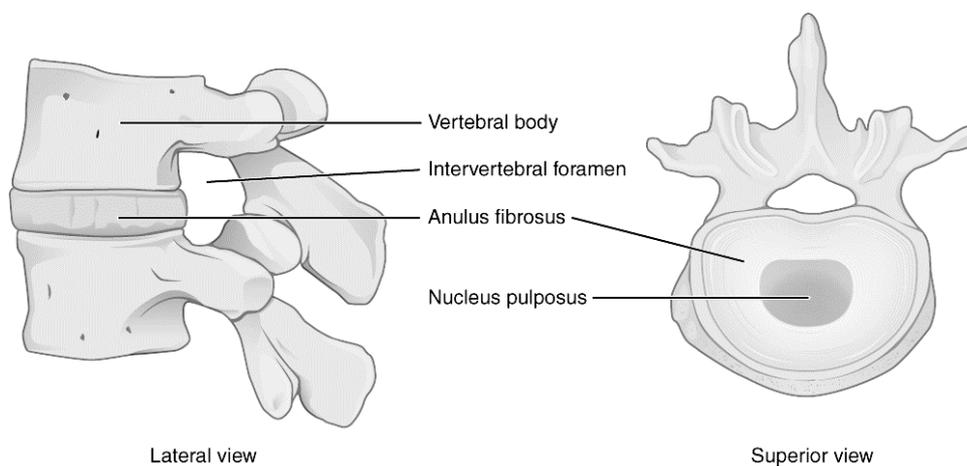
Figure 2-4, Anatomy of the intervertebral disc, adapted from (Betts, 2013).

2.1.2.2.   Facet Joints

The facet joints, or zygapophysial joints, are a pair of synovial joints between the processes of each vertebrae in the spine, see Figure 2-3. They are located between the superior processes of one vertebra and the anterior processes of the adjacent vertebra, and have articulating cartilage surfaces allowing for motion between vertebrae and a joint capsule formed by ligaments. Specifically they allow flexion, bending and torsion in the spine, transmitting shear forces from these motions through the functional spinal unit (FSU), which

comprises two vertebral bodies, intervertebral disc and ligaments and is used as the smallest spinal unit representing the behaviour of the whole spine. Additionally, it has been shown that the facet joint capsule plays a significant role in limiting motions of the spine, proving stability and transferring tensile loads (Serhan et al., 2007).

2.1.3. The Osteoporotic Spine

Osteoporosis is a condition affecting the bone, typically seen in the elderly and characterised by a loss of bone mass. The disease makes predominant load-bearing trabecular structures such as the hip, wrist and vertebrae particularly susceptible to fragility fractures. It is characterised by a deterioration of trabecular micro-architecture, including the discontinuity of secondary or horizontal struts. Osteoporosis is caused by a number of age-related contributing factors, including decreased osteoblast function resulting in an imbalance of the bone remodelling process, with more bone resorption than bone deposit; a decrease in calcium absorption, and oestrogen deficiency (Riggs, 1991). At the microscale level osteoclasts, the cells responsible for bone resorption during remodelling, adhere to the surface of the bone and dissolve both the organic and mineral components of the bone, creating cavities which over time leads to an overall reduction in bone mass (Pernelle et al., 2017).

In the spine, osteoporosis causes vertebral compression fractures, back pain and a loss of vertebral height, or kyphosis. Typically osteoporosis is not diagnosed until fracture has occurred, at which point the disease may have progressed severely. Example radiographs of a healthy lumbar vertebra and an osteoporotic lumbar vertebra are shown in Figure 2-5,A and B respectively (Dougherty, 2010). The severe reduction in bone volume and deterioration of trabecular microarchitecture can be seen, resulting in vertebrae with lower mechanical strength.
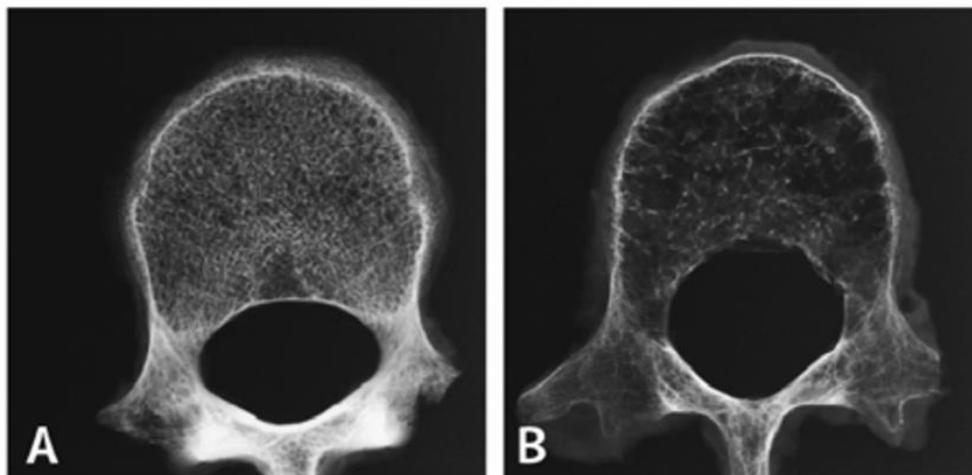
Figure 2-5 Radiographs showing A) healthy lumbar vertebra and B) osteoporotic lumbar vertebra, (Dougherty, 2010)

2.2. Mechanics of the Spine

The mechanical behaviour of the spine is complex, and is different in normal and pathological spines, with changes seen in loading, movement and posture. Understanding loading and motion in the spine and vertebrae is an essential part of assessing changes due to pathology and treatment. Vertebral strength, stiffness and range of motion all affect patient outcome; and such understanding is essential to provide insight into the best pre-clinical testing methods and simulation.

The current work predominantly concerns the vertebrae in the spine, therefore the following evaluations of the literature will focus on the biomechanics and simulation of the vertebrae, rather than the soft tissue structures.

2.2.1. Loading and Motion in the Spine

The spine transmits loads through the vertebral body, intervertebral discs and facet joints/posterior elements. In axial compression, the majority of the load is transferred through the vertebral body and discs, the proportion between vertebral body and posterior elements is dependant of the posture of the spine, with load increasing when the spine is in flexion or lateral bending. In extension, the load in the vertebral body is decreased as a

larger proportion is transferred through the posterior elements. In axial compression the load is distributed relatively evenly across the endplates. (Niosi and Oxland, 2004). The range of motion in the human spine varies between anatomical regions, with the greatest flexion and extension range seen in the cervical spine, the highest range of axial rotation in the thoracic spine and the greatest degree of lateral bending in the cervical spine (Wilke et al., 1997b).

2.2.1.1.   Viscoelasticity

It is known that soft tissues such as IVD (intervertebral disc) and ligamentous tissues highly viscoelastic due to hydration and fibre alignment, with mechanical response dependant on loading rate as well as magnitude (Troyer and Puttlitz, 2011; Panjabi et al., 1994). However, it is also seen that the hard tissue in the vertebrae is also viscoelastic. Shim et al. conducted a series of quasi-static and dynamic compressive tests on human trabecular bone from the cervical spine, and demonstrated the increase in compressive strength from approximately 5 MPa for a strain rate of $10^{-5}\,\mathrm{s}^{-1}$ test to approximately 20 MPa at strain rates of over $10^{-2}\,\mathrm{s}^{-1}$. As this was for specimens of length 8mm, these rates equate to approximately 0.0008 mm/sec and 0.8 mm/sec. Additionally, across the same range of strain rates, they showed that the higher the strain rate the greater difference is seen between static and dynamic loading in terms of strength and stiffness (Shim et al., 2005). In addition to an increase in strength and stiffness with increased strain rate, the hysteresis seen in the axial compressive loading of vertebrae and trabecular bone is well established, demonstrating stress relaxation and creep (Pollintine et al., 2009). This work shows there is need for pre-conditioning of vertebrae before compressive or tensile testing (Wilke et al., 1998), however it should be noted that the changes in mechanical properties over a number of cycles are generally small under small strain rates but more significant where high strain rates are used (Keaveny and Hayes, 1993).

2.2.2. Loading in Daily Activities

In order to accurately model and predict the outcome of spinal interventions using *in vitro* experimental and computational procedures, it is necessary to have a thorough understanding of *in vivo* loading conditions. However, it is inherently difficult to measure these loads *in vivo*, and there are few studies which have done so directly. Some studies have measured the intervertebral disc pressure to investigate load transfer through the functional spinal unit (Nagaraja et al., 2005), although it is difficult to directly translate this data to values of loads in the vertebral body.

Rohlmann et al. conducted a number of studies using instrumented vertebral body replacements to collect data for the forces and moments experienced in vertebrae (Rohlmann et al., 2014). The measurements were performed in five patients for a number of different typical activities such as walking, lifting and using stairs. They then recorded the activities which produced the greatest forces and moments, finding that the loads in the spine vary greatly between patients even for the same activity, however, for daily activities the loads typically fall in the range of up to 1kN, Figure 2-6. Activities which generate the greatest axial load generally involve lifting a weight in front of the body, standing up from sitting, tying shoes and walking. The greatest resultant axial force measured was 1.65 kN which occurred when a patient lifted a 10kg weight from the floor. Walking typically generated loads varying between around 100-300N for the lowest load point in the gait cycle and up to 400-800 N at the point of greatest load. Details of the loads recorded by the vertebral body replacements can be seen in Figure 2-6.
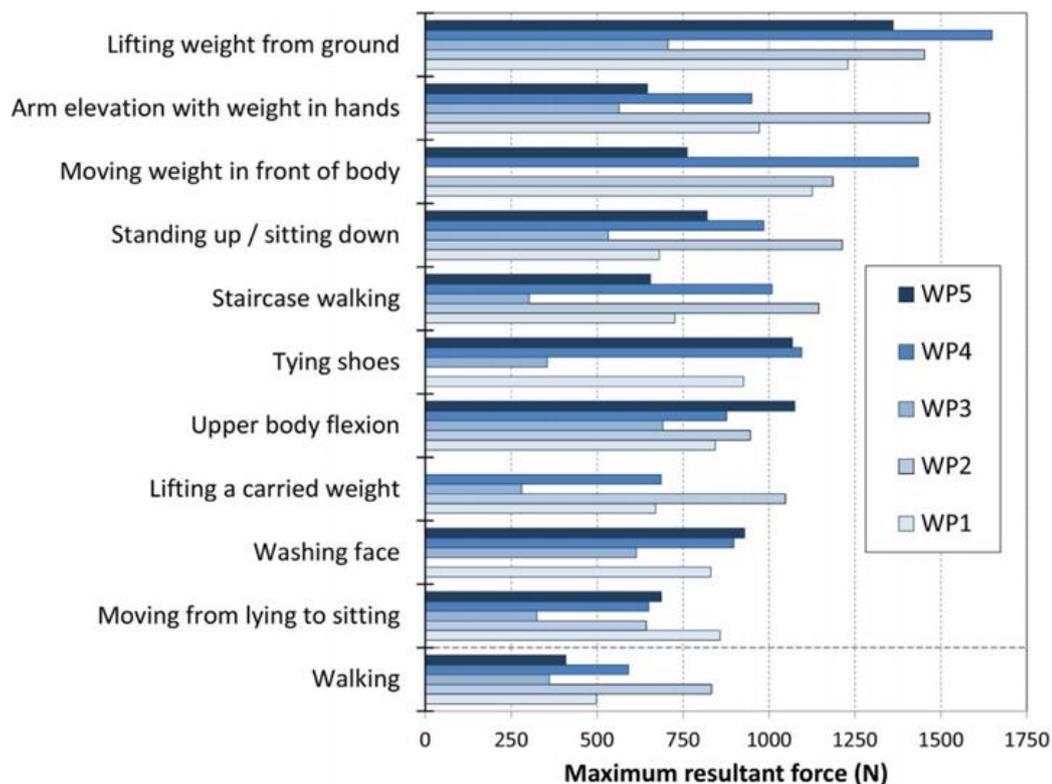
Figure 2-6, Activities with high resultant force for the five patients (WP1-WP5) with instrumented vertebral body replacements (Rohlmann et al., 2014).

This data is extremely useful as there are few studies directly measuring spinal loads; however Rohlmann et al. was a very small study only taking measurements on five patients, and there was found to be already a large amount of variation between individuals. The authors also highlight that the resultant force measured by the vertebral body replacement underestimates the load experienced by the natural vertebra, as the load in the instrumented spine is shared between the vertebral body replacement, an internal fixation device and the bone. Due to these limitations, the results of this study are not likely to accurately represent the loads experienced in a healthy vertebra, however they do provide a good indication of the magnitude of loading and the types of activities that increase the load. Additionally, the study concluded that there was a large variation seen between each patient, in some cases more than twice the load was measured for the same activity, however no speculation as to the causes of these variations was presented.

Han et al. used an analytical musculoskeletal model to show the variance in axial compressive loads experienced by the lumbar spine for different body weights and heights, and found the loads varied almost linearly with an increase in both parameters for all activities. This study showed loads between around 300 and 1900 N for the various tests, which is in agreement with the range of loads found by Rohlmann et al. Load was seen to increase by approximately 50% for a change in body weight from 50 kg to 120 kg, whereas much smaller changes were seen for changes in height from 150 cm to 200 cm. One limitation of this study was that only two values of body weight and two values for body height were evaluated (Han et al., 2013). This knowledge is important clinically when trying to predict fracture risk for a patient, as well as knowing the range of loads experienced by the spine for mechanical experimentation.

A small number of studies have predicted loads in the spine through measurement of *in vivo* IVD pressure measurements (Nachemson, 1966; Wilke et al., 1999). Sato et al. used a pressure transducer to measure the IVD pressure in lumbar discs of healthy patients and those with back pain, then used this value and the cross sectional area of the vertebrae, found using MRI, to determine the loads in the vertebrae (Sato et al., 1999). The average spinal load calculated from the L4–L5 disc pressure for eight healthy patients was 144 N in the prone position, 240 N in a lateral lying position, 800 N in the upright standing, and 996 N in the upright sitting positions. This is similar to the values seen in Figure 2-6, and despite the level of patient variation, can be said to be of a comparable order.

2.2.3. *In Vitro* Mechanical Testing of Vertebrae

In vitro testing of vertebrae typically comprises of compressive testing, or compressive testing with a range of other motions such as rotation and bending. A large body of work has been published on *in vitro* mechanical testing of vertebrae or functional spinal units because these methods have been used to evaluate a range of spinal treatments and instruments (Kothe et al., 2004), examine disease states (Heini et al., 2001) and predict fracture risk (Rapillard et al., 2006). The majority of studies test vertebrae under quasi-static loading

conditions, however there has been some investigation of the fatigue behaviour and mechanical properties under dynamic loading. With the exception of testing for spinal implants and intervertebral disc replacements, there is no standardisation for the *in vitro* laboratory testing of vertebrae or FSUs (Holsgrove et al., 2015).

2.2.3.1. Quasi-Static Testing

Static testing methods typically involve the constraint of the vertebrae or FSU around the endplates and mechanical loading in a materials testing machine. The load values used vary depending on the goal of the testing and which parameters are being investigated. Generally, load-displacement data is collected for vertebrae, as stress-strain is difficult to evaluate given the geometry and variations in cross-sectional area of vertebrae and functional spinal units. For the general evaluation of material properties of vertebrae or bone specimens, the specimens are typically loaded to failure under a low strain rate in order to determine elastic stiffness, yield or failure properties, broadly under axial compression although sometimes with the addition of varying postures. In this case a low strain rate is considered to be sufficiently slow to not see the effects of an impaction load, but does not necessarily entirely negate the effects of visco-elasticity. Example stain rates used for such tests are 1mm/min (Wijayathunga et al., 2008) and 5mm/min (Chevalier et al., 2008). Where whole vertebrae or FSUs are tested, load is typically applied via a loading plate or surface, to evenly distribute the load across the endplate, whilst the inferior surface is constrained (Cheng et al., 1997; Wijayathunga et al., 2008; Chevalier et al., 2008). It is challenging not to over-constrain the specimens during *in vitro* testing, which would make the test less representative of the *in vivo* situation, however methods have been developed to allow for the rotation of the surface on which load is applied, for example by applying compressive force to the specimen via a steel ball. This rotation allows for more physiological loading to occur without the intervertebral discs present (Wijayathunga et al., 2008; Mengoni et al., 2016; Tarsuslugil et al., 2014).

2.2.3.2.   Fatigue Testing

Vertebral fractures do not only occur as a result of impact or trauma but can often be caused by the accumulation fatigue damage, particularly in osteoporotic vertebrae (Lambers et al., 2013). Fatigue damage can be defined as structural weakening or failure resulting from repeated cyclic loading, and may cause failure at values lower than the typical yield stress of the material. This type of fracture may often go undiagnosed, as it does not result from a single noticeable event. Due to constant bone remodelling *in vivo*, it is likely that fatigue damage accumulates over a relatively small period of time, such as days to weeks, rather than years (Adams and Dolan, 2011). The available information on the fatigue behaviour of healthy vertebrae will be investigated in this section, and will be used as a basis for comparison to treated vertebrae later in this Chapter.

There is some evidence in the literature regarding the fatigue response of whole vertebrae. A number of *in vitro* studies were evaluated by the present author and the outcomes are summarised in Table 2-1. Fatigue life can be evaluated through characteristic S-N curves, where S is the stress amplitude of the test and N is the number of cycles to failure. Whilst this is standard for engineering materials, it has not been widely reported here due to difficulties in determining stress in vertebrae due to the non-uniform shape. Some fatigue properties can be deduced from investigating the internal structure of failed vertebrae.

From Table 2-1, it can be seen that the fatigue properties of human vertebrae are affected most by age, as may be expected due to the reduced BMD (bone mineral density) seen in older patients. However, it can also be seen from Gallagher et al. and Huber et al. that the flexion angle of the spine has an effect on the fatigue performance, suggesting some types of activity will have a greater effect than others. Most studies, with the exception of Huber et al., use a low-cycle high-load fatigue process. This is partly because it is not possible to take into account the bone remodelling process observed over time when using *in vitro* studies, which would start to take effect after a few weeks to a month *in vivo*, as well as the practicality of long term testing of biological tissue. The amplitude of the applied load varies

between each study and is in all but one case set as a percentage of the ultimate compressive

load (UCL) of the vertebra sample. This normalises the load across different specimens and

reduces variability in the results, however this method is limited by the need to estimate or

predict UCL, usually found from compressing other samples to failure or using BMD as a

predictor.

It is also worth noting that because fatigue is by nature an accumulation of small amounts of

damage, the point of failure may be difficult to define. As a result, the point at which to stop

a test is subjective and defined by the author of the study in each case, usually as a percent

reduction in stiffness or vertebral height. Additionally, there may also be pre-existing

damage to the specimens, particularly in the cases where older samples are used, so the

cycles or loads to failure may not be an accurate representation of what happens *in vivo*.

Table 2-1, Details of experimental fatigue investigations of the human lumbar spine.

Author	Fatigue Test	UCL/Load Determination	Failure Point Definition	Results
Lui 1983(Liu et al., 1983)	2-vertebrae FSUs, n=11. 22N up to 37-80% ultimate load (UCL) (depending on vertebral level) for 10000 cycles at 0.5Hz.	Mean values of failure strength from White and Panjabi (Panjabi and White III, 1980).	Abrupt height loss signified compression fracture.	5 specimens fractured below 2000 cycles, 6 experienced gradual height loss, but did not fail.
Hansson 1987 (Hansson et al., 1987)	17 FSUs. Applied load between 60-100% UCL for maximum 1000 cycles at 0.5Hz.	Predicted from bone mineral content.	Audible cracking and/or sudden increase in deformation.	1 specimen did not fail. All others failed before 950 cycles.
Brinckmann 1988 (Brinckmann et al., 1988)	111 FSUs. Applied load 700N to between 20-70% UCL, cycled to failure at 0.5Hz, 36.5°C and 100% humidity. Maximum 5005 cycles or 4mm deformation.	Using UCL from 1 vertebra to predict UCL in all other levels of that spine, assuming the value varies by ~0.4kN per level.	Sudden increase in deformation, visible or audible cracking.	18 specimens did not fracture before the end of the test. Specimens fractured between 2-2700 cycles.
Gallagher 2007	18 FSUs, categorised as either 'old' or	Load values obtained from	10mm displacement	Av. cycles to failure:

(Gallagher et al., 2007)	'middle aged'. Loaded at 1.3kN at 0° flexion, 2.4kN at partial flexion and 3.15kN at full flexion, all at 0.33Hz up to 10020 cycles or to failure.	literature – database for lifting tasks.	after the period of creep deformation.	No flexion: -Old 8267 -Middle aged 10020 Partial flexion: -Old 3261 -Middle aged 7124 Full flexion: -Old 236 -Middle aged 3929
Huber 2010 (Huber et al., 2010)	N=18 FSUs. Three groups (n=6 per group): Old, un-flexed; Young (20-40 years) Un-flexed; Young flexed. Loaded between 0-2kN up to 3000000 cycles or to failure at 5Hz.	Based on previous studies.	Distinct discontinuity in creep behaviour	6 specimens failed by 3000000 cycles Age and flexion both affect fatigue behaviour.

2.3. Spinal Fracture

The mechanisms behind compressive vertebral fracture are complicated and typically do not just involve the catastrophic failure of the primary vertical trabeculae but rather are a result of the accumulation of fractures of the oblique trabeculae and microscopic cracks of the vertical trabeculae (Palastanga and Soames, 2011). This damage pattern allows for some recovery of the structure to its initial shape, giving the vertebrae perceived viscoelastic properties (Fyhrie and Schaffler, 1994).

The microarchitecture of the trabecular structure is known to play an important role in the prediction of fractures, and a number of imaging tools and techniques for interrogating this structure are used in diagnostics. The most common of these techniques is dual x-ray absorptiometry (DXA), used to determine bone mineral density (BMD) or the amount of bone mineral per unit area. Micro computed tomography (μCT), and can be used to determine bone volume fraction, which gives a ratio of bone volume to total volume of the internal trabecular structure, and is a useful way of investigating changes in bone density.

2.3.1. Classification

In order to produce repeatable fractures, clinical classification can be used to help classify *in vitro* specimens. Magerl et al. have proposed a comprehensive method of classifying thoracolumbar injuries creating three main categories based on the main mechanism of injury, pathomorphological criteria and prognostics (Magerl et al., 1994). This is built on work by a number of authors such as Holdsworth (Holdsworth, 1963), Whitesides (Whitesides Jr, 1977) and Dennis (Denis, 1983; Denis, 1984) who introduced the ideas of classification of stable and unstable injuries, mechanistic classification and the introduction of the three column model. Three main categories of spinal injury are defined depending on a typical fundamental injury pattern: Type A, vertebral body compression; type B, anterior and posterior element injuries with distraction and type C, anterior and posterior element injuries with rotation. Type A is the most common type of thoracolumbar injury, with over two thirds of the cases in the Magerl study falling into this category. Each category is split into three subcategories. This study will focus on type A, vertebral compression fractures, which can be split into impaction fractures; split fractures and burst fractures. Each of these can again be defined in further detail. These classifications are useful when trying to create reproducible fractures *in vitro*.
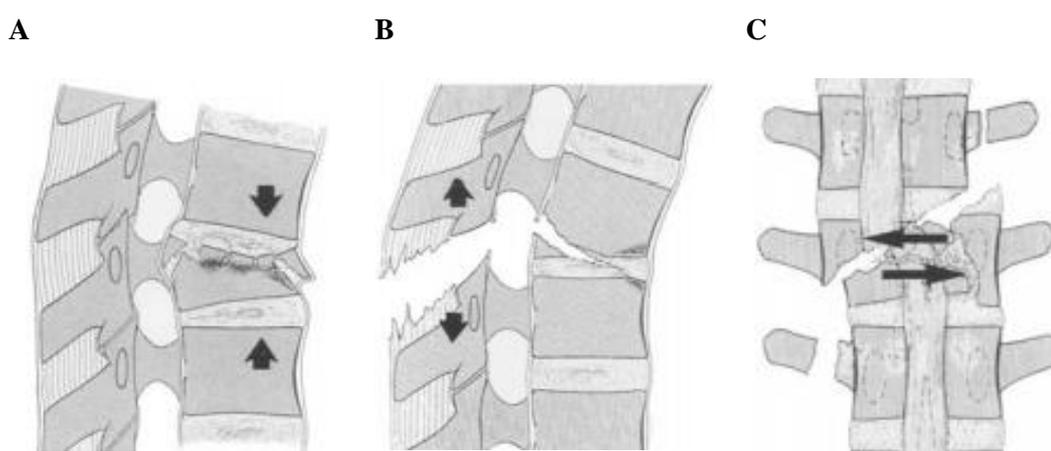
Figure 2-7, Classifications of Spinal Fracture, showing Type A, vertebral body compression, Type B, Distraction with anterior and posterior injury, and Type C anterior and posterior injury with rotation, adapted from (Magerl et al., 1994).

A large number of studies have attempted to use testing and imaging to improve current fracture prediction methods. The microarchitecture of the vertebral trabecular structure is known to play an important role in the prediction of fractures, and a number of imaging tools and techniques for interrogating this structure are used in diagnostics. The most common of these techniques is DXA, used to determine the amount of bone mineral per unit area. Micro computed tomography (μCT) can be used to determine bone volume fraction. Understanding key factors that play a role in the fracture of vertebrae is necessary when creating an *in vitro* fracture model.

2.3.2. Experimental Fracture Generation

There are a number of *in vitro* fracture creation methods reported in the literature which attempt to recreate physiologically accurate, repeatable vertebral fractures. Many studies using osteoporotic human vertebral specimens often create fractures through static compressive loading applied either centrally or eccentrically until failure, or through a single impact from a drop rig (Rüger and Schmoelz, 2009; Tabensky et al., 1996; Dall'Ara et al., 2012). Failure is defined in these cases as a pre-defined loss of vertebral height, as the peak of a force-displacement graph of the compression, or through observing visible fracture failure. Alternatively, a number of studies have created a defect in the vertebral body prior to fracture creation to generate a more repeatable fracture (Kayanja et al., 2004; Hitchon et al., 2001). This method is less physiologically representative, however may be necessary to create consistent, repeatable fractures. The artificial defect is typically a notch or hole created in the anterior edge on the vertebral body (Chiang et al., 2009; Wang et al., 2008).

2.3.2.1. Failure Behaviour

As strength varies with strain rate, in this section the yield behaviour under quasi-static testing is considered (Palastanga and Soames, 2011). Healthy human lumbar vertebrae are known to have a compressive strength of 7-9 kN when loaded at physiological strain rates; this high compressive strength is provided by internal trabecular structure of the vertebrae. However this strength decreases with age and osteoporosis as bone density decreases, so

compressive strength reported in the literature is typically lower than this, where cadaveric specimens used are normally from older patients. Brinckmann et al. show for over 100 vertebral specimens from donors aged between 19 and 79, compressive strength varies between 2 and 12 kN (Brinckmann et al., 1989). When compared to loads seen in daily life, it can be seen that activities involving lifting a weight can apply loads of around 1.5 kN to the vertebrae, and this was expected to be an underestimate due to measurement techniques, so in elderly patients daily activities can produce loads in the spine that are close to failure loads for some people. It has also been shown by Brinkmann et al., amongst other studies, that bone mineral density (BMD) can be used as a predictor for vertebral compressive strength: for 109 vertebrae tested in compression to failure, a Pearson's correlation coefficient of 0.85 was seen between BMD and strength. This provides a potential method to derive vertebral strength non-destructively and highlights the effect of BMD on vertebral strength.

Understanding the changes in mechanical properties as a result of compressive loading or damage is essential for modelling biomechanical changes in vertebrae from high loads. There is little literature evidence describing these changes, however a study by Keaveny et al. has shown through the testing of human lumbar bone cores past the initial yield and then reloading the cores past the yield point, that large reductions in both yield stress and Young's modulus occur. Modulus was seen to reduce by up 85% were seen for plastic strains of up to 3%. Yield stress was shown to reduce between approximately 5% and 60% for plastic strains between 0.5% and 3%. This work demonstrates the substantial change in material properties of trabecular bone as a result of relatively minor overloading (Keaveny et al., 1999).

2.4. Vertebroplasty

Vertebroplasty is a minimally invasive technique used to stabilise fractured vertebrae with bone cement in an attempt to restore the structural properties of the vertebra, reduce pain and restore movement to the patient. Bone cement is injected into the vertebral body through the

spinal pedicles under local anaesthetic, where-upon after setting it is thought to inhibit motion between the fractured bone fragments and minimise pain, Figure 2-8. Vertebroplasty is typically used for osteoporotic vertebral compression fractures, however the efficacy of the procedure has been the topic of debate for a number of years, and the exact mechanisms of pain reduction are unclear (Wilcox, 2004; Sun and Liebschner, 2004).
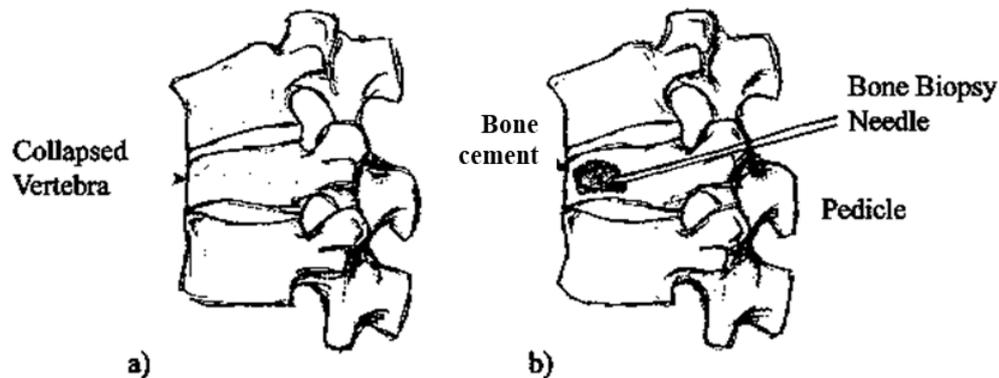
Figure 2-8, Diagram showing vertebroplasty process, with a) vertebral compression fracture and b) bone cement injection through the pedicle, adapted from (Sun and Liebschner, 2004).

Currently the most common type of cement used for vertebroplasty is PMMA (poly methylmethacrylate), an acrylic based cement which is usually mixed with a radiopaque marker and injected under fluoroscopic guidance through either one or both pedicles. It has been shown that PMMA has sufficient mechanical properties to either restore or increase the strength and stiffness of vertebral body to pre-fracture levels (Liebschner et al., 2001; Luo et al., 2009). However it is thought that the disparity in the mechanical properties of the cement and typically osteoporotic bone can cause further problems, particularly in adjacent level vertebrae, by significantly altering the mechanics of the spine (Wilcox, 2006; Trout et al., 2006). PMMA is known to have a high polymerisation temperature which may cause local tissue damage around the fracture, and, although it mechanically stabilises the vertebra, it is unable to integrate well with the bone, remaining a foreign object inside the vertebra. To address these limitations, osteoconductive calcium phosphate (CaP) cements have been

investigated (Tarsuslugil et al., 2013; Wilke et al., 2006). These have a lower setting temperature and are known to be more biocompatible than PMMA, with the porous structure integrating better with the native bone tissue, promoting bone ingrowth and a stronger bone-cement interface in the longer term. Despite this, CaP cements are known to have inferior tensile properties to PMMA, and as a result are more brittle (Wilke et al., 2006). As such, there is still no consensus on the optimum material configuration for vertebroplasty treatment.

2.4.1. Clinical Outcomes

A large number of clinical studies have been undertaken to investigate the efficacy of vertebroplasty (Hulme et al., 2006), however there are only a small number of randomised control trials (Buchbinder et al., 2009; Kallmes et al., 2009). There are also a limited number of randomised control trials investigating the effect of kyphoplasty treatment, which even though the kyphoplasty procedure differs from vertebroplasty by the creation of a void in the vertebral body into which cement is injected, still results in a similarly augmented vertebra (Wardlaw et al., 2009; Berenson et al., 2011).

Buchbinder et al. found that vertebroplasty is no more effective at reducing pain, improving physical function or improving quality of life than a sham procedure. A study design with blinded, placebo-controlled treatment was used, and 78 patients were split into groups to either undergo vertebroplasty or a sham procedure which mimicked the vertebroplasty procedure up until the injection of PMMA. The main measured outcomes included pain and quality of life, determined through the use of a multiple questionnaires, assessed at 1 week, 1, 3 and 6 month follow-ups. Significant improvements in pain and perceived quality of life were seen in both groups at each follow-up (Buchbinder et al., 2009).

Kallmes et al. used a randomised control trial to assign 131 patients with osteoporotic vertebral fractures to either vertebroplasty treatment or a control intervention, which simulated vertebroplasty. Pain scores and the Roland–Morris Disability Questionnaire

(RDQ) were used to assess outcomes at 3 days, 2 weeks and 1 month, at which point patients were given the option to swap study groups. Both groups saw an improvement at 1 month however there was significant difference between groups. A trend towards higher rate in pain improvement was seen in the vertebroplasty group; however this was not statistically significant (Kallmes et al., 2009).

Separate studies by Wardlaw et al. and Berenson et al. used randomised controlled trials to investigate the efficacy of kyphoplasty for vertebral fractures compared to non-surgical treatment. Wardlaw et al. showed a significant improvement in physical component summary (PCS) score for the kyphoplasty group at 1 month compared to the non-surgical treatment group. Berenson et al. found that RDQ score significantly improved for the kyphoplasty group at 1 month, and saw no significant difference for the control group. Neither of these studies used blinded treatment, so cannot rule out the effect of the known treatment for patient questionnaire feedback or clinicians assessment (Wardlaw et al., 2009; Berenson et al., 2011).

A randomised controlled trial of 50 patients with osteoporotic spinal fractures by Rousing et al., in which vertebroplasty was compared to conservative treatment, found significant improvements in the vertebroplasty group, assessed using the visual analogue scale at 3 months. This study was also not a blinded test (Rousing et al., 2009).

There is a lot of debate over the outcomes of such clinical trials, especially the placebo-controlled studies (Klazen et al., 2010). The main criticism of the trails that show no difference in outcomes of vertebroplasty treatment compared to a placebo procedure is their choice of patients, which is very broad. It is clear from such debate that the mechanisms behind the treatment are complex and still not fully understood, and the range of outcomes suggests it is more suited to some patients than others. This highlights the need for investigation into the effect of vertebroplasty on different clinical groups of patients.

2.4.2. *In Vitro* Vertebroplasty Studies

Numerous investigations have been performed to study the biomechanical effects of vertebroplasty treatment *in vitro*. These tests are often similar to those conducted to create fractures as they are often simple axial compressive tests conducted to provide mechanical stiffness and strength data for augmented vertebrae as a comparison to the equivalent pre-fracture data. This information gives an idea of how much the treatment has affected the biomechanics of the system, as well as how well the treatment has improved or restored the mechanical properties of the vertebrae in question (Aquarius et al., 2014; Tarsuslugil et al., 2013; Erkan et al., 2010).

A small number of studies have investigated the fatigue response of augmented vertebrae through *in vitro* experimentation. The methods used in these studies vary substantially, utilising different test lengths, mechanical loads and output measurements depending on the experimental reasoning. Incremental load increase is used as a method of speeding up fatigue response of the system, which may not be an accurate representation of typical spinal loading but gives indication of the fatigue characteristics of bone and bone cement. Table 2-2 summarises *in vitro* fatigue tests conducted on augmented vertebrae from the literature.

Table 2-2, Summary of the available literature on experimental fatigue testing of augmented vertebrae.

Author	Purpose	Fatigue Test	Outputs
Wilke 2006 (Wilke et al., 2006)	Comparison between vertebroplasty and kyphoplasty with both PMMA and CaP cements.	100000 cycles of eccentric loading at 5Hz between 100-600N with flexion/extension and lateral bending. Human cadaveric FSUs (functional spinal units) 1 unconstrained vertebrae.	Cryosectioning showed microcracks in the CaP but not in the PMMA. Negligible difference height loss was seen in all the groups, and all were approximately 1mm less height loss than the control.
Chiang 2009 (Chiang et al., 2009)	Investigating the effect of prophylactic vertebroplasty in adjacent levels.	36000 cycles with 550-750N amplitude at 5Hz. Cadaveric motion segments with 3 unconstrained vertebrae in each sample.	Significantly lower height loss seen in prophylactically augmented adjacent vertebrae compared to control. Osteoporotic vertebral strength is increased and anterior body shift is reduced.
Oakland 2009 (Oakland et al., 2009)	Investigating the effect of prophylactic vertebroplasty in adjacent levels.	115000 cycles at 1Hz with incremental increase in load up to 3.5x body weight. Tests ended at 50% failure load using a predicted failure load from BMD. Cadaveric, three-vertebra segments.	No difference in pre- or post-augmentation stiffness. Fractures only occurred with the greatest load. Cement modulus of the intact vertebrae had no significant effect on incidence or location of fracture.
Rüger and Schmoelz 2009 (Rüger and Schmoelz, 2009)	Investigating the use of a high-viscosity PMMA to correct kyphosis of wedge fractures.	3x1000 cycles with incrementally increased loads (50-250N, 50-450N and 50-650N) at 0.5Hz. Cadaveric FSUs.	Kyphosis angle significantly reduced and remained constant during testing. No fatigue damage observed upon macroscopic inspection. ROM nearer intact value than fractured value.
Kolb 2013 (Kolb et al., 2013)	Investigating the effect of cement stiffness on risk of adjacent level fractures.	Load applied increased by 100N every 1000 cycles starting at 100N. Maximum cycles approx. 20000 at 4Hz. Human lumbar specimens with three unconstrained vertebrae in each sample.	The fatigue fracture force was significantly higher in the 50% less stiff PMMA group than the PMMA group (1.76kN compared to 1.54kN).

It is difficult to make comparison across studies from the above results for a number of

reasons. The variety of tests makes comparison difficult; however valuable information can

still be acquired from the studies. An initial qualitative result regarding the difference

between PMMA and CaP shows that CaP exhibited microcracks whereas the PMMA did not, suggesting it may be more susceptible to fatigue damage at a low loading rate (Wilke et al., 2006). Such microdamage causes a permanent degradation of mechanical properties. Both the study by Kolb et al. and the study by Oakland et al. show there is no significant difference in the incidence of fractures during fatigue loading when the PMMA cement stiffness is altered either 50% or 100-12.5% of an initial value. In the study by Kolb et al. fractures occurred in the augmented vertebrae and in the superior level with fewer adjacent level fractures being seen in the modified PMMA group.

Due to the relatively low number of cycles used in these tests the only fractures observed occurred at relatively high load values (>1kN). However loss in vertebral height, both including and not including soft tissue height loss, was seen in each case, even where low loads were used. This suggests that vertebral subsidence occurs as a result of fatigue loading and fracture typically occurs at higher physiological loads.

A range of cyclic loading frequencies between 0.5-5Hz have been used in these studies. These tend to be based on the length of the tests and how long the tests need to last logistically for keeping biological tissue fresh. Cycle numbers ranged from 1000-115000, again depending on whether the author was looking for changes in properties which can be observed at lower cycle number, such as vertebral height and stiffness, or whether the tests required loading until failure which typically need a lot more cycles, depending on load.

2.5. *In Vitro* Animal Models of the Spine

Animal models have been used for *in vitro* and *in vivo* spinal research due to the limited availability, ethical considerations and large variation in age, mechanical properties and geometry of human specimens. Large animal models specifically, such as sheep, cow and pig spines, provide a useful method of studying the spinal pathologies and treatments due to geometric and structural similarities with the human spine. For the current study, it is important to find a model that is suitable both for recreating injury and for augmentation

with bone cement, therefore mechanical properties and trabecular structure are important to consider.

It is necessary to understand the resemblances and differences of different animal models to the human spine in order to effectively decide which is most appropriate and to recognise the validity of each. It is important to consider a number of different factors when assessing suitability of animal tissue: similarities in geometry, internal structure, biomechanical properties, such as range of motion (which can be considered because it will affect the microstructure and strength) and loading, and mechanical properties of the tissue, such as stiffness and strength. Several studies have shown quantitatively that the geometry of quadruped spines are comparable with human spines in terms of size and structure of the vertebra (Smit, 2002; Cotterill et al., 1986; Wilke et al., 1997b). The biomechanical properties of porcine and ovine spines have been shown to be similar to those of human spines, with comparative similarities in range of motion across different spinal regions as can be seen in Table 2-3 (Wilke et al., 2011; Wilke et al., 1997a).

Table 2-3, Approximated average range of motion values for each spinal region based on values for individual motion segments for ovine, porcine and human specimens. In this instance C, T and L denote the cervical, thoracic and lumbar regions of the spine.

	Ovine ROM (°) (Wilke et al., 1997a)			Porcine ROM (°) (Wilke et al., 2011)			Human ROM (°) (Wilke et al., 2011)		
Motion	C	T	L	C	T	L	C	T	L
Flexion-extension	6-23	4-7	7-11	6-16	5-10	7-11	9-20	4-12	4-14
Axial rotation	7-18	2-20	1-3	2-5	2-13	3-5	4-14	3-17	2-5
Lateral bending	17-31	19-25	8-12	9-16	8-13	11-13	8-22	10-17	6-16

Depending on the purpose of the study in question, different aspects of a model will be more important than others. For example where kinematics/biomechanics/soft tissues are concerned, then the range of motion and biochemical properties might be most important. In the case of the current work, where longer-term properties and vertebroplasty are concerned,

the geometry and trabecular architecture of the vertebra is important. However, as it is more important that accurate specimen-specific finite element models can be created, it is sufficient for there to be a number of differences as long as the testing is still representative of vertebrae, modelling methods are validated and are developed to be transferable to human vertebrae. In this work important trabecular measures are spacing and thickness, or a measure of BV/TV (bone volume as a ratio of total volume), as this directly affects the amount of cement able to be injected into the vertebrae during vertebroplasty treatment.

Smit (Smit, 2002) discussed the suitability of quadruped spines as models for human spines by investigating the loading mechanisms and trabecular architecture. It was shown that both are loaded along the axis with primary loading being axial compression, and other loads being transformed by the muscular system into axial compression and facet joint loads. Smit concluded that the quadruped spine is loaded in a very similar way to the human spine. It is known that trabecular structure is closely related to mechanical loading of the system as a result of bone remodelling, generating anisotropic structures with trabecular struts and plates aligned in the direction of principal stress. As such, if the loading is axial as proposed by Smit et al., then one would expect animal and human bone to have similar trabecular orientation, and indeed this is what has been found. Comparing trabecular architecture of quadruped and human vertebrae gives further indication to the biomechanical similarities in the structure. It is shown that similarly to human vertebrae, quadruped vertebrae have anisotropic trabecular structures orientated axially. However animals also have a higher bone density suggesting quadruped spines are subjected to higher compressive forces than humans, meaning they are typically stronger. The authors concluded that different animal models are useful for different applications depending on the specific research question: porcine are the closest in size and geometry so are useful for testing devices and implants, however they have high vertebral bone density compared to humans and have been shown to be difficult to fracture consistently (Tarsuslugil et al., 2014). Skeletally mature animals are more useful for investigating biological processes (Smit, 2002).

A comparison of the trabecular structure between human, ovine and porcine lumbar vertebrae found in the literature is summarised in

Table 2-4. It can be seen that although both ovine and porcine trabecular structures are comparable to human trabecular properties, there are some clear differences. Ovine trabeculae are considerably thicker and slightly denser whilst porcine trabeculae are closer in thickness yet considerably denser than human trabeculae. This information additionally shows that it is likely that ovine and porcine vertebrae are subjected to higher axial loads than human vertebrae giving them a stronger load bearing trabecular structure.

Table 2-4, Comparison of trabecular structure parameters for human, ovine and porcine lumbar vertebrae.

	Human (Müller and Rüegsegger, 1997)	Ovine (Kennedy et al., 2009)	Porcine (Teo et al., 2006)
BMD (g/cm^2)	Healthy: 0.93 Osteoporotic: 0.64 (Wilcox, 2007)	0.823 (5-10yr ewe)	1.2
BV/TV	0.13 (Grote et al., 1995)	0.35 (Harrison and McHugh, 2010)	0.2
Trabecular thickness (mm)	0.06	0.2	0.1
Trabecular Number (mm^{-1})	1.3	1.7	2.08
Trabecular Spacing (mm)	0.65	0.52	0.35
Degree of Anisotropy	-	2.22	1.37
Index of connectivity (mm^{-1})	2.6 (Grote et al., 1995)	5	2.08

It is inherently difficult to compare mechanical properties, such as Young's modulus, yield stress and strain and ultimate stresses and strains of human and animal vertebrae due to the large variation seen in these properties within species (Teo et al., 2006). Wijayathunga et al. showed a range of stiffness values for human vertebrae tested in compression between approximately 1000N/mm and 2500N/mm (Wijayathunga et al., 2008). Zapata et al. show a range of stiffness values for different animal models, with in vitro stiffness determined to be

an average of 5200N/mm for bovine vertebrae; 5800N/mm for porcine vertebrae and 8400N/mm for ovine vertebrae. This correlates with

Table 2-4, where ovine bone is shown to have the greatest bone volume fraction, trabecular thickness and index of connectivity, providing it with the strongest and stiffest mechanical properties.

2.6. Image-Based Modelling of Vertebrae

Over the last two decades, finite element methods have become widely used in the field of spinal biomechanics to model and analyse spinal structures. One goal of such studies has been to conduct a wider analysis of parameters whilst mitigating the need to use large numbers of specimens and conduct numerous experiments. In addition, FE methods can provide information that cannot be found through *in vitro* testing. FE methods use a numerical technique to find an approximate solution to boundary value problems for differential equations. Complex structures are subdivided into smaller elements, connected by nodes, and equations for each node are developed which are then assembled and solved computationally to determine the mechanical response at each nodal point and across elements. For structural analysis, the differential equations are usually based on minimising the potential energy of the system, and can be solved to determine the displacement of the nodes, and then post processed to determine stress and strain.

Finite element analysis has been used to investigate the biomechanical response of the spine and different spinal structures and implants. This type of analysis can provide useful information whilst minimising limitations seen in *in vitro* experiments or *in vivo* trials. Finite element models have been used to provide information about the effects of parameters relating to the treatment (Wijayathunga et al., 2013); can be used clinically to provide patient specific information, such as fracture risk (Chevalier et al., 2008), and have been used to investigate the response of spinal interventions (Charosky et al., 2014). When evaluating FE models in the literature, it is important to consider the level of validation, and

model assumptions, in order to understand whether the model is a correct representation of the equivalent real life situation.

The main approach used for modelling whole vertebrae for FE analysis is to consider the bone as a continuum. That is, the trabecular structure, depicted in Figure 2-9, is represented as a continuous material without modelling individual areas of bone and marrow space. In this method, the material properties of the bone are typically assumed to be isotropic and are assigned on an element-by-element basis. The elastic modulus values are derived from the average bone density in each element. (Verhulp et al., 2006). This method does not account for the detailed trabecular bone morphology, but has been shown to produce viable models and provide a sufficient level of detail for the application of modelling whole vertebrae (Tarsuslugil et al., 2014). Trabecular level models, created with a sufficient resolution to model individual trabecular structures, may provide a method of more accurately predicting the response of the vertebrae as the behaviour of individual trabecular features can be accounted for, however in order to do this a whole vertebra model would be required to be modelled with a mesh resolution greater than 100μm. Few studies have used trabecular level modelling to investigate the response of the whole vertebrae. Eswaran et. al modelled vertebrae at a 30-40μm resolution, creating models with up to 60 million elements, and requiring powerful supercomputing to solve the model, for a linear elastic model. A similar model of a 1mm mesh resolution may contain around 200000 elements. Whilst this method is feasible, and was shown to better represent the load sharing relationship between cortical shell and trabecular bone in these case, it is not necessarily an effective use of resources for models where this specific load sharing is not of greatest interest. Additionally, Eswaran has shown that the load sharing through vertebrae can also be well represented in continuum models when compared to micro-FE models, however it was noted that strain distributions compared less well (Eswaran et al., 2006).

Key sources of error when creating models from microCT scan data are expected to be from the lack of accuracy in the representation of the boundary conditions and material properties, which need to be considered carefully regardless of where they are derived from.
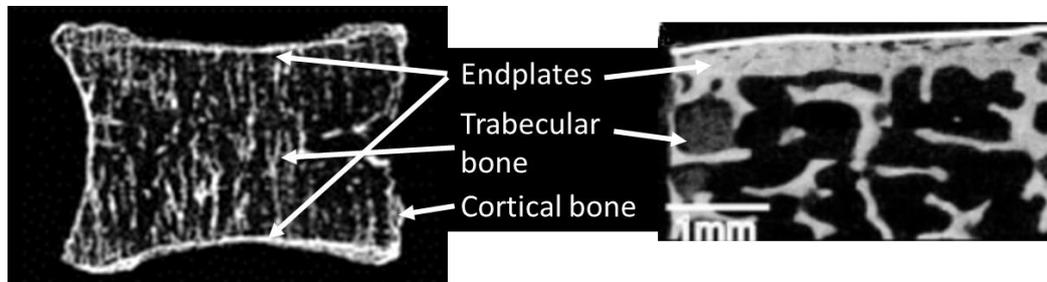
Figure 2-9, Micro-structure within the vertebral body, depcicting trabecular bone and denser cortical bone and endplate. Adapted from (Chevalier et al., 2009; Rodriguez et al., 2012).

2.6.1. Geometry and Mesh

Vertebral geometry for continuum-level FE models can be built directly from individual specimen images (specimen-specific models) or from averaging measurements taken from specimens using statistical methods or parameterised models to give a generic model (Higgins et al., 2006).

In order to build the finite element mesh, there is a need to segment the volumes of interest relating to different materials. Segmentation of vertebrae may require identification of the trabecular bone, cortical shell, soft tissues and any supporting bone cement, which is often included as part of validation experiments. The identification of these regions can be challenging considering the variation in densities captured by microCT seen between specimens (Pahr and Zysset, 2009b). Segmentation can be performed in a number of ways such as manually 'painting' voxels, signal intensity based thresholding or region-based or edge-based numerical analysis of geometries (Leventon et al., 2000).

The accuracy of the resultant model is dependent on the accuracy of the segmentation. It is known that FE solutions are sensitive to the threshold values of bone used to segment the

bone mask, as this determines the amount of bone material captured, and therefore both geometry and material properties. The accuracy is also dependent on the original image quality. It is therefore important to consider the image resolution, contrast and noise as well as user interpretation. Image reconstruction software (ScanIP, Simpleware, UK) has been used successfully to segment vertebral bodies through thresholding according to signal intensity and morphological adjustment of masks to segment bone and bone cement (Tarsuslugil et al., 2014). In this method, density-dependent material properties were assigned to the full vertebrae, avoiding the need to separate the trabecular bone centrum from the cortex; this approach has been shown to provide models with material properties in good agreement with corresponding experiments (Tarsuslugil et al., 2014).

Volume meshing is conducted after segmentation, and can be done by matching the mesh element size to the size of the voxels in the segmented three dimensional models. Modern microCT scanners can provide very high resolution scans with voxel sizes less than 5μm, however voxel based finite element models based on such scans have very high number of elements, creating FE models which take a lot of computational time to solve. To overcome this issue scans can be taken at lower resolutions or high resolution scans can be down-sampled prior to mesh generation. Whilst this improves the practicality of the modelling, information about the trabecular architecture is lost, or not captured by the scan if the voxel resolution becomes larger than the trabeculae size. Yeni et al. showed by investigating the effect of scan resolution and reconstruction resolution that creating a coarse mesh from high resolution scans more accurately represented material properties and the mechanical response of the structure than scanning at a lower resolution to match the mesh resolution (Yeni et al., 2005). It is suggested that this may be due to the lower signal to noise ratio when a lower scan resolution is used, as well as some effect of the scan resolution decrease causing effective trabeculae thickening. When down-sampling or choosing a voxel resolution for the FE model it is important to understand the sensitivity of the model to the voxel resolution. A range of voxel resolutions can be seen in the literature for use in

specimen-specific vertebrae models and a range smoothing algorithms are applied to the models. For voxel based methods, element sizes typically range from 1 to 5 mm. Jones and Wilcox (Jones and Wilcox, 2007) conducted a mesh sensitivity analysis based on FE models and concluded that a 2x2x2mm^3 was sufficient as errors created by other factors outweigh those created as a result of voxel size. Crawford et al. investigated the difference in predictive capability between a 3x3x3mm element sized mesh and a 1x1x1.5mm mesh, concluding that when developing models for a clinical application the variation seen in vertebral mechanical properties seen in the population are far greater than the differences in predicted values resulting from differences in mesh resolution (Crawford et al., 2003b). It is important to evaluate all such comparisons with the overall application in mind to apply context to the investigation. The applications in these studies, to predict vertebral stiffness and strength, match best to the applications intended in this thesis, and so therefore provide evidence on the mesh density required.

FE models are sensitive to geometry and material properties, so in order to most accurately represent the geometry of the vertebrae the smoothing algorithms can be used on the surface of the model using tetrahedral elements instead of hexahedral elements to create a smooth cortical shell and endplates (Jones and Wilcox, 2008).

As mentioned above, vertebral model geometries can also be derived from averaged data, taken either from the literature or experimental measurements, creating a non-specimen specific model. This effectively reduces the effect of inaccuracies due to the large patient variation seen in direct anatomical data, however also makes models less meaningful as they are more susceptible to errors in results appearing correct. It is currently more common to create specimen-specific models as these can be directly validated by experimental results, giving much more confidence in model outcomes (Jones and Wilcox, 2008).

2.6.2. Material Properties

The material properties of elements can be acquired from information from the microCT image, often employing a defined relationship with the image greyscale to provide element-specific values, or they can be applied from an external source such as values derived experimentally or acquired from the literature. The former approach allows for the representation of the inhomogeneity seen *in vivo* and potentially represent the variations in strain within the vertebrae, whereas a model employing homogenous experimentally-derived material properties would only be able to predict the gross response.

Assigning material properties from the image greyscale removes the need for complex and time consuming thresholding of the different types of bone and endplates, whilst keeping details of variations of mechanical properties in the model. Each voxel in the image has a value (measured in Hounsfield units or a numeric greyscale) resulting from the signal intensity of the x-ray. This value is an indication of the material density at that point, and for bone the density is known to be related to the elastic modulus (Brinckmann et al., 1989; Cheng et al., 1997). The modulus values can therefore be derived, either by using a combination of equations relating the greyscale to the density and the density to the modulus, or by directly relating the greyscale to the modulus. There is no standard equation for this relationship and a number of different equations have been used in the literature (Ebbesen et al., 1999; Kopperdahl et al., 2002). The Leeds group has developed an approach based on a linear relationship and used an iterative method to derive the equation by matching the predicted model stiffness values to experimentally derived stiffness values. This approach has been shown to successfully model the material properties of vertebrae under axial compression (Wijayathunga et al., 2008).

Alternative approaches to converting from greyscale values to Young's modulus include using the trabecular architecture and bone volume fraction within each element to derive the elastic behaviour, which may include anisotropic effects based on the fabric tensor. Methods using BV/TV have been used successfully, however this requires the scan resolution to be

high enough to capture the trabecular structure, with lower resolution scan that do not properly represent individual trabeculae likely to overestimate the modulus. This method does not account for variations in bone modulus through the vertebrae (Pahr and Zysset, 2009a; Brown et al., 2014). Using a linear scaling between greyscale value and Young's modulus allows for bone density to be accounted for in the stiffness properties but does not account for other factors which may affect the material properties, for example other morphological properties of the trabecular architecture, or hydration of the tissue.

2.6.3. Boundary Conditions and Loading

Normally loading regimes are kept simple in order to make model validation possible. This means that many of the current models have been simulated under simple axial loads or flexion moments. Experimental methods of loading individual vertebrae often include the encasing of the superior and inferior endplate surfaces and some of the vertebral bone in a potting cement in order to provide a smooth flat surface on which to apply loads. This can help ensure an evenly distributed load across top surface of the vertebrae whilst providing an even geometry inferiorly to stabilise or secure the specimen with. The potting cement is often included in the models with boundary conditions applied to these loading plates (Liebschner et al., 2003). This matches the models with the experimental set up as best as possible, which is important because it is known that the models are sensitive to the applied loading and boundary conditions (Jones and Wilcox, 2007).

The loading conditions used depend on the specific application of the model. One common approach is to apply an axial compression representing body weight when standing. The reported load values range from 300 to 1000 N, with most using 400 N for static axial loads (Erdem et al., 2013; Li et al., 2014; Lu et al., 2014; Unnikrishnan et al., 2013). In these instances, the load is either applied as a distributed pressure over the superior surface of the model or potting cement, or by modelling an analytically rigid plate that is in contact with the superior surface of the endplate or loading plate and applying the force at a known reference point on the plate (Unnikrishnan et al., 2013; Tarsuslugil et al., 2014).

There has been some exploration into the difference made by having the vertebral bodies loaded via solid cement loading plates rather than via less stiff intervertebral disc material seen *in vivo* (Lu et al., 2014). It was found that the comparative IVD model did not correlate significantly better or worse than the cement loaded vertebrae. It is worth considering how relevant simplified models are with respect to *in vivo* situations, such as those that omit soft tissues, however it is more important in model development that the FE model is validated sufficiently. This may mean simplifying the loading and physiological accuracy in order to be able to match experimental validation studies to the model. Additions of soft tissues may introduce more error into a model as they are difficult to accurately represent using FE methods and may significantly increase computational time, and Lu et al. concluded that IVDs are not worth adding until a model is fully validated (Lu et al., 2014).

2.6.4. Predicting Response to Cyclic Loading and Failure

Only a limited number of studies have investigated the cyclic response and failure behaviour of vertebrae using finite element methods. It is therefore challenging to compare between studies, particularly as approaches vary substantially between these limited studies. Tsouknidas et al. used an explicit finite element solver (Abaqus Explicit) to model gait analysis data of a patient's heel strike motion, and subsequently used vertical reaction force information as the model input. They showed a predicted stress and deflection curve for the full range of input forces over the cycle for a range of healthy and treated vertebrae in a full lumbar model (Tsouknidas et al., 2013). This approach is certainly a step forward from static loading and is ideal for short dynamic analysis such as burst fracture mechanisms (Zeng et al., 2013). However these models have a high computational cost and simulating only a single cycle would not be sufficient to provide a true fatigue response evaluation.

In order to monitor the fatigue response of vertebrae using FE methods, it is important to include damage criteria. That may mean including plastic behaviour in the model past a given yield stress, or a removal of elements that pass a defined plastic strain to simulate fracture, as presented by (Garo et al., 2011). The removal of elements then reduces the

model stiffness, simulating the drop in stiffness seen in fractured specimens. Chevalier et al. speculated that damage criterion developed from methods used to analyse non-biological solid materials such as the Drucker-Prager equivalent yield stress condition adopted by Imai et al. are not sufficiently accurate for modelling damage in trabecular bone, as they do not take into account hydrostatic pressure (Chevalier et al., 2008; Imai et al., 2006). Instead, the authors proposed a constitutive law taking into account elasticity, plasticity and damage in vertebrae which was shown to predict the non-linear behaviour, capturing the plastic strain in the system and stiffness reduction. Utilising this, Chevalier et al. show good correlation between FE and experimental vertebral strength, however see poorer agreement for stiffness, however results evaluating direct agreement are not shown. As mechanical stiffness is an important factor in assessing the effect of vertebroplasty, it will be important to consider a method which can provide agreement between both FE and experimental stiffness and yield behaviour. The method of determining failure can be very subjective due to the range of failure mechanisms seen *in vivo* and can add uncertainty into the comparison of methods. Failure can be defined by a sudden change in a force-displacement relationship, or by a given height change in the vertebrae.

A number of studies have used FE methods to predict failure in spinal segments either before or after treatment, with the investigations focussing on whether this is a more reliable fracture prediction method than DXA (dual-energy X-ray absorptiometry) scans, which are the current clinical gold standard (Dall'Ara et al., 2010; Matsuura et al., 2014; Imai et al., 2006; Silva et al., 1998; Mirzaei et al., 2009; Hosseini et al., 2014). One approach has been to determine failure criteria for the FE model and compare the predicted failure strength with that seen experimentally. Alternatively predicted fracture characteristics and location can be qualitatively compared with experiments. Crawford et al. established that vertebral strength predicted from CT-based voxel FE models correlated more strongly with experimental compressive strength than BMD based measures from QCT scans. It was suggested that BMD data does not take into account mechanical factors that affect strength such as

geometry and density inhomogeneities, so cannot accurately predict vertebral strength (Crawford et al., 2003a).

FE methods of differing complexities have been shown to successfully predict fracture sites and fracture patterns (Imai et al., 2006; Mirzaei et al., 2009; Hosseini et al., 2014). As such it is necessary to consider the requirements of the model, for example Hosseini et al. used mathematically complex damage models in order to predict fracture behaviour under very large deformations, however this study was for an increasing step-wise load rather than the load-unload behaviour seen in fatigue loading. Mirzeai et al. showed it is possible to achieve good agreement for smaller deformations using a linear-elastic, linear-plastic material model where failure points were considered as elements with non-zero equivalent plastic strain, identified at each load step (Hosseini et al., 2014) (Mirzaei et al., 2009). However, the results in the Mirzaei paper were shown in cases where damage had been induced via a drill (in order to augment the specimens in a later step) which meant the fracture patterns were relatively repeatable between experimental specimens and not necessarily representative of an *in vivo* situation.

Review of these studies has highlighted the variation in approaches, and limited evidence available to allow for the assessment of each approach. There are no standardised methodologies for defining failure in vertebrae experimentally or in finite element models; or for the best use of material properties, and often the addition of complexity does not seem to provide a clear improvement in results, often at greater computational cost.

2.6.5. Modelling Vertebroplasty

A number of attempts have been made to create FE models of cement augmented vertebrae with the purpose of investigating various characteristics of vertebroplasty such as cement properties, general biomechanical effects of the treatment, effect on adjacent level vertebrae and the potential for prophylactic vertebroplasty (Aquarius et al., 2014). An image-based CT method can be adopted from modelling vertebrae to modelling augmented vertebrae through

the use of manual thresholding and segmentation at the bone-cement interface, then applying previously derived material properties for the cement. This method was used by Matsuura et al., Figure 2-10, and showed good results with the use of tetrahedral elements to more closely represent the complex geometry of the cement than would be possible with hexahedral elements (Matsuura et al., 2014). However in the Matsuura study only correlation was assessed rather than agreement, and whilst fracture load correlation was good, stiffness correlations, including for intact vertebrae, were moderate (R^2<0.4). Xu et al. incorporated bone cement by removing areas of cancellous bone from the model and replacing them directly with cement material approximately matching the area seen in clinical CT scans and x-rays (Xu et al., 2014). Similarly Liebschner et al. approximate the cement volume using a cylindrical shaped bulk material (Liebschner et al., 2001). This method may seem inaccurate, however it has been shown that cement volume does not have a significant effect on mechanical properties of augmented vertebrae, and as the models are only approximations, any small errors due to this simplification would be insignificant (Wijayathunga et al., 2008). Another limitation is in most models the cement fills a void or replaces bone completely as a bulk material, whereas in reality there is still a combination of trabecular bone and cement. This assumption will affect the mechanical properties of the structure as in reality the cement-bone interface is a complex scenario which few studies have investigated. It is difficult to model these interactions on a detailed trabecular level scale when assessing whole vertebrae due to impractical computational times. Typically, as presented in the cases by Matsuura et al., Xu et al. and Wijayathunga et al., the bone-cement interface in the model is tied, so there is no movement or interaction at the surface (Wijayathunga et al., 2008). This assumption may be a large cause of error in fracture prediction models where the interface is likely to be a cause of weakness or failure initiation. (Sikora, 2013) showed that better agreement is seen if this interface is modelled with a less stiff material with plasticity.
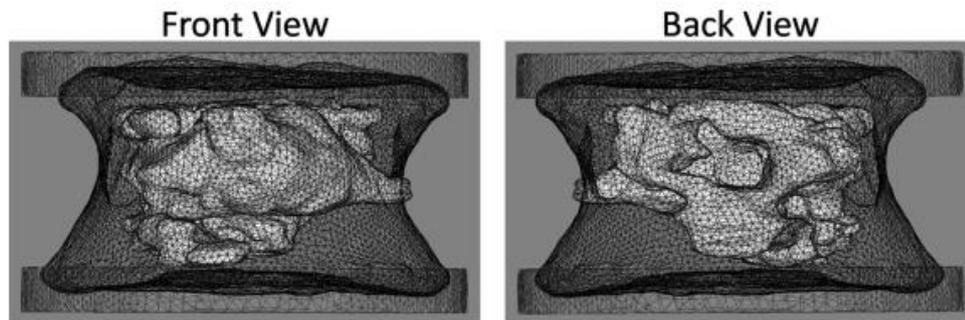
Figure 2-10, FE model showing distribution of bone cement in the vertebra (Matsuura et al., 2014).

2.7. Model Validation

Validation of an FE model is an essential step in confirming that the model is accurately representing a real scenario and thus providing useful results. A common method of model validation is direct comparison with corresponding experimental data, which may demonstrate whether the model can represent the experiment, but the wider clinical application will depend on whether the in vitro simulation is a relatively good representation of the true in vivo scenario. Alternatively, models can be validated by comparison with experimental data or clinical data from the literature but this is usually less robust due to the greater differences in replicating the geometry, material properties and boundary conditions. A summary of the validation process and results reported in finite element studies of vertebrae is presented in Table 2-5.

Table 2-5, Validation methods and techniques seen in the literature for a number of modelling approaches, including elastic models, fracture prediction, augmented vertebrae and models of cyclic loading of vertebrae. Showing the level of validation and results.

Author	Validation Type	Validation Results
FE Vertebrae models		
(Erdem et al., 2013)	Validation with experimental and analytical results from the literature of stiffness, displacement, ligament stresses and ROM.	Reported similar values to literature.
(Unnikrishnan et	No validation	No validation

al., 2013)		
(Li et al., 2014)	Qualitative comparison of fracture location (which vertebrae) with clinical results.	FEA results were consistent with clinical observations.
(Lu et al., 2014)	Experimental strength comparison in models loaded via PMMA and models loaded via an IVD.	Exp/FE-PMMA: R²=0.68 Exp/FE-IVD: R²=0.71

FE Fracture prediction models

(Silva et al., 1998)	Experimental comparison of yield load. Qualitative comparison of predicted strain with failure pattern.	$R^2 > 0.86$ Some correspondence of strain with fracture patterns.
(Imai et al., 2006)	Comparison with experimental yield loads, fracture loads, minimum principal strains, and fracture sites.	Yield loads r =0.949 Fracture loads r = 0.978 Strain r = 0.838
(Mirzaei et al., 2009)	Experimental comparison of strength Qualitative comparison of augmented vertebrae fracture patterns.	Strength R^2 = 0.84 Good failure pattern comparison.
(Dall'Ara et al., 2010)	Experimental comparison with strength prediction	Stiffness R^2=0.49 Strength R^2=0.79
(Hosseini et al., 2014)	Qualitative evaluation of fracture locations comparing with experimental results. Comparison of volumetric strains.	Strain R^2 = 0.74

FE Augmented vertebrae models

(Dickey et al., 2012)	Qualitative validation with models in the literature.	'Showing good agreement'; no evidence given.
(Kinzl et al., 2012)	Experimental comparison of stiffness, strength and loading plate contact pressure.	*Stiffness* CCC=0.94 low modulus cement and 0.89 standard modulus cement. Strength CCC>0.95 Pressure CCC>0.67
(Liang et al., 2014)	Validation through the use of a previously validated model.	Previous model validated
(Purcell et al., 2014)	Validation through the use of a previously validated full thoracolumbar model.	Previous model validated
(Matsuura et al., 2014)	Experimental comparison of predicted fracture loads and stiffness.	Failure loads R^2=0.78 Stiffness R^2=0.39
(Tarsuslugil et al., 2014)	Experimental comparison of fractured augmented vertebrae stiffness	Stiffness concordance = 0.69

Cyclic Testing Vertebrae

(Schmidt et al., 2010)	Comparison with literature values for axial displacement and pore pressure in IVDs.	Good agreement with literature values.
(Tsouknidas et al., 2013)	Comparison with experimental data from the literature.	Agreement with literature values.

As can be seen from Table 2-5, Validation methods and techniques seen in the literature for a number of modelling approaches, including elastic models, fracture prediction, augmented vertebrae and models of cyclic loading of vertebrae. Table 2-5, there is a wide range of results presented in these validation studies so it is important to consider what level of agreement is sufficient, whether it be with experimental results or literature. This predominantly depends on the application of the model in question. It could be said that the error presented as a result of the non-perfect validation is required to be less than the change seen in the model for any given property. For example, Wijayathunga et al. showed that a large change in cement modulus changed the stiffness of the model by 0.7-3.3% and, if this were within the error value determined by the validation, then the model would not be sufficiently accurate to investigate such changes. So the validation error, along with other likely sources of error, has to be smaller than the size of changes that are likely to be seen in the model as a result of its intended use. It can also be said that the validation accuracy has to be sufficient to determine variations between groups of patients for use in a clinical setting. It can be seen that it is possible to achieve very good agreement for vertebral strength and in some cases for vertebral strain, particularly for fracture prediction models. Stiffness validation is, in general, less robust than strength, however Kinzl et al. have shown excellent agreement (concordance coefficient of 0.94).

When evaluating validation results, it is important to note whether the correlation between model predictions and validation values is given as a Pearson's correlation coefficient (R^2 or r^2) or as a concordance coefficient. Concordance evaluates variables with a 1:1 relation which measures degree of linearity between two variables. This is more useful in validating models than linear regression, which only measures the degree of linearity between two variables and not their 1:1 fit.

2.8. Summary of Literature Review

There is still considerable debate over the best methods of treating vertebral fractures. Experimental and FE methods have been established to investigate the use of vertebroplasty

treatment through biomechanical analysis. These have shown promising results and have provided ways of investigating spinal fracture treatment whilst mitigating the limitations of *in vivo* trials (Wilcox, 2004).

Experimentally, studies of vertebroplasty have focussed on examining the static biomechanical response, although a small number of studies have investigated the fatigue behaviour of augmented vertebrae through cyclic loading tests. It has been shown that cement material properties and load magnitudes are both highly important factors in the fatigue behaviour of augmented vertebrae. However there is no standardised method for fatigue testing of vertebrae, as was highlighted by the number of approaches seen, including using and increasing load during the tests, a wide variety of loads and frequencies used and varying length of tests in terms of number of cycles. The fatigue behaviour of non-augmented specimens has been sparsely investigated so there is little with which to compare with treated specimens.

Computationally, studies have predicted the yield strength of vertebrae under static axial compression, however only a limited number of studies have used FE analysis to predict plastic deformation behaviour of vertebrae. Mirzaei et al. and Hosseini et al. have shown that it is possible to predict fracture behaviour with the use of multiple loading steps, however there is little published work on predicting the fatigue behaviour of augmented vertebrae using FE models (Hosseini et al., 2014; Mirzaei et al., 2009). These studies are not truly representative of fatigue loading however, as the first models very high strains representing catastrophic damage of the vertebra and the second uses an induced defect creating more reproducibility between specimens than would be seen *in vivo*. Additionally many of the studies reviewed in this chapter do not show direct validation with experimental data, or do not discuss agreement of predicted results with experimental data.

While there have been significant advances as outlined above, there is a need to develop more robust experimental and FE methods to evaluate the fatigue performance of vertebrae

in both their fractured and augmented state. This will allow for a fuller understanding of whether the augmentation can affect the long term biomechanical behaviour of vertebrae.

2.8.1. Study Aim and Objectives

As a result of the literature review findings, the following aim was determined for the project:

To investigate the mechanical fatigue behaviour of vertebrae through the development of combined experimental and computational methods, with a view to understanding the longer term behaviour; and to apply developed methods to the investigation of the efficacy of the cement augmentation of spinal vertebrae.

To achieve this aim the following objectives were defined:

- Develop a method of creating reproducible, physiologically relevant fractures in an *in vitro* animal model, utilising findings from previous work carried out at the University of Leeds and in the literature on the experimental characterisation of vertebrae.

- Apply the method to create a set of vertebral specimens that can be fractured and augmented using vertebroplasty techniques, and tested to characterise their mechanical behaviour.

- Construct specimen-specific FE models of tested vertebrae from the experimental studies, and validate the FE predictions against the experimental data.

- Define a protocol for fatigue testing of augmented vertebrae *in vitro* using the available materials testing equipment, to characterise the changes in fatigue and multi-cycle loading after vertebroplasty.

- Develop methods to model the fatigue behaviour of bone using FE, using literature evidence defining relationships to describe the changes in material properties over a number of high load cycles (Keaveny et al., 1999).

- Validate the results of FE fatigue analysis by direct comparison with the experimental results.

3. Experimental Methods and Selection of *in vitro* Model

3.1. Introduction

In this chapter, methods used for the development of an *in vitro* animal model are discussed, including specimen preparation and data analysis techniques. First, the general methodologies used throughout the development are presented, including testing, data processing and imaging methods. Then the development of an *in vitro* model using animal tissues that is suitable for investigating fatigue failure and vertebroplasty treatment is presented.

3.2. General Methodologies

The processes used to prepare individual vertebral specimens for mechanical testing are detailed below. The vertebral specimens were required to be of relatively similar size to human vertebrae so that they could be treated in the same way for the vertebroplasty methodologies; and they needed to be readily available so that specimens could be taken from multiple spines and reasonable sample sizes would be achievable. These criteria limited selection to certain food chain animals: cow, sheep and pig; to specific ages available at slaughter; and to certain spinal regions, for example only tail tissue was available from cows due to the way they are sectioned following slaughter. Specimens from pigs were discounted because previous studies have shown these vertebrae have very dense bone with low mineralised bone content, and have been shown to be difficult to fracture consistently (Tarsuslugil et al., 2014). Therefore, specimens from two species were tested for suitability in this study after the above criteria were met: initially, ovine thoracolumbar were selected for investigation due to similarities in geometry and size with human vertebrae, relative homogeneity and evidence in previous studies showing their usefulness for testing spinal therapies. The use of ovine bone as a suitable animal model is discussed in Section 2.3. Ovine vertebrae have a higher mineral content than human vertebrae, and are therefore

stronger, so it was not appropriate to use loads physiologically relevant to loading ranges typically seen in human vertebrae. Skeletally mature ovine bone taken from sheep aged 3-5 years was used, specifically from the thoracic and lumbar regions.

Bovine bone was subsequently investigated because it has a lower bone mineral density than ovine bone, negating the main disadvantage of using ovine vertebrae. It also has a suitable geometry and size compared to human vertebrae for the testing of spinal therapies. For this study, bovine vertebrae from the tail section were used due to their availability and also their smaller size compared to other regions in the spine.

Similar dissection and preparation methods were used for both types of bone, with the goal of creating consistent vertebral specimens suitable for both mechanical testing and subsequent representation in finite element models.

3.2.1. Specimen preparation

Spinal sections were dissected into individual vertebrae and embedded in PMMA cement endcaps to provide flat, parallel loading surfaces. There were some variations in the processes required to dissect ovine and bovine vertebrae due to differences in anatomy, therefore both preparation methods are discussed below, however the goal of isolating bone from soft tissues and creating consistent specimens was the same in both cases.

The process of dissecting ovine thoracolumbar sections is depicted in Figure 3-1. All soft tissues were removed, including muscle and ligamentous tissue, as shown in Figure 3-1 A and B. The ribs were then removed by dissecting through the costovertebral joints, Figure 3-1 C, and the section was divided into individual vertebrae by cutting through the intervertebral disc and facets. Disc tissue was removed from the endplates, dissecting as close to the endplate as possible, Figure 3-1 D. Transverse and spinous processes were trimmed from the lumbar vertebrae and posterior processes were removed from the thoracic vertebrae using a saw blade, allowing specimens to fit within the constraints of the microCT scanner later in the process.
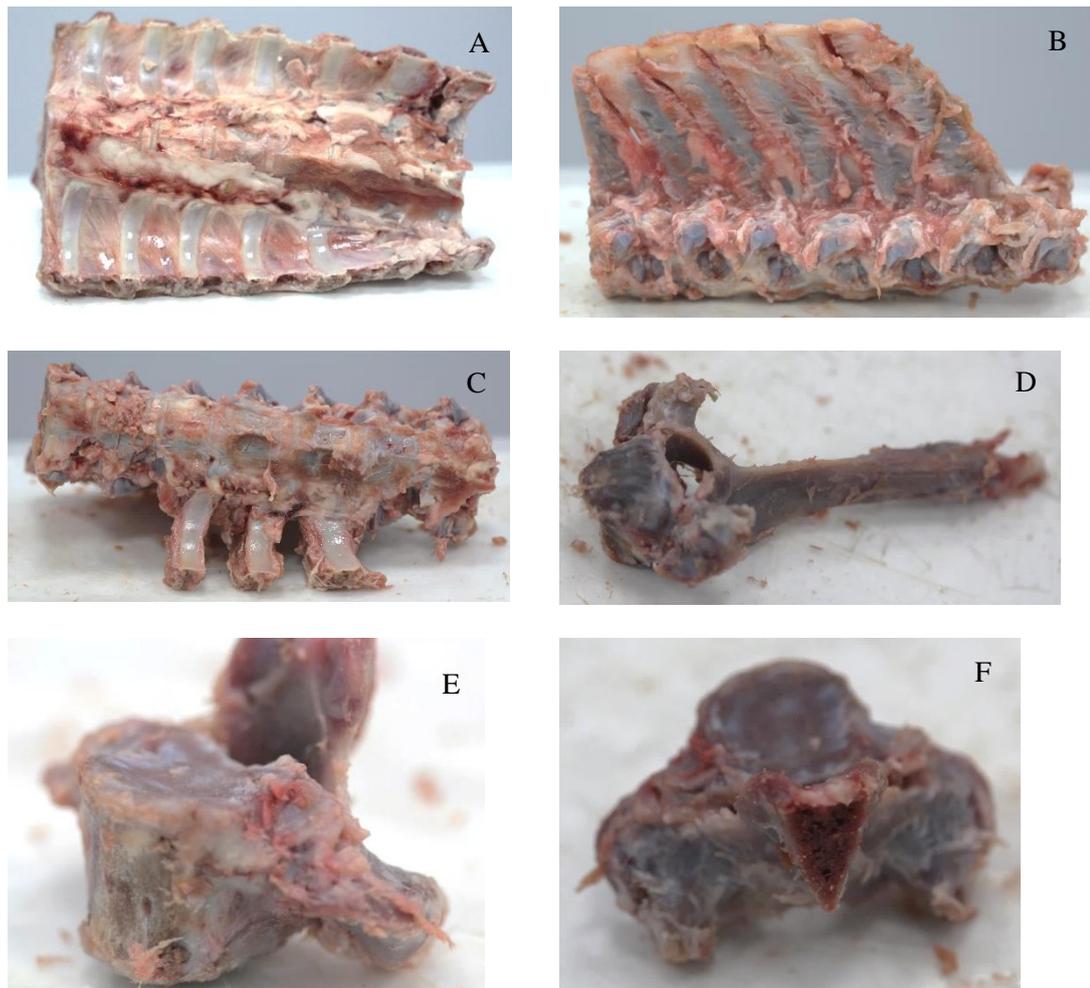
Figure 3-1, Dissection process in an ovine thoracic region showing A) Section T1-7 anterior view showing ribs, B) Lateral view showing posterior elements, C) Removal of ribs, D) Individual vertebrae, E) Anterior view of individual specimen and F) Removal of posterior element.

Bovine tail vertebrae do not have ribs, facet joints or large posterior elements. Additionally there is greater variation seen along the tail with regards to size and shape of the vertebrae compared to thoracic and lumbar regions of the ovine spine. To reduce this variability, the smallest vertebrae at the distal end of the tail were discarded (approximately CC11-CC18, where 'CC' stands for coccygeal vertebra). Due to natural variations between animals, and variation between the spinal level at which the tail was removed initially, some specimens had larger processes than others resulting in them not fitting into the moulds used to create cement endcaps. In these cases the processes were trimmed with a saw blade, removing only the bone necessary to allow the specimen to fit in the mould. The dissection process is show

in Figure 3-2. Two tail sections before removal of any tissue are shown in Figure 3-2 A, followed by a five vertebrae section after tissue removal in Figure 3-2 B, and complete soft tissue removal and dissection into single vertebrae in Figure 3-2 C.
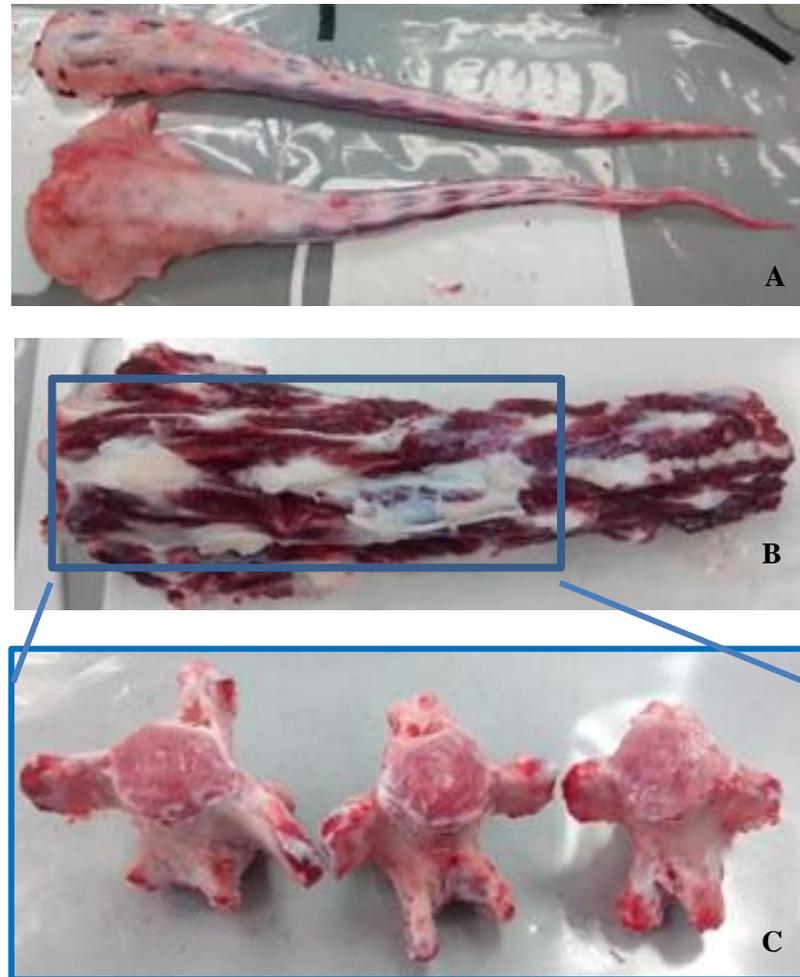
Figure 3-2, Dissection of bovine tail vertebrae showing A) two full tail section prior to any dissection or removal of soft tissues, B) Five most cranial vertebrae (CC1-CC5) after removal of some muscle tissues and C) Individual bovine vertebrae with all soft tissues removed.

3.2.2. Embedding in PMMA

PMMA bone cement was used to create flat parallel plates on the inferior and superior endplates, providing a surface for compressive loading of the specimen in the materials testing machine and producing even load distribution over the endplate (Figure 3-3). For this study, commercially available PMMA cement was used (Cold Cure, WHW Plastics, Hull,

UK), prepared at a 2:1 weight ratio of acrylic powder component to liquid methyl methacrylate. The powder and liquid components were mixed until the powder had dissolved and the cement was then used over the next few minutes before the cement began to solidify.

In order to align the specimens so that the cement plates were parallel, a steel rod was inserted into the spinal canal and secured against the anterior edge of the canal using sponge. The rod was then held in place above the mould for the PMMA using an adjustable retort stand, with the vertebral endplate approximately 2mm above the base of the mould, Figure 3-3 A. The mould was then filled with PMMA and left to set. This method created a hole concentric with the canal, which was used as a reference point for the location of the applied load. Once one side of the specimen was embedded in PMMA, the vertebra was then inverted and a spirit level was used to ensure the second plate would be parallel to the first, and the process was repeated, Figure 3-3 B.
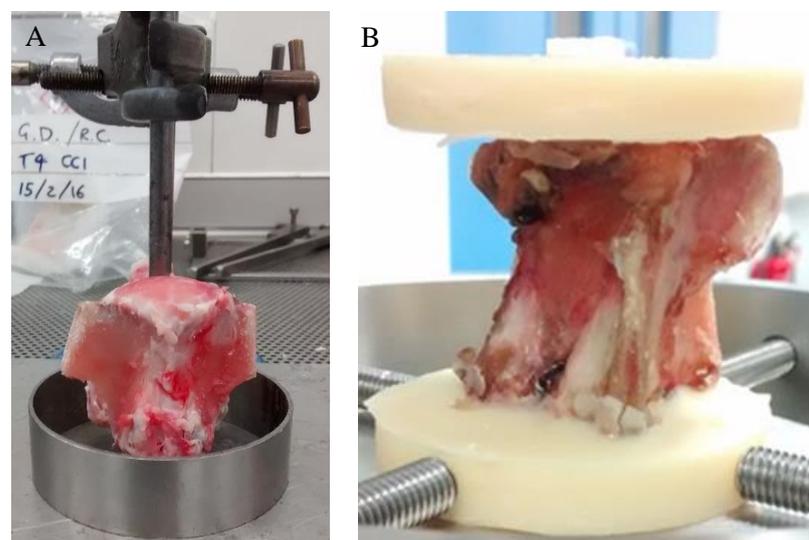
Figure 3-3, A) Method for creating PMMA loading plates using stand with dowel through neural canal to align specimen vertically, and B) Vertebrae in cement housing constrained for testing.

3.2.3. Load location

The distance from the anterior edge of the neural canal to the anterior most edge of the specimen was measured and recorded, to define the point of loading consistently between specimens. Two positions for the load application were tested during the method development, the first directly through the central vertical axis and the second at an anterior position. The central load was likely to be more representative of the neutral position of the spine and the anterior load was more likely to create an anterior wedge fracture. The central load location was half the distance between the anterior margin of the neural canal and the anterior edge of the vertebrae along the sagittal axis, so it was in effect at the central point of the main body of the vertebrae, Figure 3-4 A. The anterior load position was defined as 75% of the distance between the canal and the anterior edge of the vertebrae, Figure 3-4 B. It was thought that this load location would allow for an anterior wedge fracture to be created, whilst still allowing sufficient load transfer through the rest of the vertebral body to ensure the structure would be stable during loading. Radiopaque markers were then attached to the location where the load was to be applied using superglue, Figure 3-5.
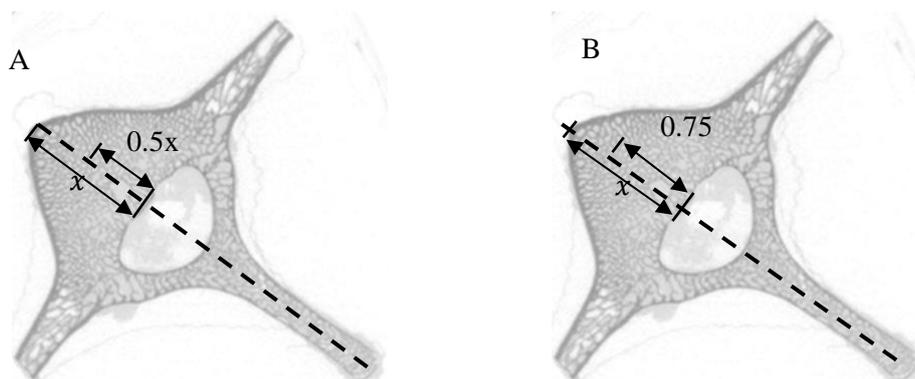
Figure 3-4, A) location of the central load position, and B) the anterior load position, shown on an example microCT scan of an ovine thoracic vertebra. The dashed line shows the sagittal axis.
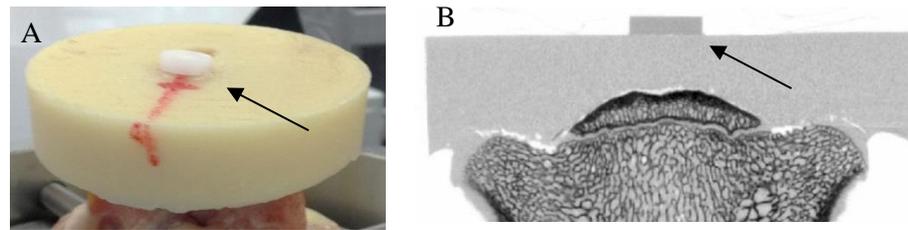
Figure 3-5, Radiopaque markers used to identify load application location in experimental method and microCT images with A) marker glued to upper cement plate, and B) marker shown in microCT image.

3.2.4. MicroCT Imaging Methods

Specimens were imaged using microCT in order to characterise the vertebral architecture and level of damage, as well as to generate specimen-specific finite element models. Single vertebral specimens were scanned using a microCT scanner (XTremeCT, Scanco Medical AG, Brüttisellen, Switzerland). Specimens were imaged after preparation and at multiple points throughout the testing process. The same imaging process was used throughout and is described below.

For the specific microCT scanner used, the specimen remained stationary whilst the x-ray source helically rotated around the specimen to collect projection data. Projection data was then reconstructed into volumetric slices of the specimen via proprietary computer algorithms. All scans were undertaken at a resolution of 82µm with a slice thickness of 1mm. An integration time of 300ms was used with a voltage of 60 kV and a current across the x-ray tube of 900 µA. These settings were used based on previous experience within the research group (Zapata-Cornelio et al., 2017), and have been shown to give a sufficient image quality for creating homogenous voxel-based finite element models and to examine the trabecular structure in the vertebrae. A higher image resolution could have been achieved using the equipment available, however this would have created larger datasets, making the images more time consuming to work with and extended scan duration times. The amount of trabecular detail that can be seen at this resolution is shown in Figure 3-6.

The image reconstruction generated proprietary 'ISQ' image files which were converted to tiff image files using a custom Matlab script built in house (M. Preutenborbeck, University of Leeds). This converts the Hounsfield units from the scanner which range from $\pm$ 32000, defining the full greyscale spectrum, to 256 greyscale values. A linear scaling factor was used, whereby the Hounsfield unit was given as a fraction of the total Hounsfield units and then multiplied by 255. Any values less than 0 were considered to be noise and set at a value of 0. The tiff images were then viewed or reconstructed in image processing software ScanIP (Simpleware Version 7.0, Synopsis, UK). This allowed them to be visually analysed or subsequently used to create finite element models.
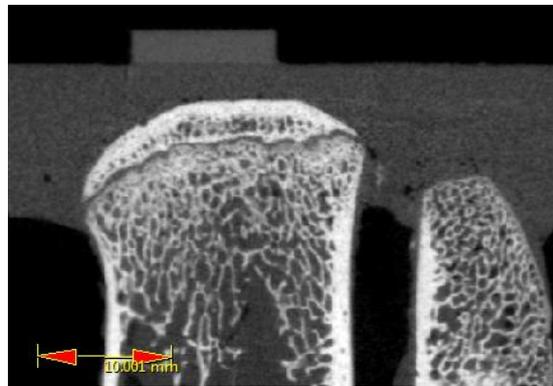
Figure 3-6 Level of trabecular detail visible at 82µm resolution shown on superior half of bovine tail vertebra specimen, scale bar 10mm.

3.2.5.   Static Compressive Testing

A compressive testing methodology was used throughout the study to generate the initial fractures in the vertebrae, as well as to measure the elastic stiffness of the undamaged vertebrae. Specimens were tested in a universal materials testing machine (Instron 3366 10 kN, Instron, UK). The cement plates were constrained to steel platens using screws, and load was transferred to the upper platen via a steel ball, located in a hole above the radio-opaque marker. This allowed for rotation of the upper cement plate so the system was not over-constrained and anterior wedge fractures could be created. The fixture configuration, used for all static and fatigue testing, is shown in Figure 3-7.
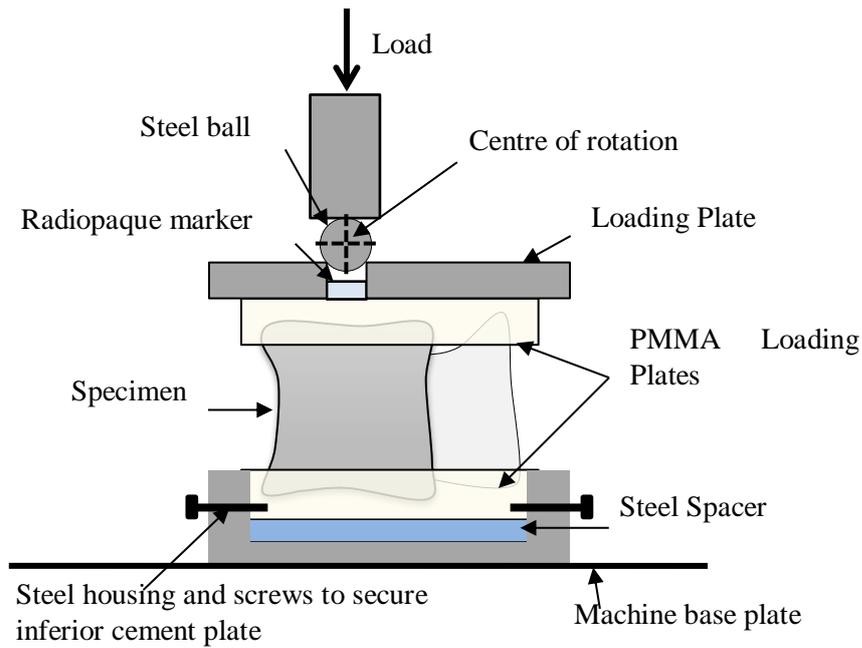
Figure 3-7, Diagram depicting experimental compressive load test set up inside the materials testing machine.

Loading was conducted in displacement control mode at a loading rate of 1 mm/minute, a rate slow enough to reduce strain rate dependency of results due to the visco-elastic effects of trabecular bone. Initially specimens were loaded to 50N to ensure full contact across the loading platens, then a cyclic preload of 50-300N was applied for 15 cycles to condition the vertebrae and further reduce visco-elastic effects. To create initial damage or failure in the vertebrae, specimens were then compressed axially to 9.5 kN, the maximum capability of the machine, or to failure, where failure was defined as non-linear behaviour seen on the force-displacement curve or where damage was first induced.

3.2.6. Data Analysis

3.2.6.1. Calculating Elastic Stiffness from Static Load Data

In order to compare mechanical behaviour between specimens and make comparisons with specimen-specific finite element models reported in Chapter 7, it was necessary to develop a consistent approach to determining the elastic stiffness of each specimen. A Matlab script was written to determine the maximum elastic stiffness from the load-displacement response of each vertebra. In the code, the stiffness was calculated from the force-displacement data over consecutive 0.6 mm intervals with an increment of 0.1 mm, starting after the pre-cycling, as shown in Figure 3-8. This approach had been found previously to give a consistent measurements across specimens (Tarsuslugil et al., 2014). The largest value from these calculations was then defined as the elastic stiffness. As the non-linear portion of the graph always has a reduced stiffness as the specimen starts to fail, and the toe region of the graph increases in stiffness towards the linear region, the largest value calculated consistently gave the steepest section of the linear region for different specimens.
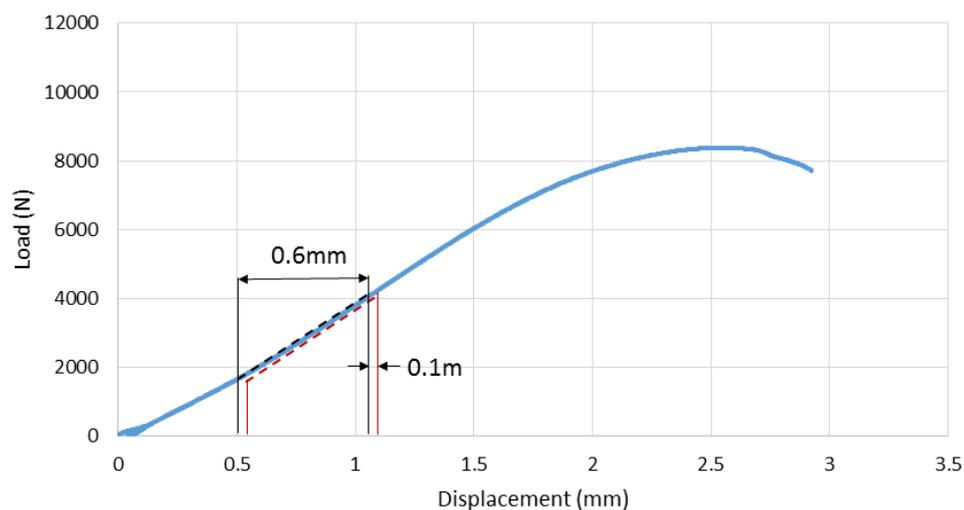
Figure 3-8, Determining the gradient of the linear elastic region to approximate elastic stiffness.

3.2.6.2. Calculating Yield Load from Static and Cyclic Data

Strain was calculated by determining specimen height from microCT images taken before testing, by reconstructed the image data and using measurement tools in the reconstruction software to calculate vertebra height from scan thickness and number of image slices. Change in height was derived from the material testing machine load-displacement data after first subtracting any initial displacement of the crosshead before the load application. Change in height could then be normalised against initial height to give strain.

As the exact yield point of the load-displacement curve was not always obvious, a method of defining yield was determined to keep the calculation consistent between specimens. Failure was defined as the intercept of a 0.2% strain offset of the linear elastic region of the force-strain curve (Figure 3-9). This was calculated by finding the gradient of the linear elastic region and using this to create the offset line, employing the Matlab script described above for calculating stiffness. The intercept of the offset line and the failure curve was then found, giving yield load and yield strain. Change in height was normalised against initial vertebra height in order to calculate a 0.2% offset strain to find the engineering yield value, as the yield point was not easily determinable from the load-displacement data. Initially, stress values were not calculated due to the varying cross-sectional areas of the vertebrae, meaning even calculating an average value through the specimen would be difficult to achieve consistently. However, in the latter part of this thesis, a largely approximated value for stress was used, calculated by dividing the test load by the total vertebra volume.

A similar method was used for the fatigue tests to find the number of cycles to failure. Cycles were plotted against peak strain for each cycle, and a 0.2% strain offset was calculated from the linear region of the graph. The point where this intercepted with the cycles-strain curve was defined as the point of failure (Figure 3-10).
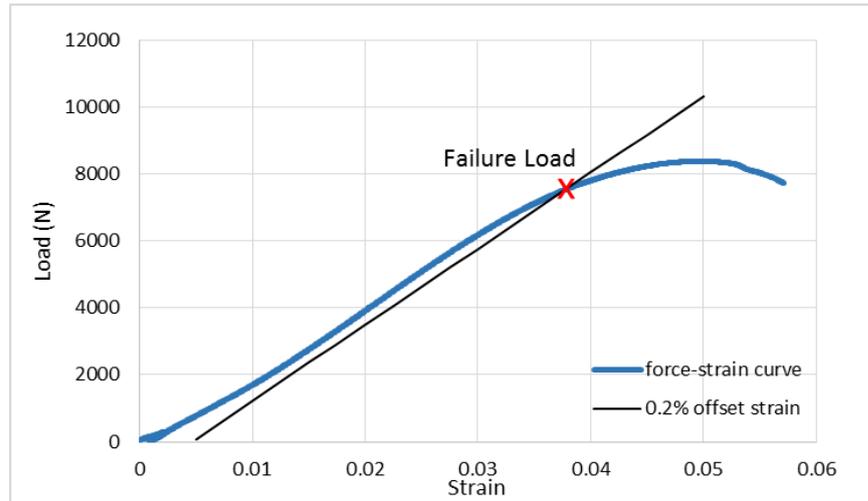
Figure 3-9, Determining the failure point of the load-strain curve using the intercept of a 0.2% offset strain line with the failure curve, shown on an example failure curve.
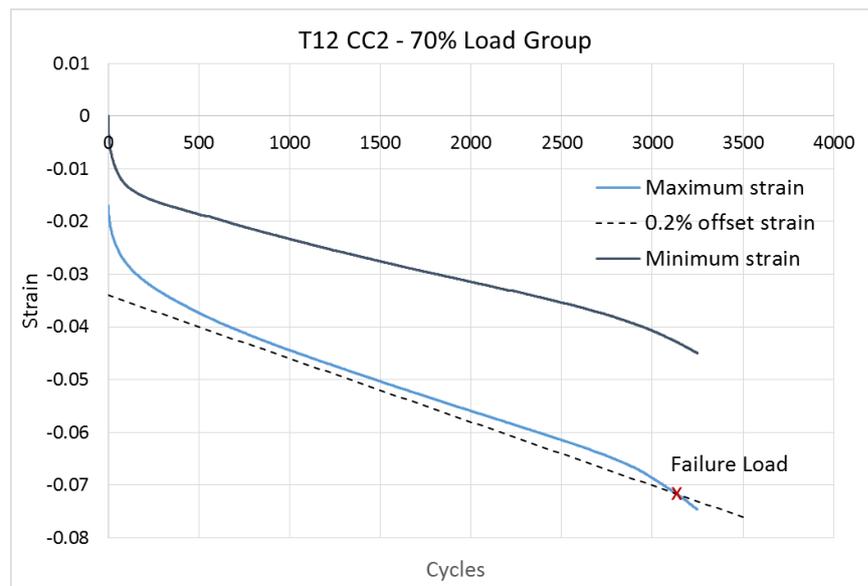
Figure 3-10, Method of determining failure point from cyclic test using intercept of a 0.2% offset line with strain against number of cycles data, shown on an example fatigue graph.

3.2.7. Statistical Analysis

Statistical analysis was used to compare mechanical properties between different groups throughout, and to compare the response of the same specimens at different points throughout testing, specifically paired t-tests and analysis of variance (ANOVA) with

Tukey's test to compare between groups. This was performed using standard statistical tools (SPSS Statistics v.22, IBM, Portsmouth, UK). Statistical significance was considered where $p<0.05$.

3.3. Development of an *in vitro* Fracture Model using Animal Tissue

In order to be able to develop fatigue testing methods and investigate vertebroplasty *in vitro*, it was essential to develop an *in vitro* model of a fractured vertebra with which the treatment could be tested. The fractures needed to be reproducible and comparable to a clinical osteoporotic fracture, with respect to showing a loss of height due to compression, ideally as an anterior wedge fracture. As discussed in Section 3.2, animal tissue was used rather than human for this work. For this study, the clinical vertebral 'fracture' was identified by non-linear force-displacement behaviour under compression (i.e. yield-like behaviour), or by visible plastic deformation or visible fracture. Methods of both quasi-static compressive fractures and high energy burst fractures were explored. The following section describes the process followed to decide upon the compressive fracture method and the most suitable animal model. As explained in Section 3.2, two types of animal bone were tested, ovine and bovine, and the following describes the different compressive testing methods explored to create fractures in these vertebrae.

3.3.1. Ovine Vertebrae

Previously excised thoracic and lumbar regions, stored at -20°C and defrosted for approximately 12 hours at 5°C were used for testing. Eight lumbar and five thoracic vertebrae (T6-T10) were excised from three spines to be used for method development. It was evident from initial testing that healthy, intact ovine vertebrae typically did not fail before 9.5 kN, therefore a number methods of manually inducing a small amount of damage to the bone to initiate fracture were trialled. The methods involved inducing fracture by making a series of cuts or notches in the anterior wall of the vertebrae. Previous studies from the literature that utilised a similar methodology are discussed in Chapter 1. This approach

had the potential advantage of creating more reproducible fractures in terms of severity and location.

Table 3-1 shows the series of tests undertaken in sequential order, with details of the test, and the load-displacement response seen. It was found that a relatively large defect was required to cause a failure response, with smaller cut defects causing no change in response, even under repeated loading where no change in stiffness was observed between tests on the same specimen (see

Table 3-1, Test 2). This method would allow for reproducible fractures and would mitigate for some of the variation seen naturally between specimens by forcing damage to occur in the same location. Additionally a burst fracture method was assessed for feasibility on six 3-vertebrae segments, using a technique previously developed at the University of Leeds (Hanlon, 2012) and illustrated in

Table 3-1 (Test 6). Briefly, three-vertebra spinal sections were constrained in PMMA on the superior and inferior vertebrae to ensure fracture in the central vertebra, housed within the drop-mass equipment and held in place by a guide shaft. A variable mass (5.1 – 9 kg) was then dropped from a pre-defined, variable height (0.8 - 1.4 m) along the guide shaft. It was not possible to consistently fracture specimens to a reasonable degree using this process, as frequently no fracture occurred or considerably too much damage was caused, as shown in

Table 3-1 (Test 6). This resulted in a large number of wasted specimens, so was not pursued.

Table 3-1, Pre-damage methods used during development to investigate a way of inducing non-linear plastic behaviour in ovine vertebrae with loads under 10 kN.

Test	Details	Image	Typical Response
1	Single static load to 9.5 kN, loaded anteriorly or centrally, showing no difference. (n=2).		

2	Static load to 9.5 kN then unloaded, test repeated ten times. (n=2). Tests 1 and 10 depicted in graph. Vertebra gets stiffer.		
3	6 mm cut made into anterior wall using saw blade, loaded to 9.5 kN. (n=1).		
4	12 mm cut made into anterior wall using saw blade, loaded to 9.5 kN. (n=1).		
5	6 mm x 6 mm notch cut into anterior wall using saw blade, loaded to 9.5 kN. (n=12).		
6	Burst Fracture method using drop rig. Different masses investigated on 3 vertebrae sections of spine. Process difficult to tune (n=6).		Two typical cases: Fracture energy A) too high, and B) too low to fracture.
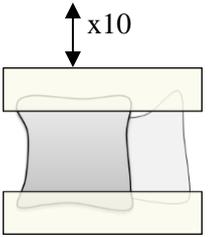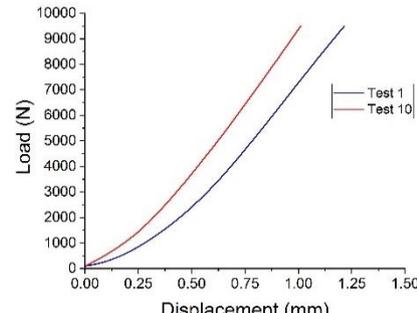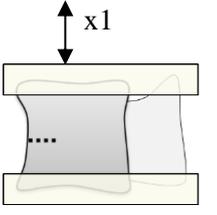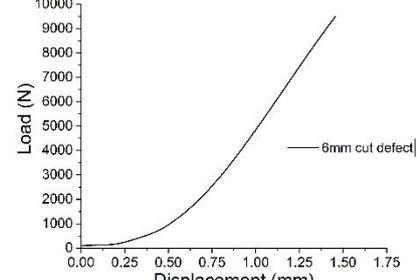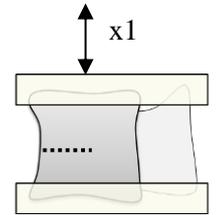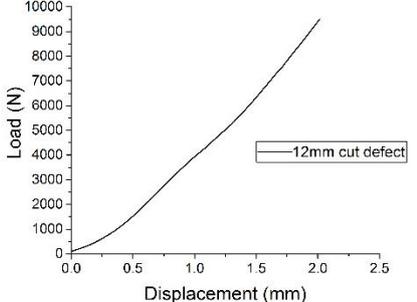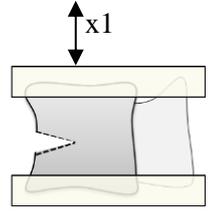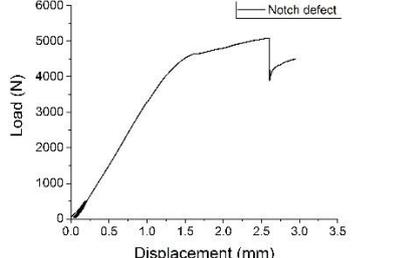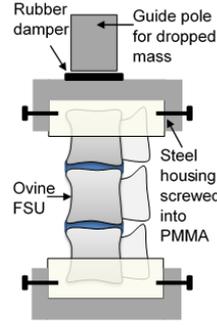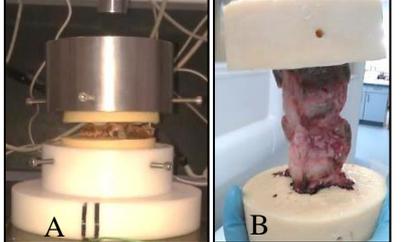
Using the method 5 from Table 3-1, Pre-damage methods used during development to investigate a way of inducing non-linear plastic behaviour in ovine vertebrae with loads under 10 kN., the remaining ten prepared thoracolumbar specimens had notch defects cut

into the anterior wall and were then compressed to failure. Elastic stiffness was measured before the notch was created by a compression test to 1 kN, i.e. before any failure or damage had occurred, where average intact stiffness was found to be 3983 ± 901 N/mm. From the load to failure curve where average notched stiffness was 2278 ± 346 N/mm; and after the load to failure test by means of a second compression to 1 kN, where stiffness with failure was found to be 3443 ± 504 N/mm. A two-tailed paired t-test was used to assess the effects of the defect and compressive testing. No significant difference was seen in mechanical stiffness as a result of creating the notch defect ($p>0.05$), however a significant difference was seen in elastic stiffness of the vertebrae after the compressive load to failure ($p<0.05$). These stiffness changes are shown in Figure 3-11 and Figure 3-12. A potential source of variation in the experimental stiffness results is the position of load application. It has been shown through finite element sensitivity studies that such loading situations are highly sensitive to this position, and even though care was taken in the measurement and position of the load markers this is still a likely source of error as the central point of the anterior wall of the vertebrae is estimated by eye. Additionally, this position may move as a result of tilt in the upper cement plate caused by the cuts or defects in the vertebrae (Jones and Wilcox, 2007).
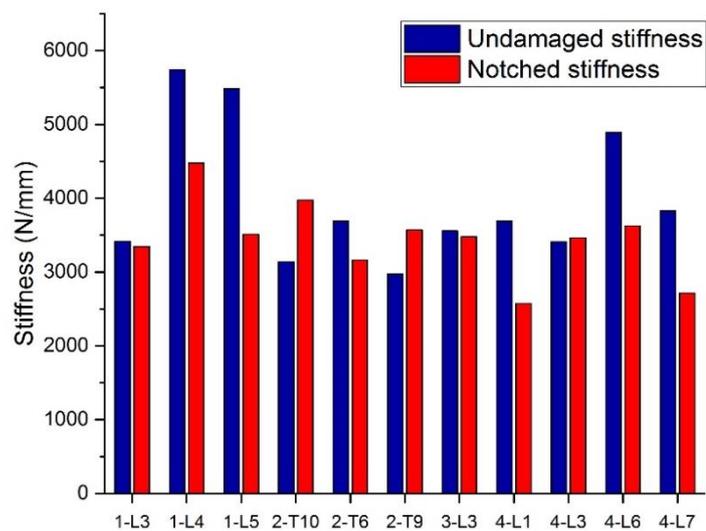
Figure 3-11, Change in elastic stiffness as a result of the notch defect cut in the anterior wall of the vertebrae ($p>0.05$).
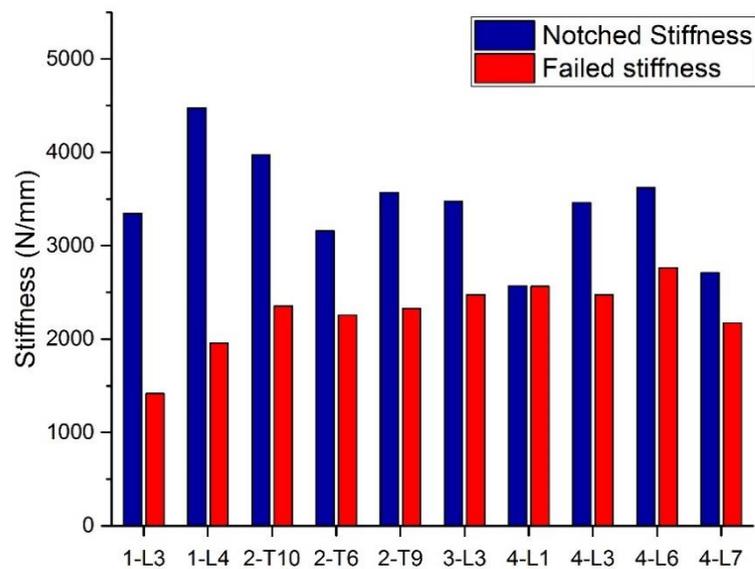
Figure 3-12, Elastic stiffness for the notched vertebrae and the same vertebrae after load to failure, significant decrease in stiffness seen (p>0.05).

It was observed that the elastic stiffness of the vertebrae did change as a result of the notch defect, typically causing the specimens to become less stiff. However this difference was not seen to be statistically significant. Compressive load to failure did however cause a significant reduction in elastic stiffness. Therefore this method could be used as a failure model for vertebrae, providing a model measurably different from undamaged controls with which vertebroplasty augmentation could be tested. However due to expected limitations of the defect model, such as difficulties with the vertebroplasty process and an expected increase in cement leakage, a different species of bone was also investigated for use as a failure model. The following section discusses the use of bovine vertebrae as a model, including the process of testing to determine the suitability of this type of bone.

3.3.2. Bovine Caudal Vertebrae

Initially 16 bovine tail vertebrae from the first to the eleventh level were dissected from four bovine tails (where the first level is taken as the most cranial vertebra), taken from cattle

aged between 2 and 5 years. For this preliminary testing, the majority of specimens were taken from levels 5 to the end of the tail, typically around level 9, as this tissue was available already in the laboratory. Vertebrae specimens were frozen after dissection, wrapped in PBS-soaked paper, and thawed prior to testing by defrosting overnight at 5°C; they were then refrozen and defrosted again before any subsequent testing in later experimental procedures. Initially all specimens were loaded in compression through a centrally located axis to 9.5 kN or failure, according to the methods described in section 3.2.5. It was noted that the geometry of the vertebrae changed through the spinal levels, becoming narrower towards the distal end; however as the height was approximately similar, vertebrae effectively have a more severe aspect ratio and appear elongated. The narrower vertebrae were found to be more likely to come loose from the cement plates during loading. In cases where this happened, testing was continued as the compressive load kept the cement and bone in contact, however the effect of this occurring on the test outcome is unknown.

Compression resulted in failure in almost all cases, where failure was defined as yield-like behaviour identified on the force-displacement curve.. However in some cases a large amount of tilt was seen in the top plate, often before failure had occurred, but still whilst within the load capabilities of the machine, meaning that frequently the test had to be stopped to ensure the top plate did not collide with the bottom plate. This was also seen only in vertebrae with a smaller cross-section. A summary of the typical geometry and mechanical response seen for different levels is shown in Table 3-2. At this stage it was challenging to identify where the point of failure occurred in the vertebral body, as the damage did not present as a visible fracture and did not create identifiable discontinuities the microCT scans. All specimens from the level 9-11 group saw failure behaviour according to the force-displacement curves, and specimens from levels 5-8 had a greater chance of failure than those from levels 1-4; however even in this group more than 80% of specimens saw failure behaviour.

Table 3-2, Images and typical force-displacement responses of representative spinal levels through the bovine tail section.

Spinal level	Image	Typical Response
Levels 1-4 (n=1)		
Levels 5-8 (n=12)		
Levels 9-11 (n=7)		
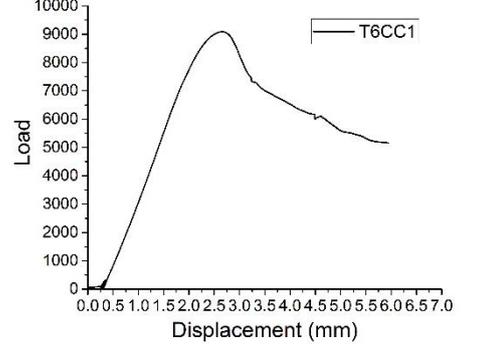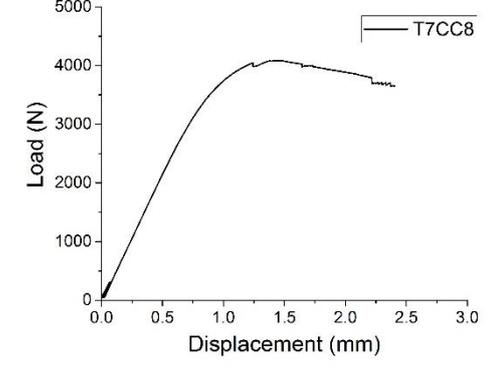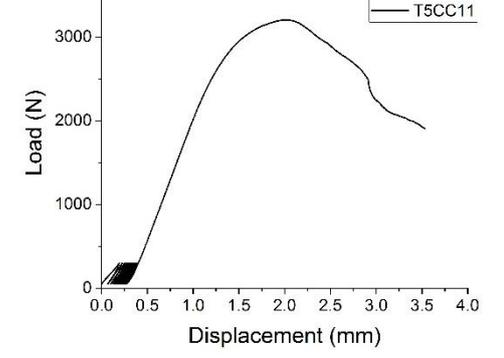
3.4. Finalised Experimental Methods

From the above set of experiments, it was evident that bovine caudal vertebrae were more suitable than ovine vertebrae, as there was a greater chance of inducing failure and displaying non-linear force-displacement behaviour in the bovine vertebrae within the available experimental conditions, and without the need for artificial induction of fracture.

Only the four most superior vertebrae were used for subsequent tests to avoid issues resulting from the narrow shape seen in lower level vertebrae and as these are more representative of the human vertebral shape.

Three sets of specimens were prepared for testing, the first (n=15) for the purpose of static compression to failure and for use in the development of specimen-specific FE models. The second set (n=20) were used for developing a fatigue testing methodology. The third set of specimens (n=11) were tested with the vertebroplasty treatment. All of the specimens were prepared using the methods described in Section 3.2.1.

3.5. Fatigue Testing Methods

After developing a suitable static testing method, it was necessary to develop a dynamic test method capable of investigating differences in fatigue response of vertebrae, and subsequently to investigate the longer-term performance of vertebroplasty. All vertebrae used in the fatigue tests were loaded statically to 9.5 kN or failure as described above. This was done primarily to investigate yield behaviour but also provided a control set for vertebroplasty treated vertebrae that would allow for a direct comparison of the mechanical behaviour before and after cement augmentation. To mitigate for some of the natural variability seen between specimens, loads were normalised against the initial yield load measured in the static test, vertebrae were then split into four groups (n=5) and tested to a proportion of their individual yield load. This approach has been taken by other authors and is shown in Section 1.2.3, and appeared to suitably account for variation whilst still providing sufficient use of varying load for a fatigue tests.

Specimens were tested at a frequency of 1 Hz with a sinusoidal waveform input cycling between 50 N and the maximum compressive load determined for that vertebra using a standard fatigue test machine (Instron Electropuls E10000, Instron, UK). The intention was to simulate high loads experienced in daily living rather than a specific activity, so a physiologically relevant loading rate of 1 Hz was chosen, which is representative of a slow

walking or repetitive lifting frequency. The group of fractured specimens were tested to either 90%, 80%, 70% or 60% of the yield load determined in the initial test. The loading regime for the vertebroplasty specimens is presented in Chapter 7. Specimens were tested to failure, determined as a rapid increase in strain rate, or until 10000 cycles were reached, at which point the test was stopped. The same constraints and loading mechanism, via a steel ball, were used as in the initial load to failure tests. The lowest and highest strain in each cycle were recorded and plotted. Yield points were determined using methods described in section 2.2.6. All vertebrae were microCT scanned at 82µm before and after fatigue testing.

A custom in-house Python script (developed by Dr S. Sikora, University of Leeds, 2017) was used to process the output data from the fatigue test to calculate the elastic stiffness during every cycle, so the change in stiffness could be tracked over time. The script extracted load-displacement data for the loading ramp for each cycle and took the middle third of these data points over which to calculate stiffness.

3.6. Summary

Developing a suitable model of vertebral fracture using animal tissue is challenging, previous studies have highlighted the merits and limitations of the use of different animal bone for investigating vertebroplasty. It was shown in this preliminary work that ovine bone is too strong to fracture within reasonable load limits. A study by Wu et. al (Wu et al., 2007) has overcome this by performing ovariectomies and utilising low calcium diets on live sheep before harvesting vertebra, inducing low bone mineral density in the animals (BMD). A number of methodologies were explored to create a suitable fracture model in ovine bone without the need for *in vivo* interventions. Previous studies have investigated burst fracture techniques (Tarsuslugil et al., 2014), however burst fracture investigations were difficult to tune and utilised specimens inefficiently.

Tarsuslugil et. al (Tarsuslugil et al., 2013) have shown porcine vertebrae are typically not skeletally mature when they are acquired from the abattoir, meaning bone is highly

cartilaginous and the resultant low porosity means it is difficult to inject cement into the vertebrae.

Due to perceived limitations with the defect methods explored in ovine vertebrae and the problems associated with porcine bone, bovine bone was investigated. Bovine bone has been used as a model for vertebroplasty in the form of bone cores (Helgason B. et al., 2013) suggesting the bone is of suitable porosity; however no evidence was found to suggest whole bovine vertebrae have been used as an *in vitro* vertebroplasty model. In this study, a bovine tail vertebrae model was successfully developed for examining the performance of fractured and repaired vertebrae under fatigue loading, as described in the following chapters of this thesis.

4. Experimental Results

4.1. Introduction

This chapter presents the results for the experimental testing conducted on bovine tail specimens under axial compression. The load-displacement behaviour for both static and dynamic tests are presented including the results from the initial tests to failure and the subsequent fatigue tests. Additionally, micro-computed tomography (microCT) image data from before and after testing is shown. This data provides information about the characteristics and locations of fractures seen in bovine vertebrae under high-load low-cycle fatigue loading. The load-displacement data from these tests and microCT image data is then used to create and validate specimen-specific computational simulations, as reported in the subsequent chapters.

A Summary of all the test groups, number of specimens in each and measured outputs in shown in Table 4-1. This includes details of vertebrae used for vertebroplasty, results of which are discussed in detail in Chapter 7.

Table 4-1, details of specimens used throughout the experimental testing,

Group	Number of Specimens	Tests and Outputs
Group 1	10	Single load test to 9.5 kN - Elastic stiffness and yield load and strain
Group 2	20	Single load test to 9.5 kN - Elastic stiffness and yield load and strain Fatigue Test – Cycles to failure, yield strain.
Group 3	11	Vertebroplasty group Single load test to 9.5 kN - Elastic stiffness and yield load and strain. Fatigue Test – Cycles to failure, yield strain.

4.2. Static Tests

Initially, a set of ten bovine tail vertebrae were loaded axially in a materials testing machine to failure or 9.5 kN (details of experimental methods were discussed in Chapter 3.2.5). Load-displacement data was collected in order to determine the elastic stiffness and yield behaviour. The load-displacement curves for each vertebra tested are shown in Figure 4-1. In most cases the initiation of failure was seen, where failure is defined as an increase in rate of change of displacement and the onset non-linear behaviour. In these cases, the test was stopped manually when the initiation of failure was seen. In a number of vertebrae there did not appear to be any initiation of damage, and linear-elastic behaviour was observed until the test stopped at 9.5kN, the maximum load capability of the machine. Similar levels of total displacement, and similar elastic stiffness values were seen across the set of specimens, however it was noted that the vertebrae that did not fail appeared to have a greater stiffness. A typical response from a vertebra that did show failure is shown in Figure 4-2A, and similarly a vertebra that did not fail before 9.5kN is shown in Figure 4-2B.

The pre-cycling used to condition the vertebrae before the load to failure showed in all cases a decrease in the hysteresis between each cycle, highlighting the visco-elastic properties of the vertebrae. An example of the typical response to ten pre-conditioning cycles is shown in Figure 4-3. Some vertebrae saw greater initial displacement than others over this period of cycling. However this was not seen to correlate with the failure behaviour of the specimen. This can be seen in Figure 4-2A and Figure 4-2B where the two examples have very similar toe regions but show different failure behaviour, with the first specimen exhibiting clear failure and the second only linear-elastic behaviour. During pre-loading cycles it is possible that the response seen is due to fluid becoming less viscous due to heat, and is moving out of the vertebrae under load causing a greater proportion of the response to come from the bone rather than marrow, and therefore cause a stiffening effect. It is also possible during these loading cycles that space is being removed that was between the cement and the bone, compressing any air out.
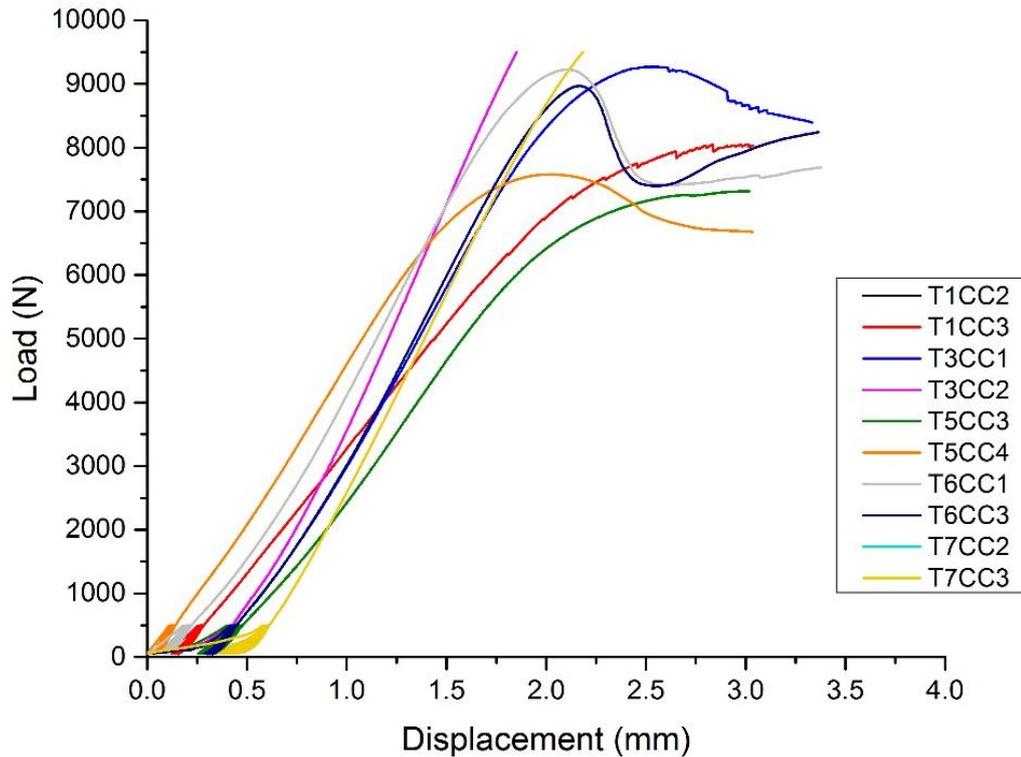
Figure 4-1, Load-displacement data for ten vertebrae loaded axially under static load to failure at a rate of 1mm/min. Specimens names are denoted using with T number giving the tail they were extracted from and CC giving the level (CC1 being the most cranial level vertebra).
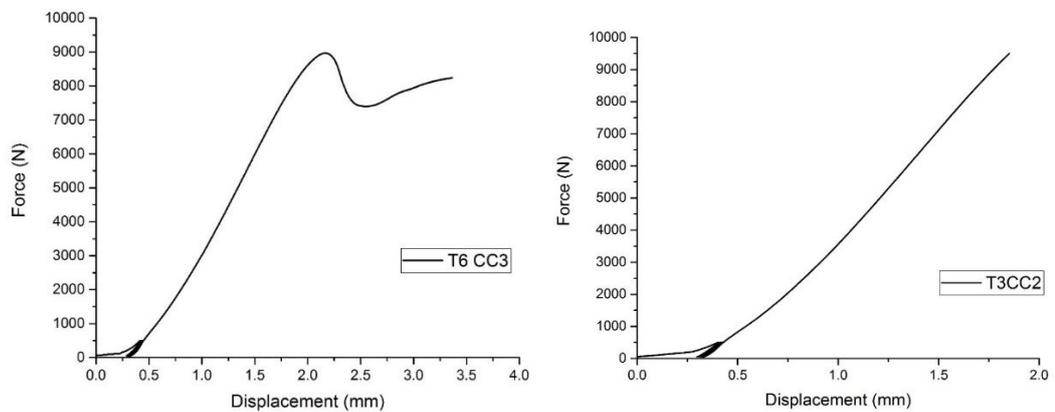
Figure 4-2 A), Load-displacement behaviour representative of the vertebrae that failed before maximum load was reached, B) Vertebra that did not fail before the maximum load was reached, displaying only linear-elastic behaviour
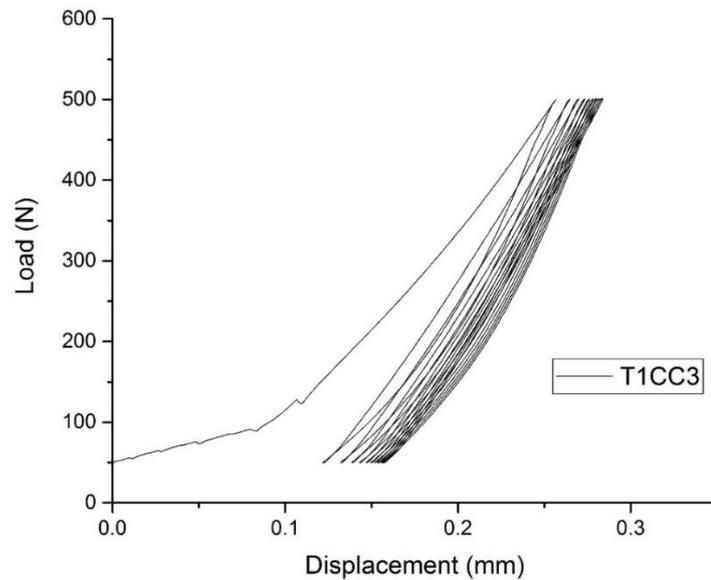
Figure 4-3, Load-displacement data from the pre-cycling period of a single vertebrae, T1 CC3, showing the hysteresis decreasing over 15 cycles.

To investigate the relationship between the elastic stiffness and yield load, the two variables were calculated for each vertebra from the load-displacement graphs, using the methods described in Chapter 3, Section 3.2.6. A second set of data from additional vertebrae tested statically to failure for use in fatigue tests and vertebroplasty testing was also included in this analysis. This brought the total number of vertebrae available to be analysed to 41.

The yield load for specimens that did not show clear yield behaviour was set at 9.5kN, nine vertebrae in total, because in all cases where this occurred, some non-linear behaviour was seen as the load reached 9.5kN. The average stiffness, yield stress, yield strain and yield load values are presented in Table 4-2, with standard deviation and standard error of the mean for all vertebrae tested in this study. An additional parameter, yield stress, was calculated by determining an average value for cross-sectional areas by dividing vertebra volume by vertebra height, both determined using measurement tools in image reconstruction software (ScanIP, V.7, Simpleware, Exeter, UK).

Table 4-2, Mean and Standard Deviation for all vertebrae tested statically to yield or 9.5 kN.

Parameter	Mean	Standard Deviation	Standard Error of Mean
Stiffness (N/mm)	5489	±955	146
Yield Strain	0.0386	±0.0079	0.0012
Yield Load (N)	8658	±1051	160
Yield Stress (MPa)	14.4	±2.0	0.3

Moderate correlation was seen between stiffness and yield load, shown in Figure 4-4, and between stiffness and yield strain Figure 4-5, suggesting in general stiffer specimens have greater strength. However little correlation was seen between approximate yield stress and yield strain, and a similar level of variation was seen in both parameters, shown in Figure 4-6. It would be expected that from the results shown in Figure 4-4 and Figure 4-5 that a greater yield stress would correlate to a lower yield strain, however this was not the case. This is because in this case there is no correlation between yield stress and yield load, suggesting that the vertebrae volume and height, used to calculate stress, do not affect specimen strength in the same way stiffness, or density, do.

One outlier was identified, T10CC3, which exhibited a much lower yield load than the other vertebrae, however its yield strain was close to average and the stiffness was within the range of the other specimens. There was no evidence from the scan data as to why this specimen should differ, as the geometry and greyscale distribution were also within the range of the other vertebrae.
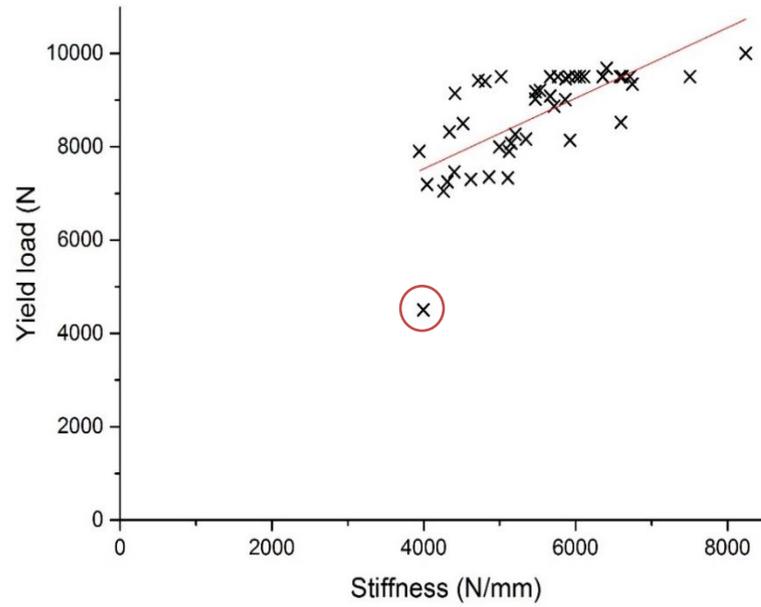
Figure 4-4, Yield load against stiffness for all vertebrae tested statically under axial load, including the group used for fatigue testing. One outlier, specimen T10CC3, is circled in red. Moderate correlation is seen, $R^2 = 0.68$.
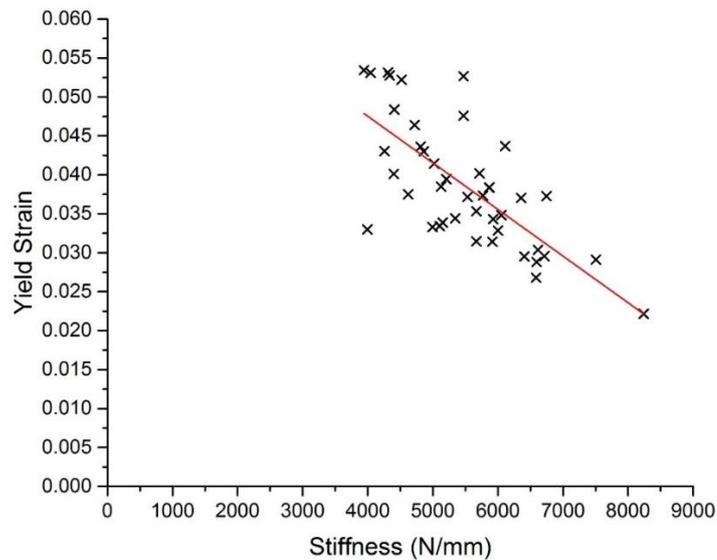
Figure 4-5 Stiffness against yield strain for all vertebrae tested under static axial load to failure or 9.5kN. Correlation between stiffness was $R^2 = 0.51$.
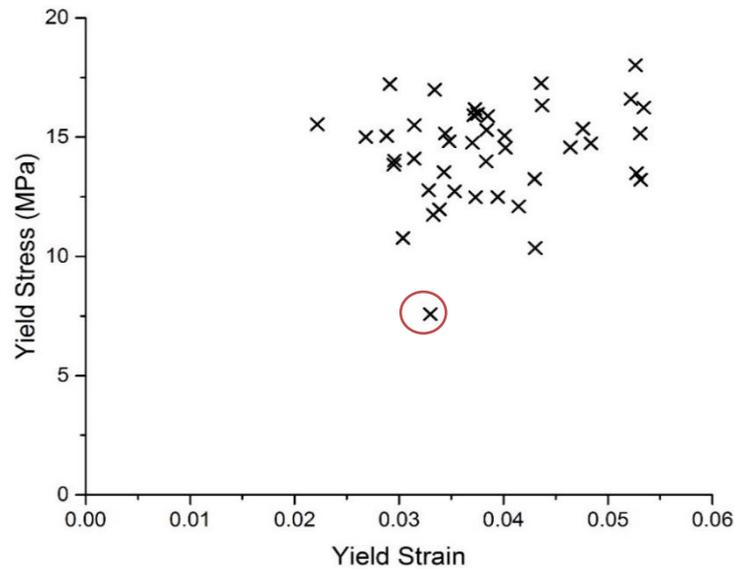
Figure 4-6, Yield strain against yield stress for all specimens tested under static axial load to failure. Outlier circled in red, specimen T10CC3. No correlation was seen between yield strain and yield stress.

The average greyscale within each vertebral specimen was calculated, as described in Chapter 3, Section 3.2.4. Briefly, image data from the microCT scanner consists of density information described by Houndsfield unit values for each image voxel. This was then converted to greyscale values in the range 0-255 to describe the density variation within the image. When the bone mask was segmented away from the background, the greyscale values for the bone only could then be determined and assessed using the image reconstruction software. This gave data for the distribution of greyscale values in the bone as well as the average greyscale value, which is directly related to the average bone density.

The relationship between average greyscale of the vertebrae and the stiffness from the load displacement data was assessed to determine whether specimen density was correlated to stiffness, and therefore strength, Figure 4-7. For this relationship $R^2=0.35$, suggesting there is not a strong correlation; however, a number of outliers can be identified, such as the specimen with the greatest stiffness and the two vertebrae with considerably lower stiffness values than the rest of the group. Although it was expected that a stronger correlation

between greyscale and stiffness would be found if the three identified outliers were to be removed, their values were left in the analysis because it is not clear why these specimens differ, therefore they cannot be reasonably discounted. Average greyscale is calculated from the greyscale values of the voxels in the down-sampled bone mask, so this value accounts for the average values of both the mineral content in the bone and the amount of bone volume compared to total volume. In the case of the outlier, the stiffness was low for the greyscale average of that specimen. The greyscale value may be high compared to the stiffness due to details of the trabecular architecture that are not captured in the down-sampled models that affect the experimental stiffness, such as trabecular architecture, anisotropy and mineral content.
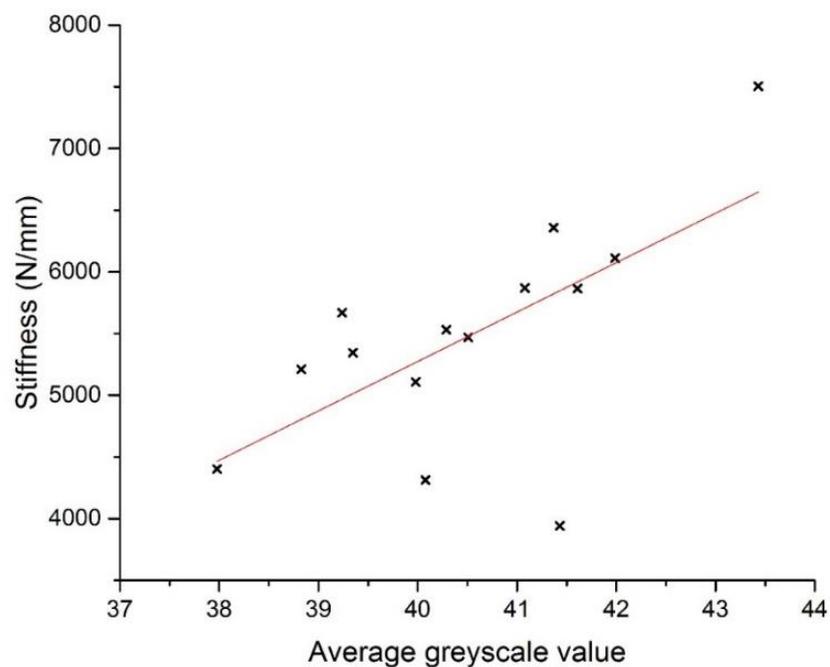
Figure 4-7 Correlation between average greyscale of the vertebrae determined from microCT data of intact vertebrae, and stiffness determined from load to failure data. $R^2 = 0.35$.

4.2.1. Image Analysis

MicroCT scans of the specimens were taken throughout the testing process, before and after the static test and after the fatigue test. These were then reconstructed into 3D images and

assessed qualitatively to look for visible signs of trabecular damage. Details of the scanning methods are described in Chapter 3, Section 3.2.4. Examples of the images acquired from the scan reconstruction from an intact vertebra are shown in Figure 4-8, showing both sagittal and transverse sections which highlight the change in cross-section through the specimen, as well as three-dimensional view. This figure provides examples of the scan cross-sections used for the results that will follow throughout the rest of the current chapter, highlighting the general area within the vertebral body where individual 2D images are taken from for comparison.
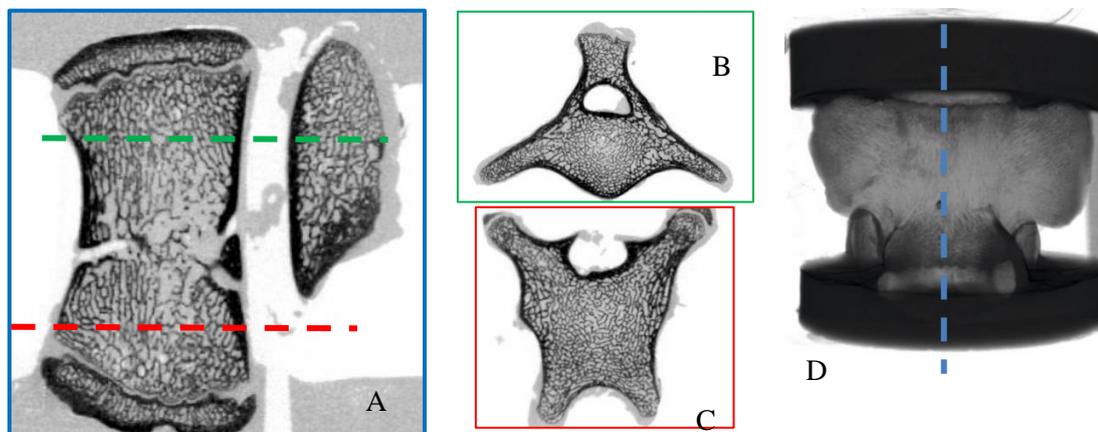
Figure 4-8, Example scan data from an intact vertebra, with image border colour corresponding with the dashed line showing where the image slice is taken from. Showing A) a sagittal view, B) superior transverse view, C) inferior transverse view and D) anterior view of a 3D reconstruction.

A series of scans from the initial ten vertebrae before and after the static test to failure onset are depicted in Table 4-3. Tiff image data has been colour inverted for clarity, so where usually CT scans denser areas of material appear brighter, here denser areas are darker and less dense areas appear bright. A cross section through the sagittal plane was taken for the comparisons. Where fractures were visible from the 3D reconstruction, images were taken from this plane, however where no fractures were seen an approximate mid-section was taken. In general, little observable difference was seen between the pre-test and post-test scans at this resolution. Fracture lines appear as areas of no density, or grey value, i.e. 'empty' lines in the structure, and are indicated by red arrows on the microCT scan images.

In the 3D reconstructed image the fractures appear to spread across the entire vertebral body on the transverse plane, however do not tend to spread in the superior-inferior direction. From the initial set of ten vertebrae, three were seen with fractures after the test, one of which was apparent prior to loading (T7 CC3). When assessed in 3D, fractures were noticed to span the entire transverse cross section of the vertebrae. Voids could be seen in the central region of a number of the vertebrae, these were lower density than the surrounding trabeculae and are likely to contain bone marrow. Very bright areas with no apparent density are vascular channels, of which anatomically there is one through the anterior wall and one through the posterior wall into the spinal canal space. No cracks appeared to propagate out from either vascular channels or trabecular voids. Determining whether fractures occur at this stage of testing was important for later fatigue analysis.

Table 4-3, MicroCT scans of each vertebrae specimen before and after static axial test to failure. Images are cross sections taken through the sagittal plane at an approximate mid-section or where fractures are seen. Fractures are indicated by red arrows.

Specimen	Initial Scan	After Static Test
T1 CC2		
T1 CC3		

T3 CC1		
T3 CC2		
T5 CC3		
T5 CC4		
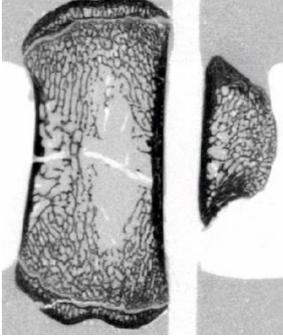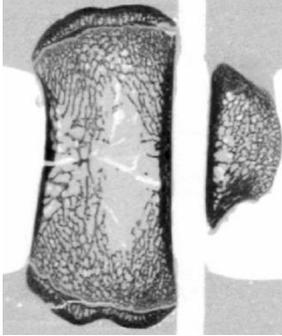
T6 CC1		
T6 CC3		
T7 CC2		
T7 CC3		
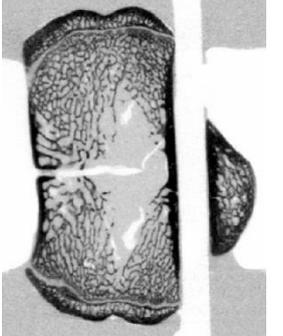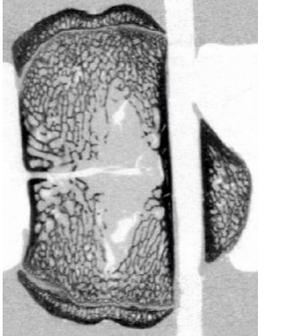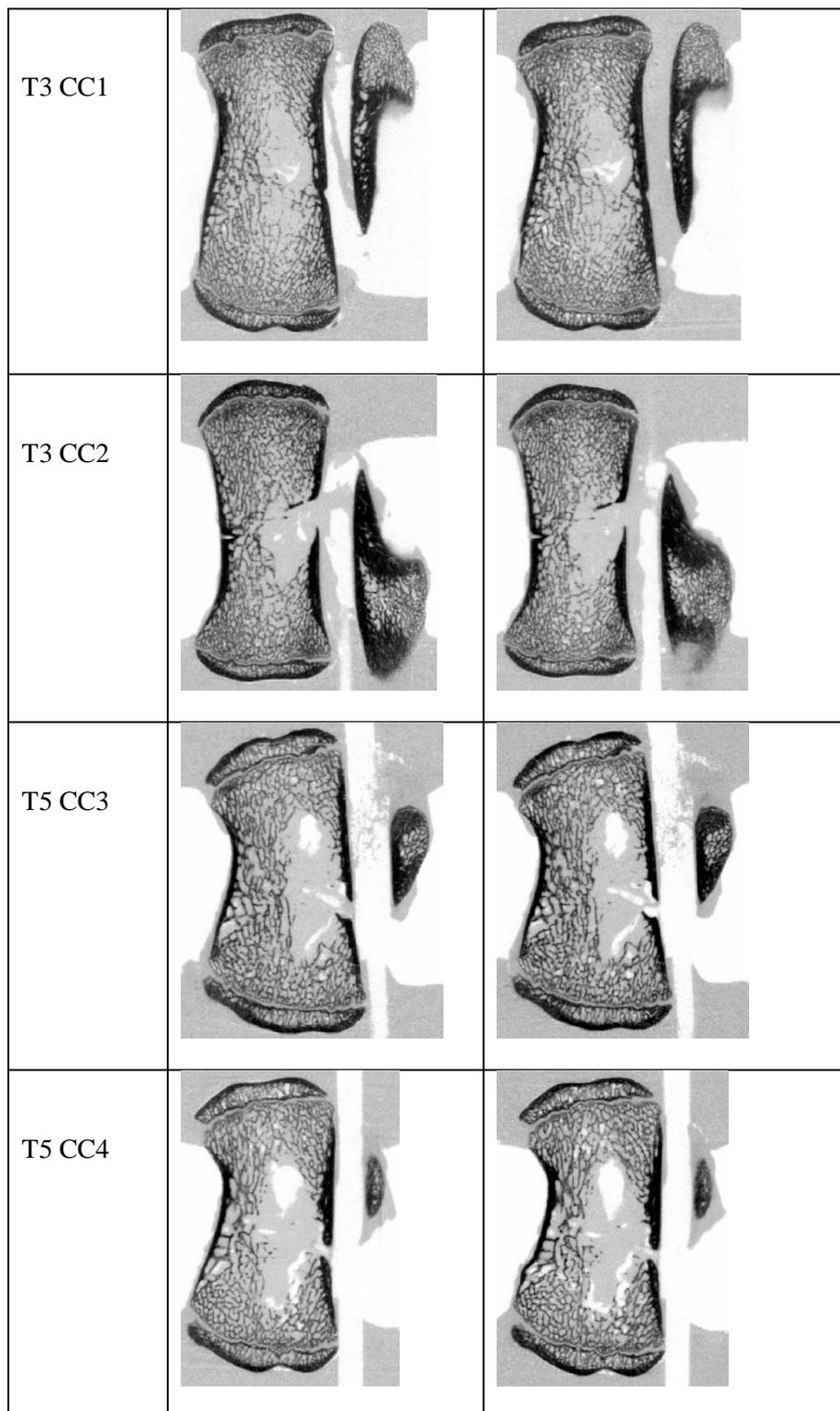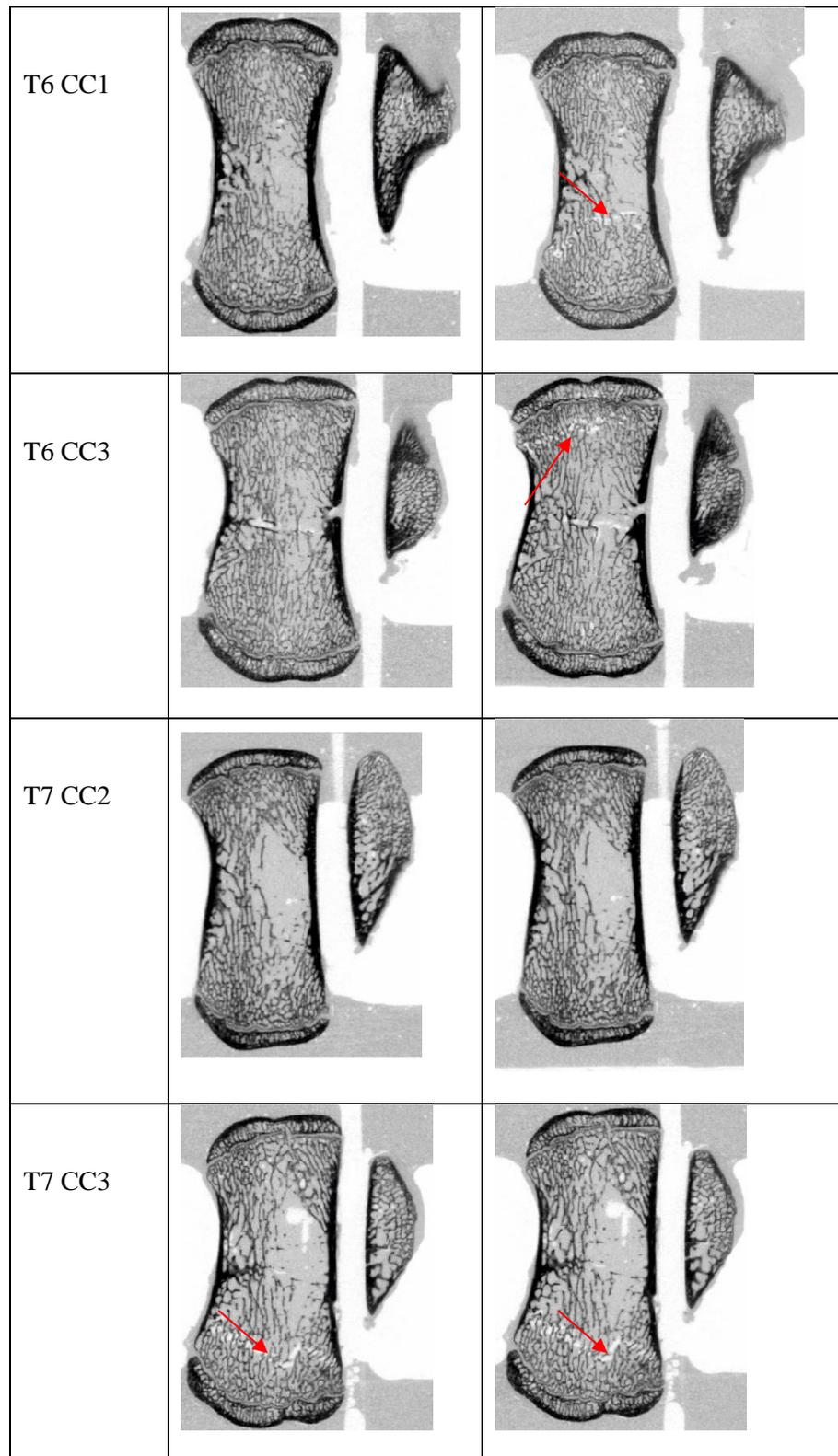
4.3. Fatigue Testing

Fatigue testing methods are described in Chapter 3, and the following section shows the results from fatigue testing vertebra after an initial static test to failure onset. Vertebrae were tested in load groups of 60, 70, 80 and 90% of the initial yield load and tested to failure or 10000 cycles.

Firstly, the incremental displacement over the number of cycles in the test for all specimens tested is shown in Figure 4-9 A-D. For each specimen, the maximum and minimum displacement during each cycle is shown. That is, the cross-head displacement at the peak load and minimum load during each cycle. These graphs highlight the variation between these vertebrae with respect to their response to cyclic loading, even within load groups. From this data the number of cycles to failure was calculated, as described in Chapter 3, Section 3.2.6.2. These results are depicted in Figure 4-10, which shows a general trend of a higher normalised load resulting in fewer cycles to failure. Cycles to failure for each load group are shown in Figure 14, with box plots depicting median, 25th and 75th percentile and range to show the spread of the data. A significant difference was seen in the 60% load group ($p<0.05$) compared to all other groups, however no significant differences were seen between the remaining groups.
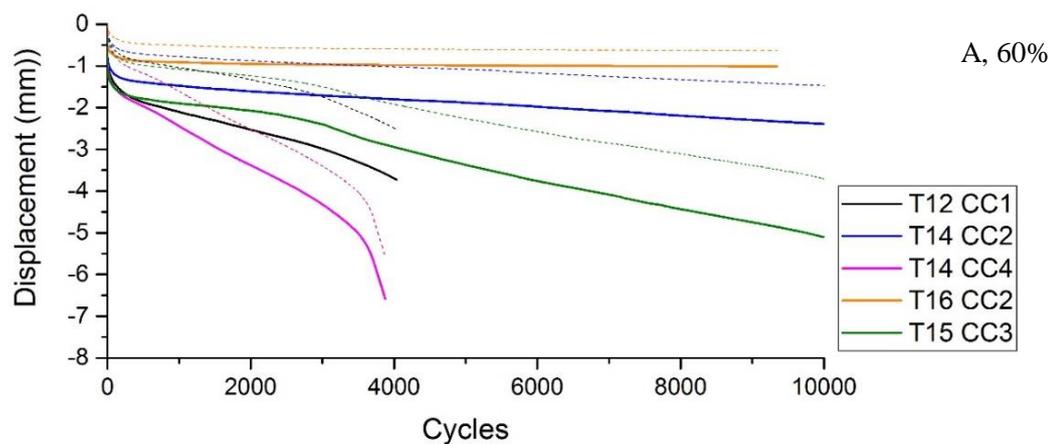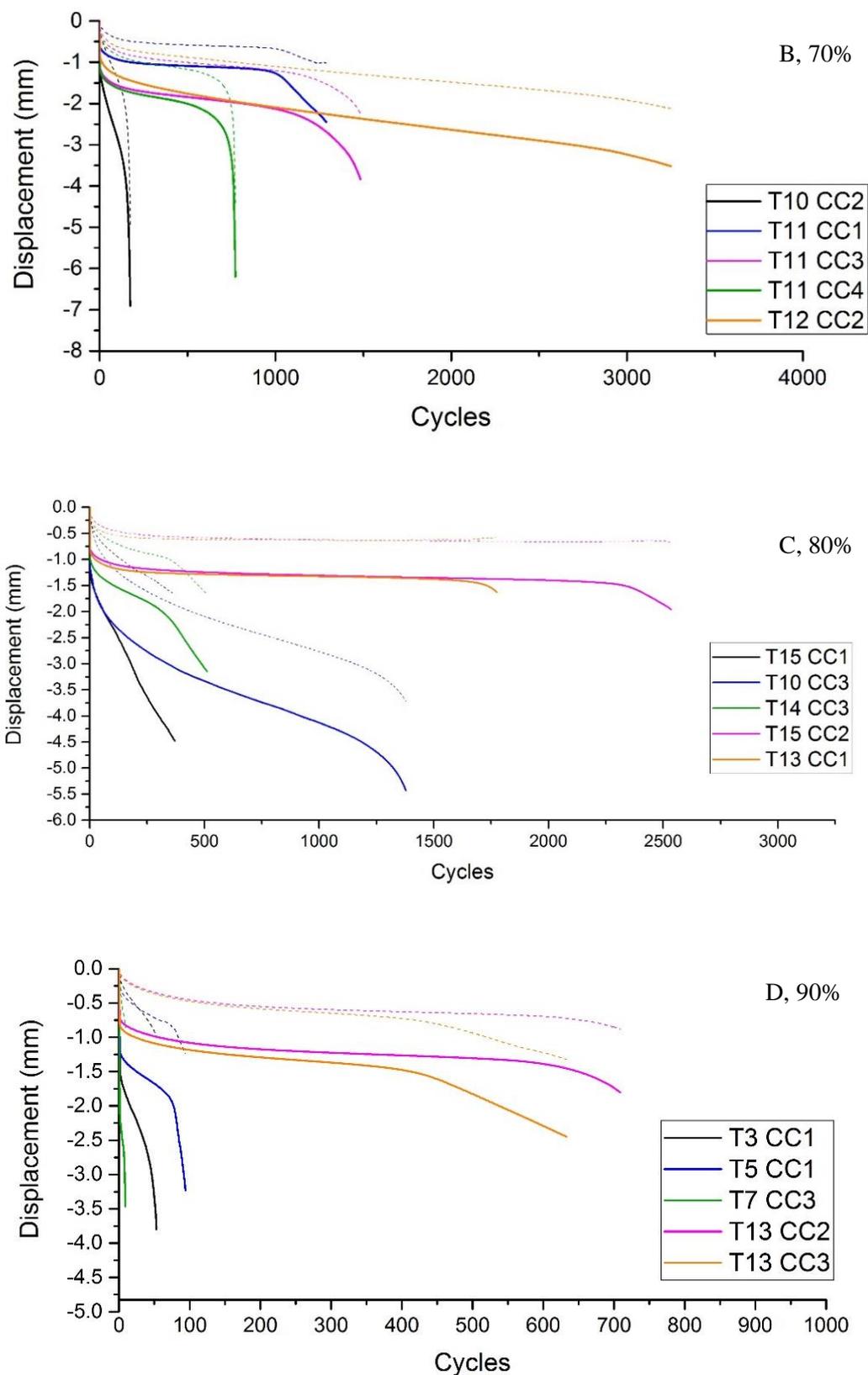
Figure 4-9 Displacement against number of cycles for A) 60%, B) 70%, C) 80% and D) 90% load groups. Solid lines depict maximum displacement and dashed lines depict minimum displacement.
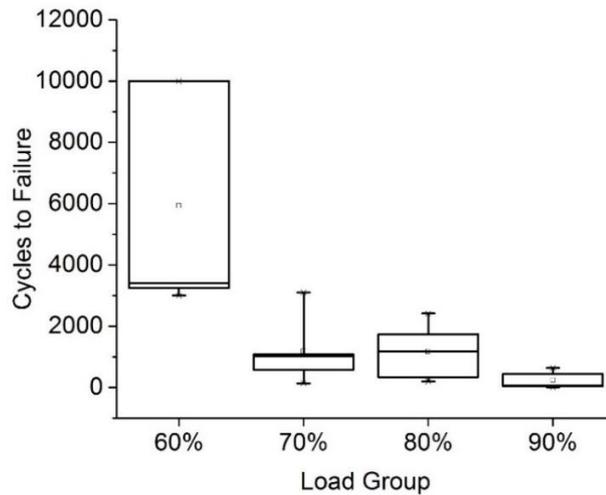
Figure 4-10, Cycles to failure for each load group tested – where peak load during dynamic testing is 60%-90% of the initial yield load of the vertebrae. Box plots show median, 25th & 75th percentile and range.

Little correlation was seen between the actual applied peak load (rather than the load group) and cycles to failure, suggesting normalising against the initial load to failure was an effective way of accounting for some of the variation seen between these biological specimens, Figure 4-11.
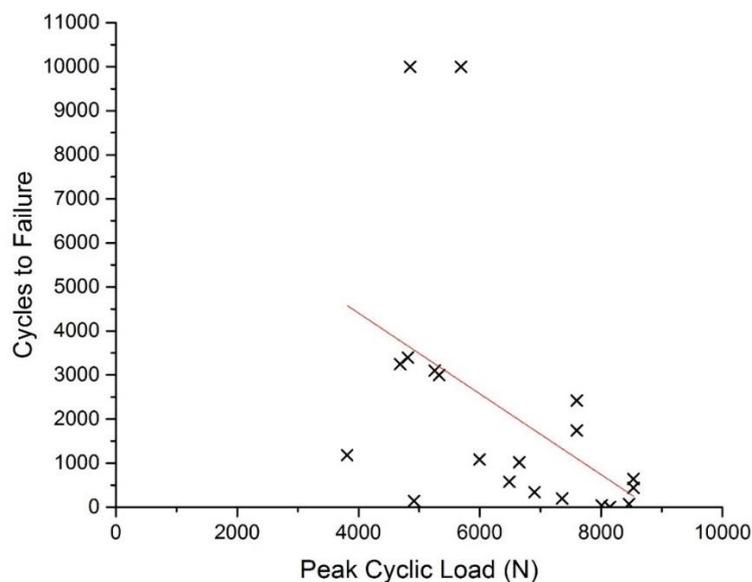
Figure 4-11, The relationship between the number of cycles to failure for each specimen and the actual peak applied load (which was calculated depending on the load group and the initial specimen strength). Poor agreement was observed

Stiffness for each cycle in each test was calculated using methods described in Chapter 3, Section 3.5, whereby a custom Python script was used to calculate each stiffness value and plot these against cycle number. Varying degrees and severity of stiffness reduction were seen as a result of failure across all four load groups. From the vertebrae that did not fail before 10000 cycles, one was seen to have a much greater stiffness than the others in the group, and increased slightly in stiffness over the course of the test, and one showed a gradual decrease in stiffness across the entire test (Figure 4-12A, vertebrae T16CC2 and T14CC2 respectively).
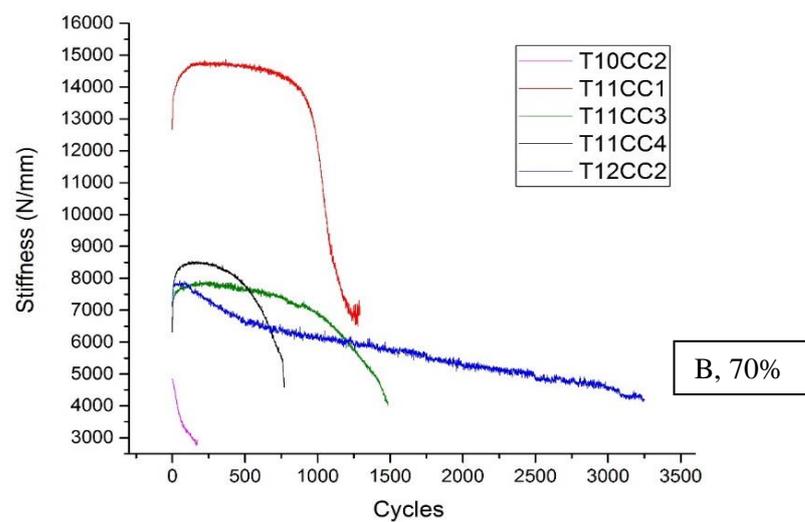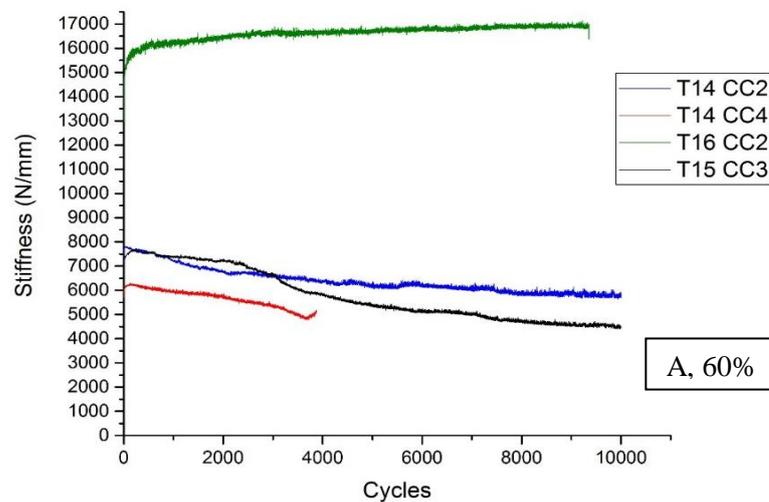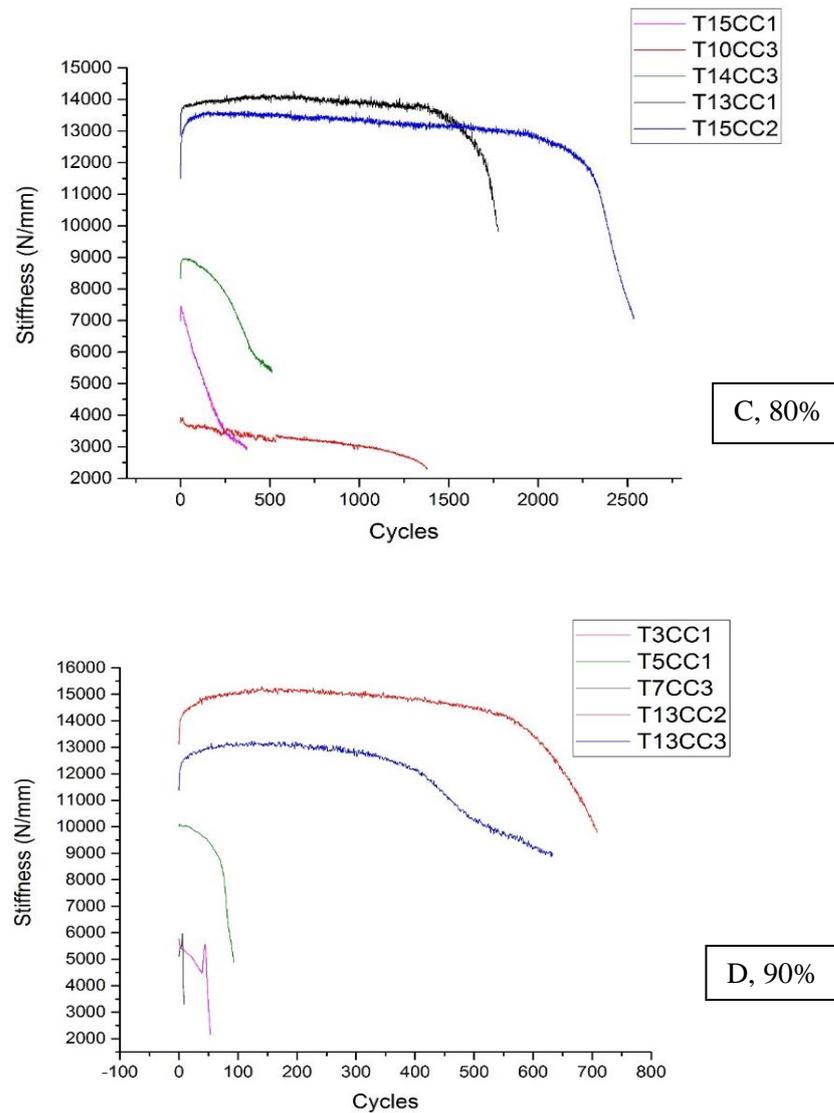
Figure 4-12, Stiffness change over the test, calculated over central third of the loading ramp of each cycle for the A) 60%, B) 70%, C) 80% and D) 90% load groups.

The change in elastic stiffness between the beginning of the test (cycle 10) and the end of the test is shown in Figure 4-13. The 70%, 80% & 90% load groups had a significant reduction in stiffness ($p<0.05$) as a results of the dynamic loading, although the 60% group did show a 34% reduction between means, the result was not significant due to the large standard deviation in the final cycle stiffness. This was due to the fact that two specimens did not fail before 10000 cycles.
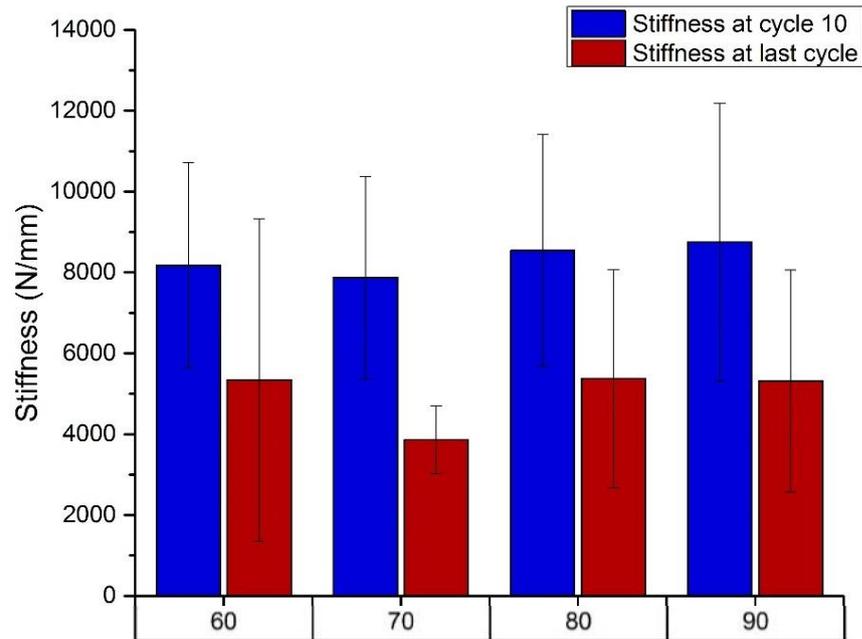
Figure 4-13, Reduction in stiffness for each load group, comparing average elastic stiffness for each group before and after cyclic testing.

Image data from all specimens testing under fatigue loading conditions is shown in Table 4-4, with load group stated next to specimen name. For comparison, images from after the static test (immediately before the fatigue test), are also shown. Fractures are seen in specimens from all four load groups, and severe fractures with relatively large displacement of parts of the vertebra wall were seen in 60, 70 and 80% load groups. Fractures were seen in both the anterior and posterior walls of the vertebrae, and were both inferiorly and superiorly located but not centrally. Severity of the fracture, determined qualitatively by assessing how much of the vertebral shell was displaced, or whether fracture was only seen in the trabeculae, did not appear to correlate with number of cycles or reduction in stiffness. This data will be used in following chapters as a direct comparison to finite element model data.

Table 4-4, Comparison of vertebrae fatigue tested after fatigue testing for each of the four load groups. Fractures are indicated with arrows.

Specimen	After Static Test	After Fatigue Test
T7 CC3 90%		
T13 CC2 90%		
T15 CC1 80 %		
T10 CC3 80%		
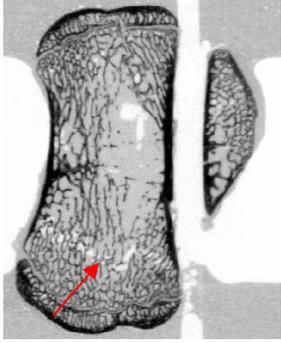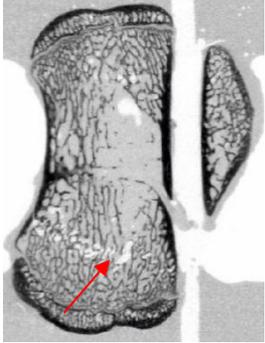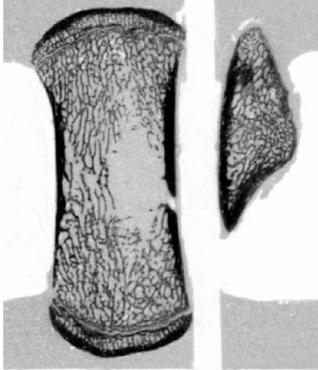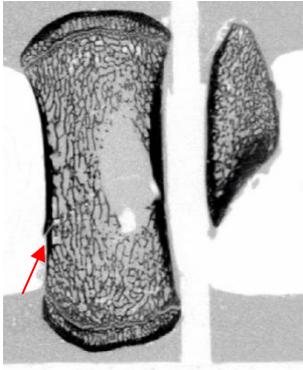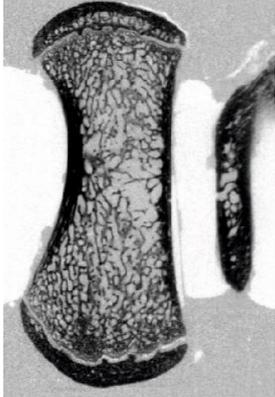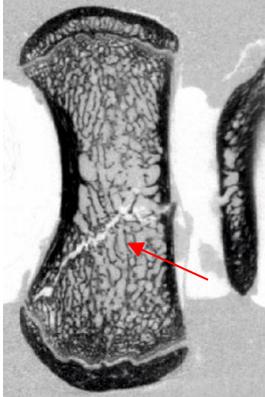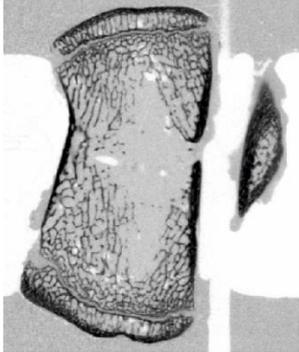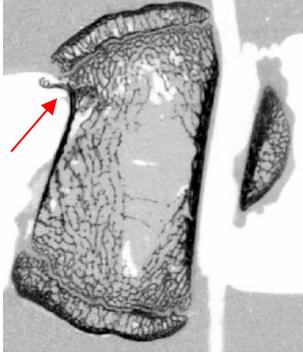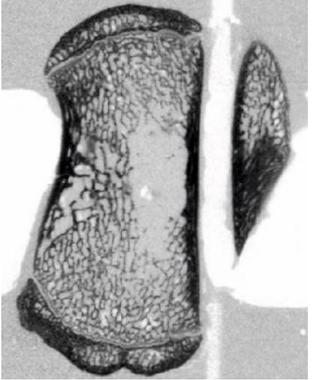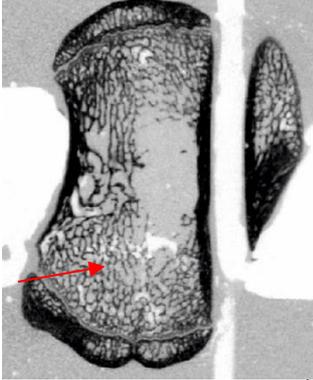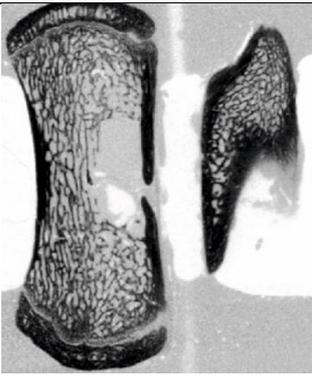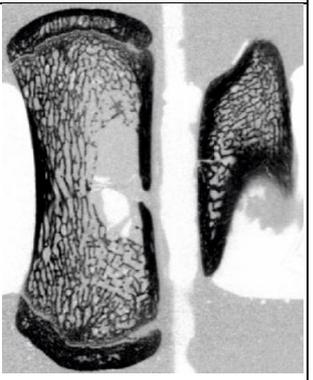
T14 CC3 80%		
T13 CC1 80%		
T15 CC2 80%		
T10 CC2 70%		
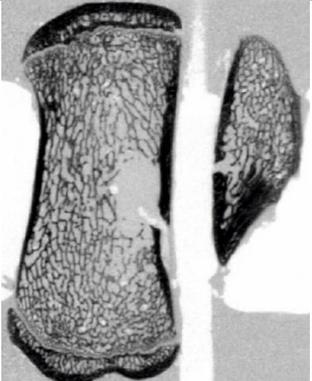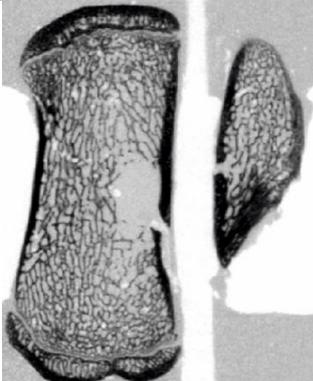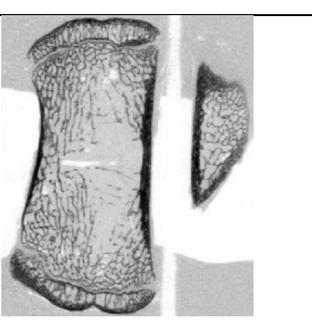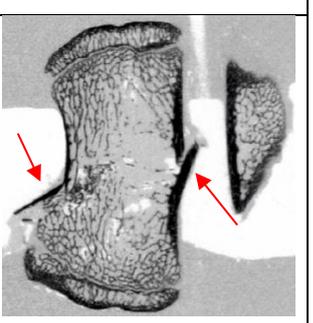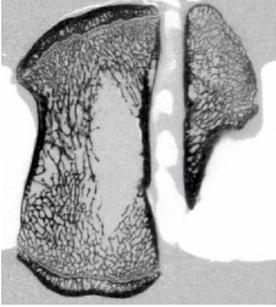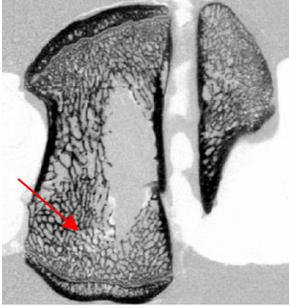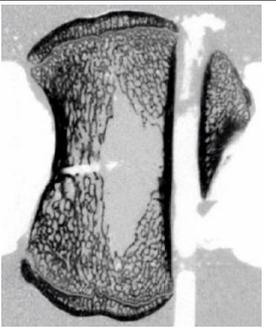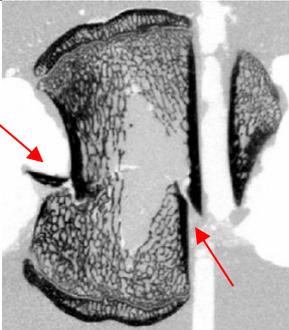
T11 CC3 70%		
T11 CC4 70%		
T12 CC2 70%		
T12 CC1 60%		
T14 CC4 60%		
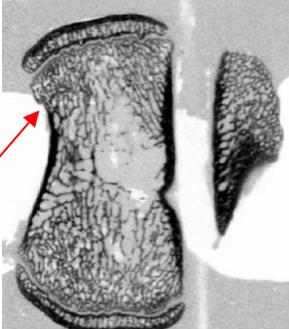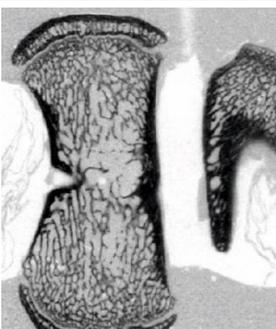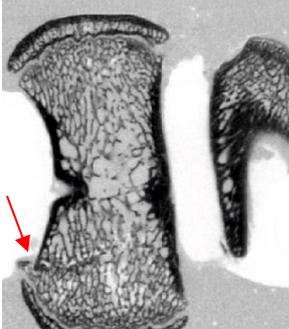
| T16 CC2 60% | | |
| T15 CC3 60% | | |
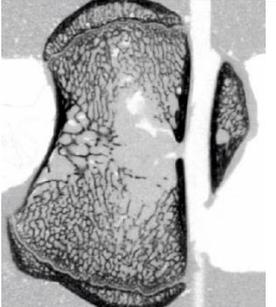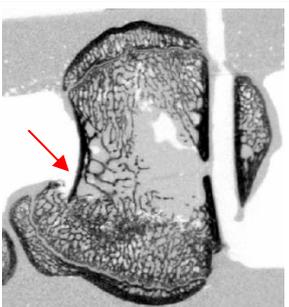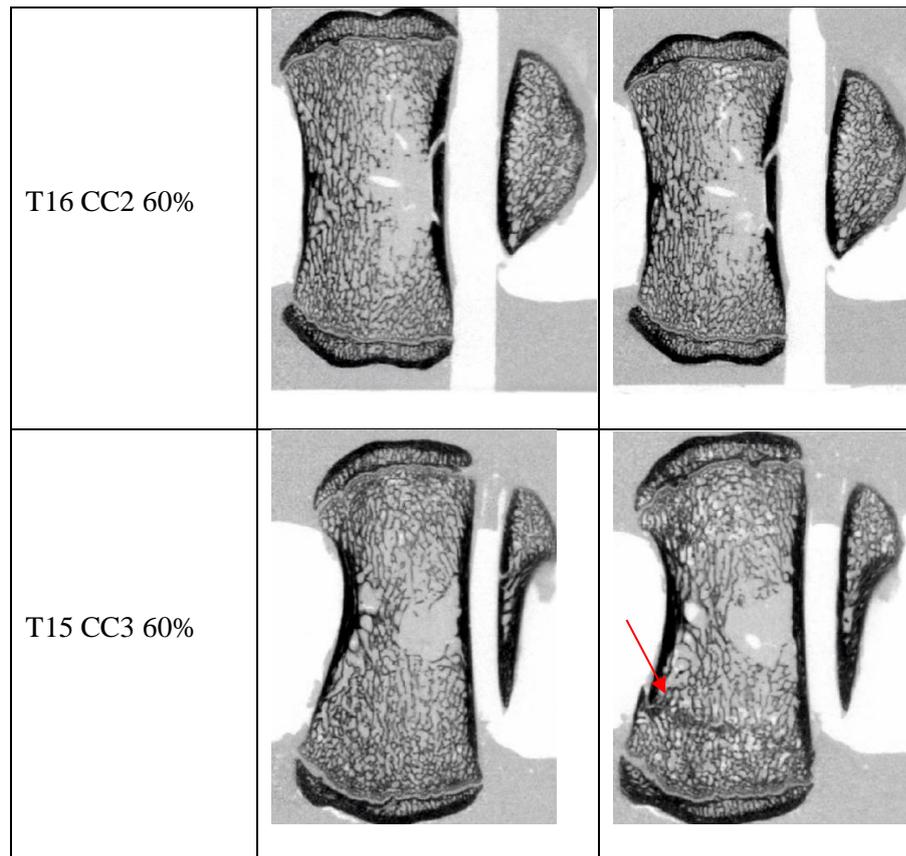
4.4. Creep tests

A creep test was performed on two specimens under high load (80% of the initial yield load, approximately 7kN for both specimens) as described in Chapter 3, to assess if any of the displacement seen over the course of the fatigue tests could be attributed to creep behaviour of the trabecular bone rather than the cyclic loading. The displacement behaviour over the course of the test for each of the two vertebrae used is shown in Figure 4-14. The rate of change of strain was seen to be low after the initial toe region following load application. Both vertebrae displayed similar results, with strain reaching a plateau after around 300 seconds. Displacement change is less than 0.2 mm from the point after the toe region in both cases. Displacement in the fatigue testing ranged largely, however in the majority of cases was greater than 0.5 mm, and was much greater in cases where failure behaviour was seen. It can therefore be assumed the creep contributions are minimal in these tests.
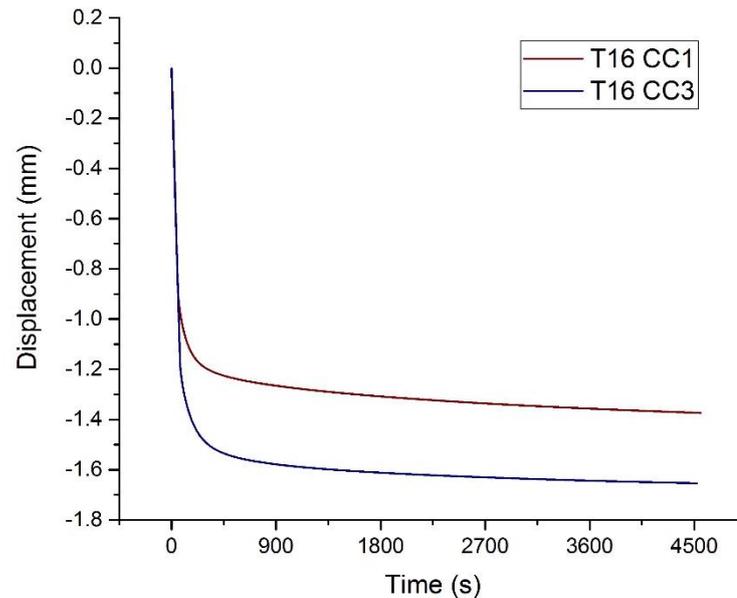
Figure 4-14, Displacement against time for two vertebrae held under constant high load for 4500 seconds.

4.5.Discussion and Conclusions

4.5.1. Static testing

Static testing to 9.5kN was able to initiate damage to the specimen, seen as non-linearity in the load-displacement data, however fractures were not consistently observed utilising this method. This means there are measurable mechanical changes in the vertebrae that can now be assessed through the course of testing, and future vertebroplasty, however the model can still be improved as ideally fracture would always be caused at this stage. Initial elastic stiffness of the vertebrae was seen to correlate with yield load, which agrees with literature data showing density can be used as predictor of fracture (Brinckmann et al., 1989; Cheng et al., 1997).

4.5.2. Fatigue Testing

The purpose of the fatigue testing was to characterise the behaviour of vertebrae under cyclic loading and understand which parameters play the greatest role in determining this behaviour. Additionally, this data was used to provide information with which to validate

specimen-specific finite element models (reported in subsequent chapters), providing a framework with which the effect of interventions on the fatigue performance of a vertebra could be assessed. Limitations of the fatigue testing methods and vertebroplasty procedure are discussed.

In engineering materials, fatigue performance of a material is typically investigated by creating identical specimens and cyclically loading them under varying loads to record the number of cycles taken to failure under a range of stresses. This data is usually presented in the form of an S-N curve (i.e. applied stress versus number of cycles to failure). Due to the variation seen in the biological specimens used in the current study and the time consuming nature of specimen preparation, testing was done by splitting specimens into different groups and determining the peak load from the initial yield load to take into account some variation in initial strength. Therefore results were presented in the form of number of cycles to failure for each load group. This does not give a true indication of the engineering fatigue, rather a range of results to be expected at different load values. Change in mechanical stiffness was evaluated as an indication of damage, in addition to rapid change in displacement. However there was no immediate correlation between stiffness change, number of cycles to failure and qualitative assessment of damage. This indicates that more factors affect fatigue behaviour than either one of these parameters, such as pre-damage that is not identifiable from 82µm microCT scans, or characteristics of the trabecular architecture such as degree of anisotropy, or level of hydration of the tissue. Additionally, if the trabeculae buckle rather than actually fracture right through, then this would cause a drop-off in the load-displacement graph but when the load is released, the trabeculae might un-buckle, so there would not be an observable damage on the CT. Larger specimen numbers in load groups may highlight further differences in behaviour under different loads that could not be identified here due to variation. Additionally, knowing what, if anything, can be predictive/indicative of fatigue behaviour is extremely useful as it can be ensured that it is incorporated into specimen specific models.

Very high loads were used for the fatigue tests as a way of exaggerating the response to ensure differences could be seen before and after testing. This was necessary as even at high loads, in a number of cases, no damage was visible and no stiffness reduction seen as a result of the high specimen strength. Whilst low load tests may be deemed more physiologically relevant, they are required to be run for a much longer period if damage is to be seen, this is often not practical with biological tissue testing. Also these tests needed to be able to be replicated in finite element models, so fewer cycles and more identifiable changes were preferable.

Whilst the loads used are high, and not fully representative of *in vivo* conditions, one-off occurrences of such high loads may occur during lifting of heavy objects or trips and falls, and the testing developed here is still useful as a laboratory test. These methodologies can be used to differentiate between treatments.

The literature reviewed in Chapter 2, Sections 2.2.1 the viscoelasticity of vertebral bone is discussed and the ability to recover from compressive loading. Additionally in Section 2.5 the strength of large animal vertebrae is considered. These factors, along with the high compressive strength, both contributed to the hypothesis that the specimens could withstand high load fatigue testing. During testing, it was observed that even in the most severely disrupted structures, the vertebrae remained complete, suggesting that compaction of the trabecular bone held the vertebra together, allowing it to withstand compressive load even in this state.

MicroCT scan data

It was difficult to recognise damage of the trabecular structure after the static tests, however fracture was seen to varying extents after fatigue testing. The majority of fractures were located inferiorly and superiorly in the vertebral body rather than in the centre, even though this is the area of lowest bone density. It may be the case that the constraints on the bone by the cement loading plates cause a stress riser to occur in these areas, and this dictates the

location of damage. This is an artefact of the testing set-up, and is difficult to avoid as the specimens need to be held in place reasonably well due to the high loads used, and the cement plate allows for this, and need a flat loading platen.

4.5.3. Creep Tests

It was shown that under the current test conditions no creep behaviour was evident in two bovine vertebrae. This is in agreement with Moore et al. (Moore et al., 2004), and whilst other studies claim creep is a contributing factor to the mechanical behaviour of vertebrae this tends to be seen where there are still soft tissues surrounding the vertebra. This is likely to be the cause of the identified creep behaviour, particularly in cases where the intervertebral disc is also included in the test (Moore et al., 2004; Pollintine et al., 2009; Rimnac et al., 1993). It seems likely that viscoelastic effects are seen only during the first few cycles as was seen in the static tests, and that long-term creep does not have an effect on the measured fatigue performance.

This chapter presented the initial static testing and fatigue results. Some failure was seen in specimens during static test, although not always as a discernible fracture, however generally the loading was enough to cause some damage, as seen on force-displacement graphs. Fatigue results showed variability due to the variable specimens, although using proportional load appeared successful in limiting some of this variance. Further examination will now be undertaken using FEA, shown in the following chapters.

5. Computational Methods

5.1. Introduction

This chapter describes the methods used to create and validate *in silico* simulations of the vertebrae tested under static and fatigue loading conditions, as described in Chapters 3 and 4. As discussed in Chapter 2, there are two possible approaches taken to model bone from microCT image data using finite element methods, continuum level and trabecular level models. Trabecular level models are created using an element size small enough to capture details in the trabecular architecture of the bone, whereas to create continuum models, scan images are resampled at a lower resolution, averaging greyscale values across larger sized voxels, and have a courser mesh when modelling with a direct voxel-to-mesh size relationship. For this study, continuum level models were used due to the limitation that trabecular level models require far greater computational power and time, and previous studies within the research group have shown excellent agreement with experimental data using continuum level models (Wijayathunga et al., 2008; Zapata-Cornelio et al., 2017). Therefore this chapter will cover the conversion of microCT data into specimen-specific continuum level final element models and the methods used to simulate and validate a static loading case and a fatigue loading case. The optimisation of Young's modulus and yield strain using experimental data collected in Chapter 4 is covered. The fatigue methodologies include the use of material property reduction parameters to modify the material properties on an iterative basis to represent cyclic loading. Discussion of the development of the script used to implement these changes is also covered.

5.2. Image Reconstruction and Segmentation

This section covers the process of creating finite element models from microCT images taken of intact vertebrae and of vertebrae after the static test to failure. As discussed in Chapter 3, image files from the microCT scanner were converted into stacks of 'tiff' file images with greyscale values ranging between 0-255, with each image representing a 0.82μm transverse slice through the vertebra. These stacks of images were then reconstructed into three dimensional (3D) models using 3D image processing software (ScanIP Version 7.0, Simpleware, Exeter UK). In the models used in this study, the coordinate system was defined with the z axis in the superior-inferior direction, the x axis in the medial-lateral direction and the y axis in the anterior-posterior direction.

Firstly, models were aligned to account for any misalignment that occurred in the scanner, ensuring the cement plates were parallel to the x-axis so any axial force would be applied through the central axis of the specimen. The reconstructed images were then down-sampled from the 82μm native resolution of the scan to a $1mm^3$ voxel size using a partial volume effect averaging method, whereby the greyscale values of all original voxels that are within the new voxel are averaged with an appropriate weighting for any that are only partially within the new voxel. An example of the resampling process in shown in Figure 5-1, where a single slice from an ovine vertebrae has been resampled from an 82μm to a $1mm^3$ voxel size. It can be seen that this method allows for the geometry of the vertebrae to be kept, as well as maintaining information about the density of regions of bone. Images were down-sampled to a $1mm^3$ resolution as this was the resolution used for the finite element mesh, and a 1:1 voxel to mesh conversion included in the imaging software was used. This resolution has been shown to be sufficient for predicting the response of vertebrae under compressive load. Since models are more sensitive to other factors, such as load position, an increase in mesh resolution does not reduce errors sufficiently to justify the extra computational expense (Wijayathunga et al., 2008; Tarsuslugil et al., 2014).
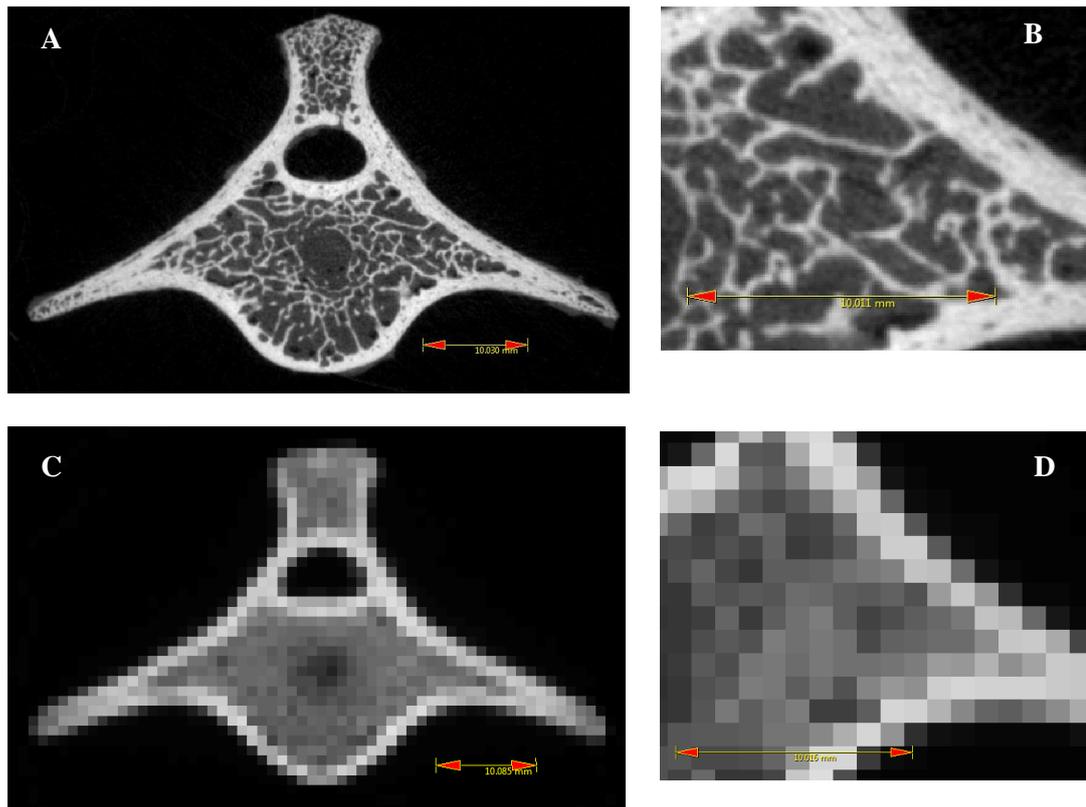
Figure 5-1, Example MicroCT image data of a bovine vertebrae showing A) 82µm scan resolution from CT scanner, B) The same scan down-sampled to 1mm3 voxel size, C) Trabecular detail visible in original scan, and D) The same volume resampled with average greyscale values shown. All dimension bars are approximately 10mm.

Following re-sampling, a threshold operation was used to segment the bone, with separate masks given to each cement plate and the vertebral bone (see Figure 5-2). Bone was thresholded between 18-255, and cement between 8-18 grey values. When creating the masks it was ensured that there were no empty spaces in the mask by manually adding voxels that had not been caught by the mask. The radiopaque load marker was removed from the model at this stage.

A   B
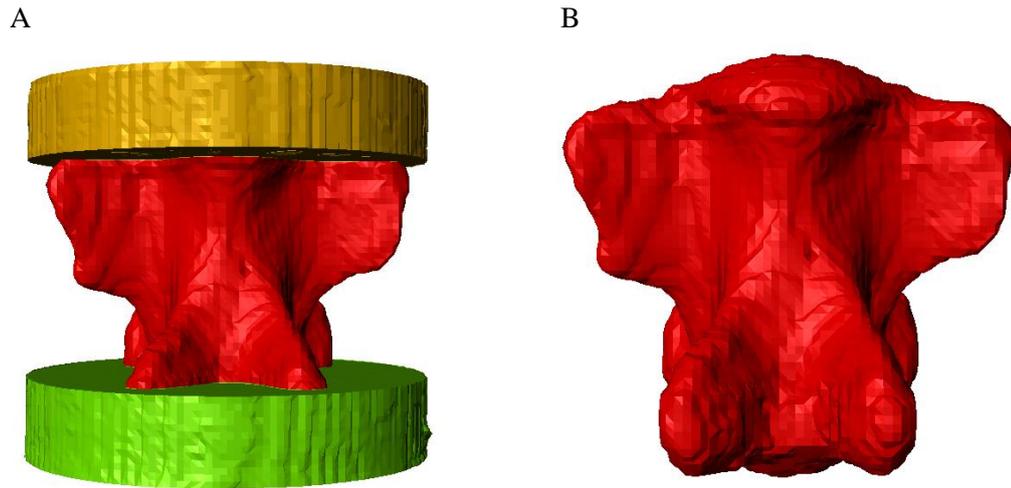
Figure 5-2, A) Thresholded masks of vertebral bone and the upper and lower cement housing, after down-sampling to a 1mm³ voxel size, and B) the vertebral body without the cement housing.

5.3. Finite element model creation

As discussed, the finite element models were generated in the 3D modelling software by approximately converting the voxel resolution of the model to a mesh of linear mixed 4-noded tetrahedral and 8-noded hexahedral elements. A built-in surface smoothing algorithm was used and mesh optimisation was utilised. This resulted in the internal structure of the vertebrae being constructed of a hexahedral mesh whilst allowing for the surface to be made of tetrahedral elements of a closer representation to the original specimen, Figure 5-3.

A   B
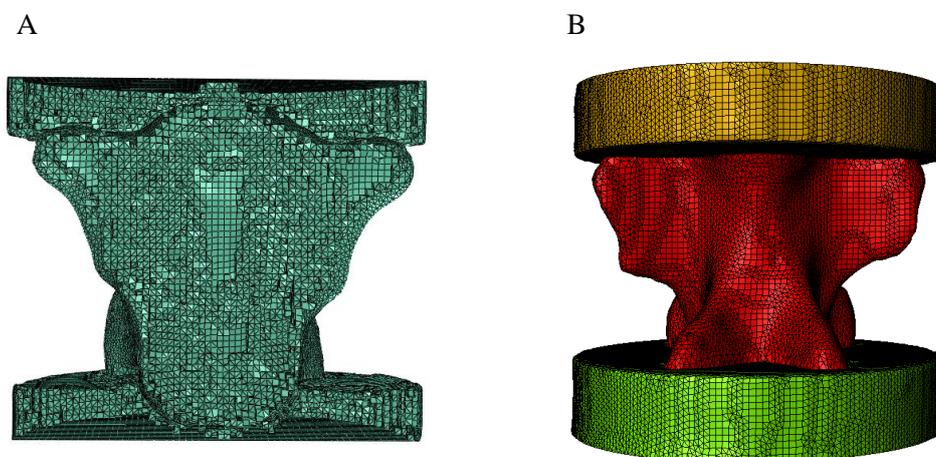
Figure 5-3, Meshed vertebra model, A) showing the internal hexahedral mesh structure and B) Smoothed surface mesh of masked vertebra and cement housing.

5.3.1. Boundary Conditions and Loading

In the 3D modelling software, some features of the finite element model were created, namely the material property assignments and definitions of surfaces and interfaces where there would be a boundary condition, or between which there would be contact. The model was then exported as input files for use in the finite element software used in this work (Abaqus/CAE V.14, Dessault Systemes, France).

In the Abaqus software, an analytically rigid plate was tied to the top surface of the superior cement plate, to evenly distribute the load applied at a specific point and model the steel loading plate in the experiment, as shown in Figure 5-4. The plate was allowed to rotate but not translate in the x-y directions in order to model the load application system used experimentally, where load is applied to the specimen via a steel ball to allow for anterior-posterior and lateral rotation. For the modelling of the static load case, a 1mm displacement was applied to the models at this reference point, as the vertebrae were seen to have a linear-elastic response in this displacement range. The inferior cement plate surface was constrained with an 'encastre' condition, where no rotation or translation is allowed in any direction. The cement plates were attached to the vertebral body via a tie constraint, under the assumption that there is little or no relative motion between the cement plates and vertebral body when under axial load. A reference point node was used to define the location on the analytically rigid plate that the load or displacement would be applied to the model. This location was determined from the microCT scan data by identifying the location coordinates of the radiopaque marker used to apply the load in the experiment using the 3D modelling software.
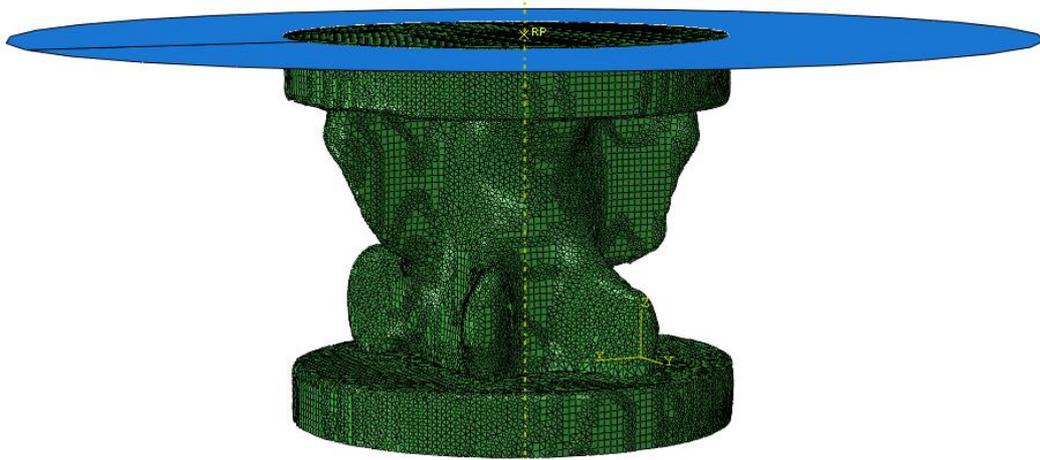
Figure 5-4, Meshed vertebra model in Abaqus with analytical rigid plate and load reference point.

5.3.2. Material Properties

Linear-elastic material properties were used initially to validate the models for the static test case. Material properties for the PMMA cement were found from the literature (Wijayathunga et al., 2008), and were assigned as homogenous material properties with a Young's modulus of 2.45GPa and Poisson's ratio of 0.3. For the vertebral body, different bone material properties were assigned to each element depending on the greyscale, or density, of the underlying down-sampled voxel in order to capture variation within the specimens. To achieve this, a density to Young's modulus conversion constant was derived through an optimisation method. Wijayathunga et al. (Wijayathunga et al., 2008) showed that assuming a linear greyscale-density relationship is as effective as a higher order relationship, therefore this approach was adopted here. Bone elements were also assigned a Poisson's ratio of 0.3.

To prepare the models for fatigue simulation it was necessary to add plasticity into the model in order to assess fatigue damage. An elastic-perfectly plastic material model was used, whereby the stress increases linearly until the yield strength was reached after which there is no increased resistance to deformation. Load-displacement behaviour for bovine tail

vertebrae covered in Chapter 3 showed that after yield is reached there is a drop in load which then starts to plateau as the test is continued. Whilst this post-yield response varies between specimens, the elastic perfectly-plastic material model was deemed a good starting point as a simplified description of the observed behaviour. For this to be implemented, yield properties of the vertebrae needed to be identified.

Both the density to Young's modulus conversion constant and the yield strain value were found through an optimisation method, with load-displacement data as the input for the process. The following discusses this process in more detail.

5.3.2.1.   Optimisation Method

An optimisation toolbox (Mengoni et al., 2015; Mengoni, 2017) written in Python for use with a set of Abaqus models was used to determine a density-modulus relationship and an element yield strain value. The user inputs include a set of specimen-specific finite element models and the corresponding experimental data for the parameter to be optimised.

The optimisation toolbox runs a set of Abaqus models to minimise the difference between the model outputs and corresponding experimental data. A gradient-based optimisation method is used, where the least square errors between the FE and the data set values are minimised. The algorithm works by minimising a function of the parameter being optimised (in this case the error between the FE and experimental values) by taking a gradient of the function to determine which direction to search for the value equating to the function minimum. The toolbox is provided with user-inputted bounds which determine the starting parameter and the highest and lowest value that can be used. Additionally, a value for the maximum acceptable value of the objective function is required, as well as tolerance values for the function and gradient, and the maximum number of iterations the optimisation can take.

The optimisation is based on Brent's method, a bracketed version of the secant method, whereby the derivative (i.e. the tangent or gradient) of the function is used to determine the

roots. This is depicted in Figure 5-5, where it can be seen that two initial values of the functions, x1 and x2 are used, and as this is a bracketed method these 'guesses' are either side of the root, and this means the derivative can be approximated using the secant line between these two points. Where the secant of the first two points crosses the x-axis, the next guess for f(x) is given, then another iteration is solved where the secant between the new value, x3, and the initial value of the opposite sign is found, and where this crosses the x axis, the next guess is found. This is repeated until convergence is seen and the zero value of the function is found. If the solution is not satisfactory for a given iteration (i.e. is not converging) the more robust bisection method is used, whereby the next value of x is always halfway between the two previous values. Brent's method can converge quicker than the bisection method alone, but being able to revert to the bisection method means the algorithm is more robust than other methods. Using this method, the optimum values for the greyscale conversion and yield strain were determined. The results for the optimisation are discussed in the following chapter.
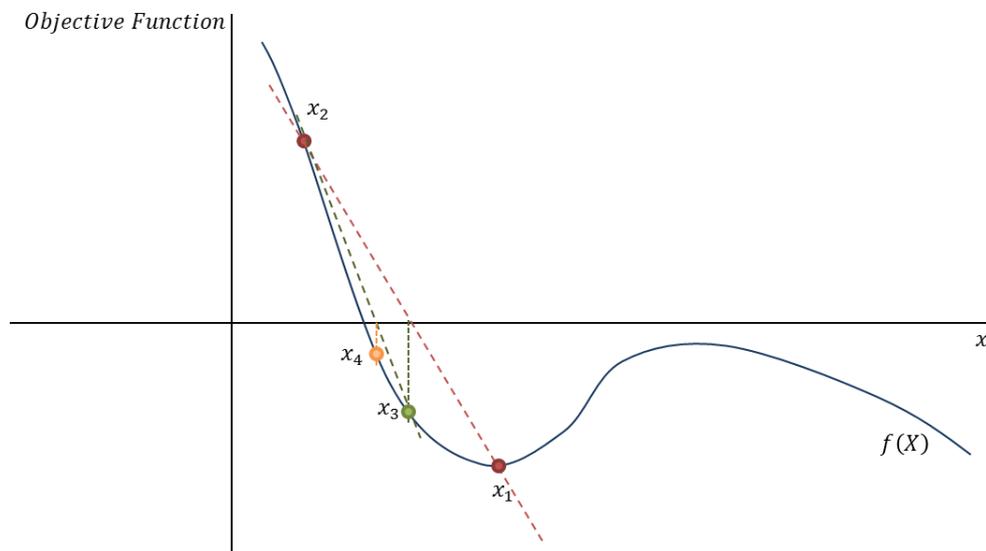
Figure 5-5, Gradient based method of optimisation, where x_1 and x_2 are the initial values, and x_3 is where these cross the x-axis. This value then provides the next tangent and the next iteration of x-axis intersect (x_4). This is iterated until the value is within pre-defined error of x=0.

For both the greyscale conversion factor and the yield strain optimisation, two groups of specimens were used, the first was used to optimise the value for the respective function and the second was used to independently validate the value. For both procedures, it was necessary to have an automated method of determining the output value parameter from the finite element model without manual input. For the greyscale conversion constant, the stiffness at the point of displacement application was required. The calculation of this parameter, load output in the z-axis divided by the applied 1mm displacement at the reference node, was included in the optimisation toolbox. However a method was required to determine the necessary parameter output to optimise a yield strain value in the elastic-perfectly plastic case, as is described in 5.3.2.2. The methods used for calculating the comparative stiffness from experimental data are described in Chapter 3.

5.3.2.2. Yield Strain Optimisation

An element-level yield strain value was determined by using the optimisation process described above. The value was altered and the resulting yield strain of the whole model compared to the experimentally derived yield strain values for each specimen by plotting a load-strain curve from output data as was done for experimental results. Having one yield strain value for all the elements representing bone still results in a different element properties across the vertebrae due to the element-specific Young's modulus, and therefore an element specific yield stress value. This allows the overall model yield behaviour to be calculated from the point of load application and compared with experimental results found in Chapter 3. Yield strain was used in this case in order to apply the 0.2% offset strain rule because the yield point of the load-displacement response was not always clear. The models were run under load control, with a maximum load of 9.5kN to reflect the experimental method.

A Python script was written to calculate the yield strain from the FE output using the same 0.2% offset strain method. This script was added into the post processing part of the Abaqus Optimisation toolbox in order to obtain a value to compare to the experimental data. In order

to get an accurate value from the FE output, the models were forced to solve in uniform small time increments, rather than automatically solving in the largest possible increment, where normally small increments are only used when a stable solution is difficult to find. The Python script was written to firstly find the maximum reaction force in the z-axis at the reference point at each frame in the solution. Secondly, the magnitude of the displacement was found at each frame from the output file, and the strain calculated for each point using the initial specimen height taken from microCT data. The 0.2% offset strain was then determined by finding the gradient of the force-strain curve. The script then compared the offset strain to the strain and created a list of index values for the points where the offset becomes greater than the original strain value. The point of intersect was found from the first point in this list, and the last point of the values where offset strain was lower than the strain, and finding the midpoint of these values. The corresponding yield load and yield strain were found using index values and the equivalent midpoint values. This can be seen in the simplified diagram in Figure 5-6, where the markers represent data points, which are directly compared between strain and offset strain lines.
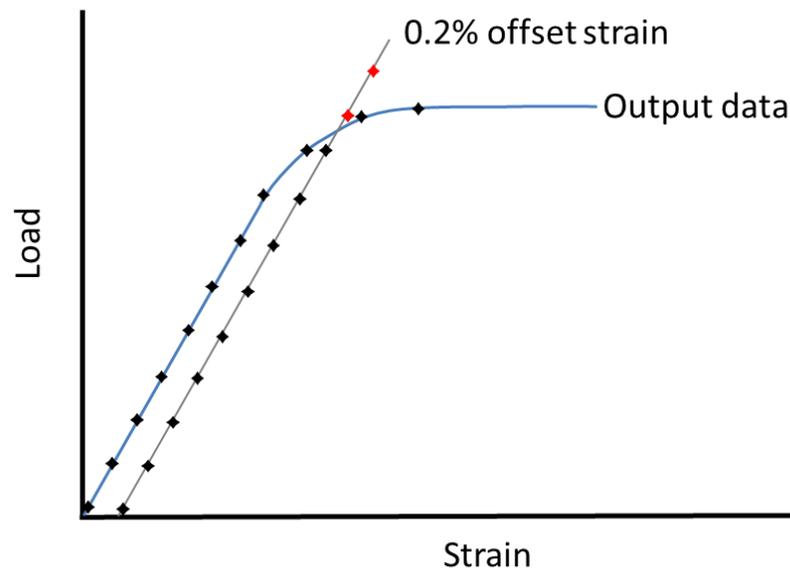
Figure 5-6, Example load-strain diagram showing the data points compared to determine the intersect point, and therefore yield point. The yield point is the midpoint between the last black and first red marker on the offset line.

During the optimisation, this yield point was calculated for each specimen and compared to the experimental yield. In some cases, particularly when the optimisation process attempted to use high values of the input yield strain value, models did not predict yield behaviour before 9.5kN. In these cases where no yield was seen, a nominally high model-level yield strain value of 10% was assumed in order to ensure the next iteration of element yield strain was low enough to allow a plastic response to occur.

5.4. Simulating Cyclic Loading

The section discusses the methods used to develop a Python script capable of simulating cyclic loading in Abaqus using the non-linear vertebrae models with the optimised Young's modulus and yield strain parameters. Based on previous studies, it was decided that a modulus reduction method would be used to simulate the accumulation of plastic strain in the vertebral bone (Corrine Hanlon 2012, Keaveney et al. 1999). This represents damage accumulating in the trabecular bone under loads great enough to cause plastic deformation, and the resulting reduction in stiffness and strength as observed in vertebral trabecular bone cores by Keaveney et al. The goal was to obtain cyclic displacement and plastic strain information to be able to directly compare with experimental displacement trends and damage location in vertebrae.

5.4.1. Material Property Reduction

After loading, Young's modulus and yield stress were reduced by a factor dependant on the plastic strain seen in each element. The equations describing the reduction relationships are shown in Eq.1 and Eq.2, which give a reduction parameter, in the form of a percentage reduction, for Young's modulus and yield stress when a percentage value of plastic strain, ε_p is used.

$$Youngs\ modulus\ reduction = \frac{111\varepsilon_p}{\varepsilon_p + 0.751} \qquad \qquad \text{Equation 1}$$

$$Yield\ stress\ reduction = 20.8\varepsilon_p - 6.4 \qquad \qquad \text{Equation 2}$$

The modulus and yield stress reductions were capped at 85% and 60% respectively. The implementation of material property changes was completely automated by utilising the ability of using scripting to interface with Abaqus. After the unload step in the finite element solution, the script read the output database and determined which elements had undergone plastic strain. These elements were then given new material properties whilst the rest remained the same. These changes were the only ones made, with the mesh, deformed geometry and plastic strain returning to the original, or 0, at the start of each model. This was done because in the experimental fatigue tests it was observed that even under large loads the vertebrae recovered the majority of the displacement that occurred after unloading right up until the point of failure, therefore this was deemed to be a reasonable assumption. After the material properties were updated, a new model was created and run.

5.4.2. Script Development

The following describes the development of the script in more detail, as development was performed on a series of models representing vertebrae of increasing resolution, firstly using a simple cube model and secondly a low resolution vertebrae model, which solve very quickly in comparison to the $1mm^3$ mesh resolution models used to optimise the material properties. This also allowed for thorough interrogation of individual elements in order to assess whether the changes being made by the script were correct, and that a reduction in material properties of one element would cause neighbouring elements to accumulate plastic strain. Each type of model had the same density-based Young's modulus and yield strain as was determined for the higher resolution models, and were set up in the same manner with load applied axially via an analytical plate. A basic flowchart of how the script works is shown in Figure 5-7, where the number of iterations, or cycles, is user-defined in the script. This level of development was necessary due to difficulties manipulating the large numbers of elements and different material sets seen in the vertebrae models which result from having varying material properties through the vertebrae. In the initial model, materials were grouped in sets of elements with the same Young's modulus value, by assigning a section

containing the relevant properties to a set of elements (rather than have an individual assignment for each element). This forms the basis of how models are manipulated.

```
┌──────────────────────────────────────────────────┐
│ Imports and runs FE model with the force used    │
│ experimentally for that specimen in the fatigue  │
│ experiment.                                       │
└──────────────────────────────────────────────────┘
                      │
                      ▼
┌──────────────────────────────────────────────────┐
│ Interrogates all vertebra elements only to read  │
│ equivalent plastic strain, and creates a list of │
│ all elements with non-zero values, identified in │
│ the list by unique element number.               │
└──────────────────────────────────────────────────┘
                      │
                      ▼
┌──────────────────────────────────────────────────┐        ┌──────────────────────┐
│ For each of these, a new section and material    │        │ Repeat using output  │
│ property, that could be modified independently   │        │ database from previous│
│ of other elements, is created.                   │        │ iteration to find new │
└──────────────────────────────────────────────────┘        │ list of plastic       │
                      │                                      │ elements, using       │
                      ▼                                      │ initial geometry and  │
┌──────────────────────────────────────────────────┐        │ mesh at each iteration.│
│ New modulus and yield stress are calculated      │        └──────────────────────┘
│ according to Keaveney equations, according to    │
│ the plastic strain in each element.              │
└──────────────────────────────────────────────────┘
                      │
                      ▼
┌──────────────────────────────────────────────────┐
│ A new .cae and job file are created and the model│
│ solved, displacement at reference point is found │
│ and the number of new plastic elements is        │
│ recorded.                                         │
└──────────────────────────────────────────────────┘
```

Figure 5-7, Flowchart showing the basic process the script iterates to simulate cyclic loading.

New sections and materials were created only when necessary, as having large numbers of these takes a large amount of time to create and solve. A failure criteria for stopping the iteration process was not determined, because it was noticed that models could no longer solve after large plastic strain were seen, so this non-convergence was taken as the end of the cyclic modelling.

Initially a simple cube with 27 1mm³ elements with greyscale values similar to those seen in bone was used to trial development versions of the script until it successfully iterated. The cube had a layer of stiff elements above and below a layer of mixed-value less-stiff elements, and the model had a load applied centrally via a analytically rigid plate and was constrained across the base. The cube model showed successful accumulation of plastic strain in elements as well as plastic strain occurring in new elements over a small number of cycles, as a result of changes in neighbouring elements, Figure 5-8. Throughout this work, the equivalent plastic strain (PEEQ), was used as the model output, as a way of taking into account all the components of the plastic strain tensor. The calculation for equivalent plastic strain is shown in Equation 3.

$$PEEQ = \frac{1}{1+v'} \times \sqrt{\left(\frac{1}{2}\left[\left(\varepsilon_{p1} - \varepsilon_{p2}\right)^2 + \left(\varepsilon_{p2} - \varepsilon_{p2}\right)^2 + \left(\varepsilon_{p3} - \varepsilon_{p1}\right)^2\right]\right)} \qquad \text{Equation 3}$$

Where v' is the effective Poisson's ratio, assumed to be 0.5 for plastic strain, and ε_{pn} is the plastic strain in the x, y and z directions.

The simple cube model allowed evaluation of the changes in all elements as there are so few, so the calculations done by the script could be checked easily, ensuring the correct changes to material properties were made for a given input and the resultant plastic strain. The accumulation of plastic strain was seen to be gradual, and is shown in Figure 5-8 for the first two cycles and then the sixth cycle, after which the model was stopped. Peak plastic strain values range from around 0.01 to 0.03. These values are not representative of what is seen in a vertebrae due to the much smaller shape, however they do appear to be in the correct order.
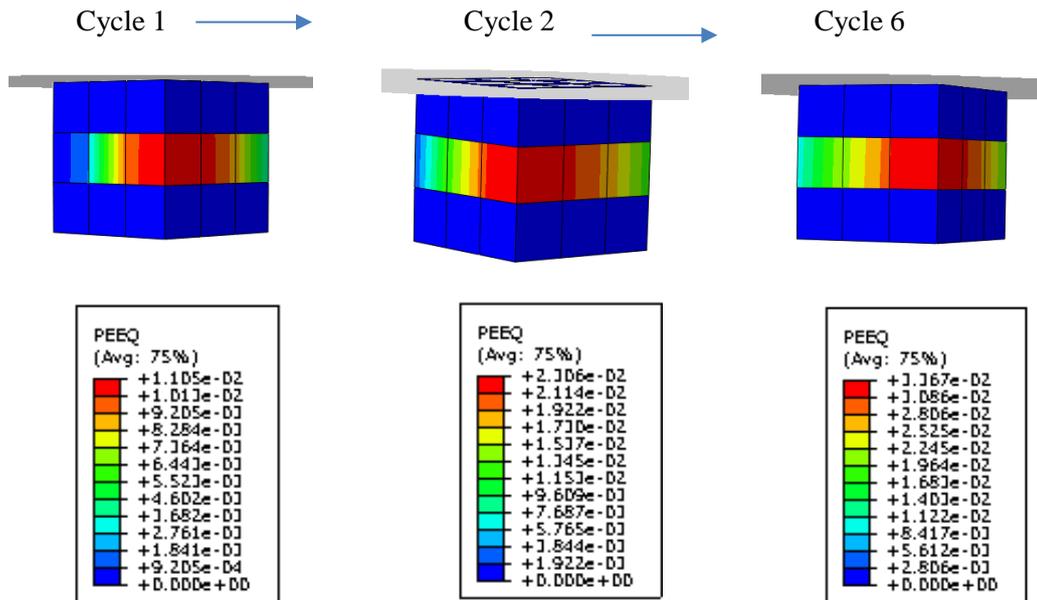
Figure 5-8, Progressive increase in plastic strain seen in the simple cube model used to develop the iterative cyclic loading script, shown at cycle 1, 2 and 6.

In order to add complexity to the cube model to develop the script for a vertebrae model, whilst keeping the number of elements low enough to allow the model to solve quickly, a very low resolution vertebra model was created by down-sampling a specimen-specific bovine tail vertebra model to a 7mm resolution, as shown in Figure 5-9. Again, the model was set up with the boundary conditions and constraints described in previously for the 1mm resolution models.
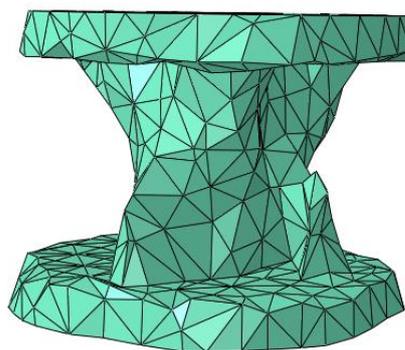
Figure 5-9, Low resolution mesh of the vertebrae model, down-sampled to a 7mm³ voxel resolution.

It was only possible to run a small number of cycles using this model, approximately 10, before plastic strain caused some elements to deform too much for the model to solve. It was noted that as there were so few elements, some were forced by the meshing tool to have more severe aspect ratios than others, and these were the elements accumulating the most plastic strain, and stopping the model from running, Figure 5-10. Further iterations of this model were made to improve the element shape by allowing the mesh to have a less accurate fit to the surface of the geometry, allowing for 0.2mm boundary space around the surface to allow for the improvement of surface element shapes. Plastic strain values from approximately 0.03 to 0.27 were predicted over four cycles (Figure 5-10 A-D).
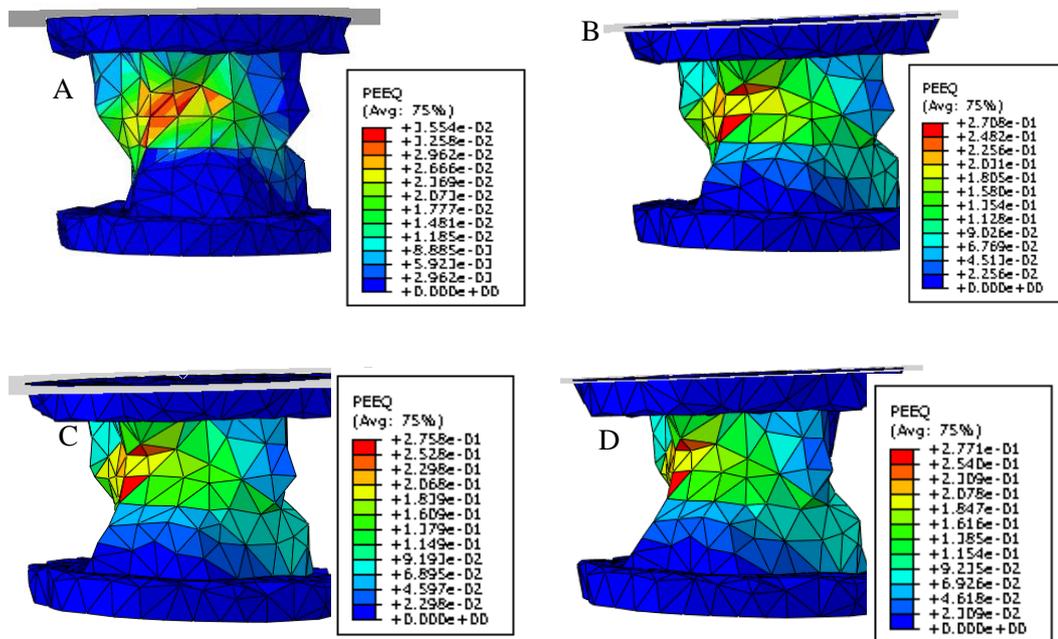
Figure 5-10, Plastic strain response of the low-resolution vertebra model at four different stages during the iterative loading (A-D, cycles 1-4 respectively), showing the greatest accumulation of plastic strain in a small number of surface elements.

At this stage a number of extra features were added into the code as a way of evaluating changes across the cyclic loading. Firstly, a continuously updating list of elements storing information regarding whether the element had been modified, the original material properties and the new material properties was created, and updated with each iteration. Secondly, a calculation was carried out at the end of each load and unload step in each cycle

to determine the displacement at the load application point. Calculations of the total number of plastic elements in the model and the number of new elements created during each step were also added. These changes allowed a .csv file with updated information about the vertebrae each iteration to be created. Information stored was the maximum and minimum displacement and the number of new plastic elements created each cycle. This was added to allow for direct comparison with fatigue experiment displacement data.

The script was then run for a 1mm mesh resolution model, which showed an accumulation of plastic strain in the anterior wall of the vertebra. The code ran for five cycles before failing to solve, and large plastic strains were predicted in a number of elements, Figure 5-11. However the general values and displacements seen were appropriate for taking the process forward to investigate the cyclic response in a group of vertebrae.

Iteration	1	2	3	4	5
Image of x-section through upper anterior wall					
Approx. peak equivalent plastic strain	6-9%	14-20%	30-40%	40-75%	60-100%
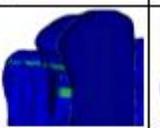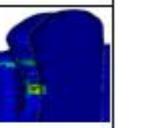
Figure 5-11, Cut though section view of a vertebrae modelled with the fatigue simulation script, showing the accumulation of plastic strain over five iterations.

5.5. Validation Methods

To validate the finite element predications of cyclic loading behaviour, outputs were compared with the experimental data produced in Chapter 4. Specifically, the number of cycles to failure were compared, additionally damage location and extent were compared qualitatively by assessing microCT scan data and the areas of high plastic strain seen in the FE output. Displacement trends were compared and the amount of displacement predicted over the cyclic loading, taken from the load application point, were compared.

5.5.1. Statistical analysis

To evaluate the ability of the finite element models to accurately predict the mechanical response of vertebrae, the static load FE and experimental data were compared using Lin's concordance correlation coefficient (CCC) to measure the agreement between the two variables (Lin 1989). To compare the relationship between parameters affecting the models, discussed further in the following chapters, graphical software was used to calculate regression analysis (Origin Pro 2015, OriginLab Corporation, USA).

5.6. Summary

In this chapter, methods were reported to scan, segment and create FE models of bovine tail vertebrae based on previous work achieved in the research group. Methods for the optimisation of greyscale to Young's modulus conversion factor for linear-elastic vertebrae models were detailed, allowing for variation of bone properties within the vertebrae to be captured in a down-sampled model. The resultant equation relating greyscale to elastic modulus is specific to the calibrated μCT scanner and specific scan settings used, which were the same for all specimens. Zapata et. al have shown it is possible to convert this value using calibrated density phantoms to derive a conversion value between scanners (Zapata-Cornelio et al., 2017). A new method of determining a single value for the yield strain input into vertebrae models with elastic-plastic material properties was developed, specifically the use of an optimisation tool to find the best case from a group of specimens, and validating this value on a different set of specimens.

A new approach was then reported to simulating the fatigue behaviour. A Script was developed to run for a user-defined number of iterations, representing fatigue loading through changes in Young's modulus and strength in proportion to the amount of plastic strain seen on an element level, adapted from literature studies for trabecular bone. Low resolution models have shown that the quality of the mesh at the surface of the model is important and badly shaped tetrahedral elements can cause the model to fail early. This will be taken into account when assessing results from high resolution models and when

considering the mesh used for these models. An example high resolution model was run to assess how effective the script was, which was then taken forward to model a group of fatigue tested vertebrae, the results of which are presented in the next chapter.

6. Computational Results and Further Development

6.1. Introduction

This chapter covers the validation of specimen-specific FE (finite element) models of bovine tail vertebrae tested experimentally. Results are presented initially for a static linear-elastic case under displacement control where the experimental stiffness is compared with the FE predicted stiffness and the level of agreement is measured. Validation of these models with the addition of a perfectly-plastic material model and optimised yield properties is also presented by assessing the agreement between FE predicted yield strain and experimentally measured yield strain.

The parameters and models from this process were then taken forward to be utilised with the cyclic loading script, the development of which is discussed in Chapter 3. Briefly, the code takes an Abaqus output file and changes the material properties, based on data derived by Keaveny et. al (Keaveny et al., 1999) from *in vitro* loading experiments. Initial results are presented in the form of displacement trends and plastic strain distributions compared to experimental displacement trends and microCT scan fracture locations for specimens-specific models.

As the original material property reduction equations were derived for the behaviour of human trabecular bone cores, it was expected that there would be error in the finite element predictions and adaptions would need to be made in the material property changes to better represent the behaviour seen in bovine bone. Utilising the adaptability of the script, sensitivity analyses were run on different parameters within the equations, and with different levels of modulus and strength reduction. These results are presented and suggested improvements to the script are discussed.

A summary of the experimental tests carried out and the corresponding FE comparisons that are made in this chapter is shown below in Table 6-1. Details of the sensitivity studies, described in Section 6.3, are also included in the summary.

Table 6-1, Summary of Finite Element Studies and sensitivity studies.

Test	Specimens	Test Details	Output Measures Compared with experimental data
Test 1	Group 1 – static test to 9.5 kN.	Material property optimisation and validation for a single load case, for linear-elastic (displacement-input) and non-linear (force-input) models.	-Elastic stiffness -Yield load and strain
Test 2	Group 2 – Fatigue group	Iterative FE modelling for cyclic behaviour in non-linear models under experimental loading conditions.	-Displacement trends -Yield strain -Plastic strain distribution
Sensitivity Studies			
Sensitivity Test 1	One example vertebra model from Group 2	Identifying relative effect of modulus reduction compared to strength reduction	Displacement against number of iterations
Sensitivity Test 2	One example vertebra model from Group 2	Modifying reduction equation to cause a greater modulus reduction for a given plastic strain	Displacement against number of iterations
Sensitivity Test 3	One example vertebra model from Group 2	Modifying reduction equation to cause a greater strength reduction for a given plastic strain	Displacement against number of iterations
Sensitivity Test 4	One example vertebra model from Group 2	Assessing the effect of limiting the amount of cumulative modulus reduction.	Peak displacement against number of iterations

6.2. Material Property Optimisation and Validation of Static Test Case

6.2.1. Young's Modulus Derivation

The optimisation method used to determine a single value to convert greyscale image data to Young's modulus values in the FE model is described in Chapter 4. Initially models were run under a defined axial displacement of 1mm with a linear-elastic material model. The elastic stiffness, calculated from the point of load application was compared with the stiffness from the linear region of the experimental data, both calculated as described in Chapter 4. Lin's Concordance Correlation Coefficient was calculated to quantify the agreement (Lin, 1989). This is a statistical measure of agreement between two variables,

where a CCC (concordance correlation coefficient) of ±1 indicates perfect agreement and 0 implies complete disassociation.

In order to find a constant that could then be validated using models that were not used in the calibration, the models were then split into two groups using a set from two tails (n=8 from tails 5 and 6) for the calibration, and a set from a separate three tails (n=7 from tails 1, 3 and 7) for validation. The greyscale to modulus conversion value, derived from the calibration set, was found to be 0.0125. A direct comparison between experimental and FE predicted stiffness for both groups is shown in Figure 6-1 with the line y=x also depicted on the graph showing where perfect agreement would lie; Bland-Altman, or mean-difference plots, are shown in Figures 6-2 and 6-3. One outlier was identified in the validation set, vertebrae T1CC1, this had a much higher experimental stiffness than all other vertebrae so was removed from the group. This can be seen in Figure 6-1, where the outlier is circled. The calibration set had a CCC of 0.607 with average errors of 8.39 ± 4.12% and the highest error was approximately 11%. The validation set had a CCC of 0.691 with average error of 8.57 ± 4.77%, and greatest error approximately 15%. It can be seen that in the calibration set there is a relatively even spread of data above and below the line x=y, however when the results were used with the validation set, the FE models tended to under-predict the stiffness values in these particular tails. Despite this the concordance coefficient was better in the validation set, indicating the greater spread of data seen in the calibration set, likely due to there being more specimens. However, the validation set still shows good agreement with the derived values, comparable with results found in the literature.

Bland-Altman plots, depicting the mean of the two values against the difference, are shown for both the calibration and the validate sets in Figure 6-2 and Figure 6-3 and respectively, with the horizontal lines depicting the mean difference and ±1.96 standard deviation away from the mean, i.e. the 95% confidence interval. This more clearly shows the spread of data. With the validation set it can be seen that the specimen with the lowest stiffness had the best

FE prediction, whereas the specimens in the calibration set have a much more even spread

and the mean difference is close to zero but with a greater standard deviation.
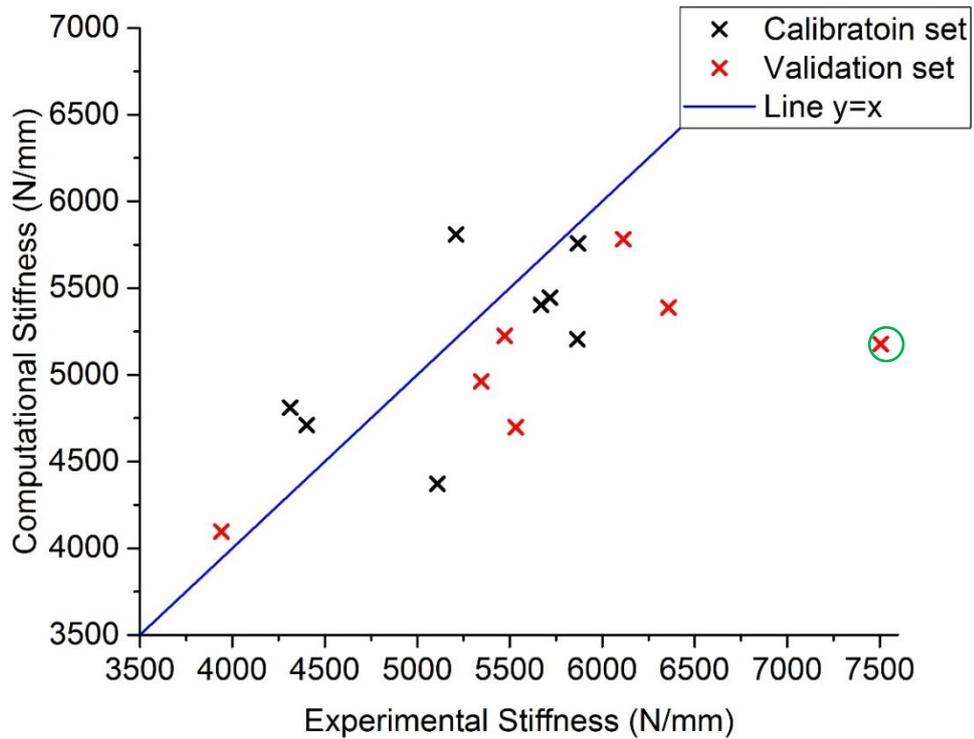
Figure 6-1, Experimental stiffness against FE predicted stiffness for both calibration and validation sets of vertebrae, with line y=x showing perfect agreement. Calibration set CCC = 0.607; validation set CCC=0.691.
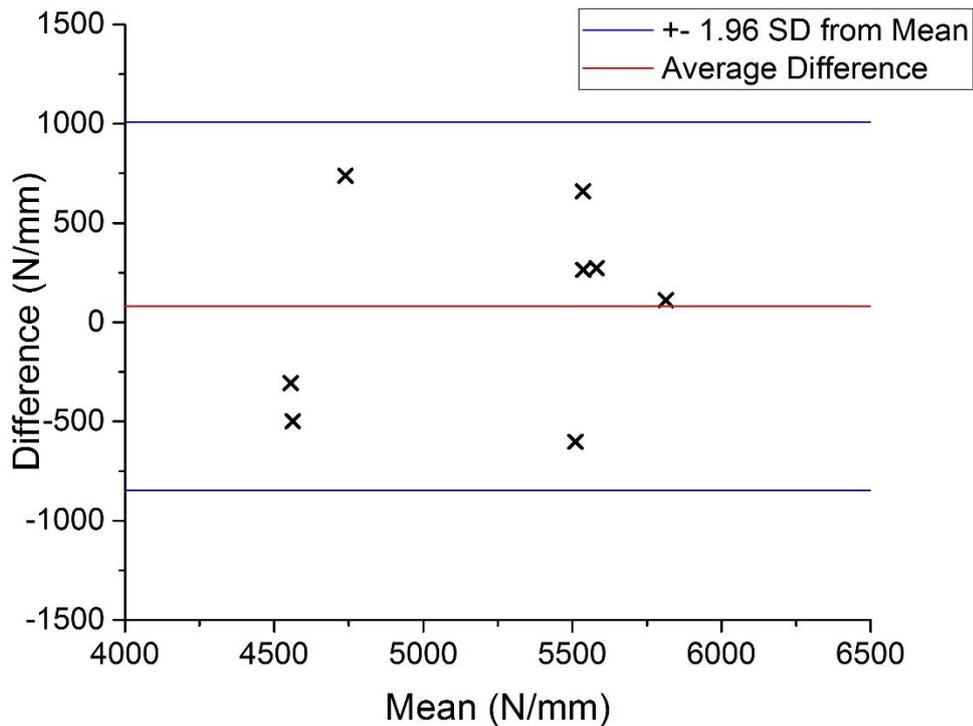
Figure 6-2, Bland-Altman plot for stiffness calibration set showing agreement over the range of means in the dataset, with average mean and ±1.96 standard deviation lines representing the 95% confidence interval.
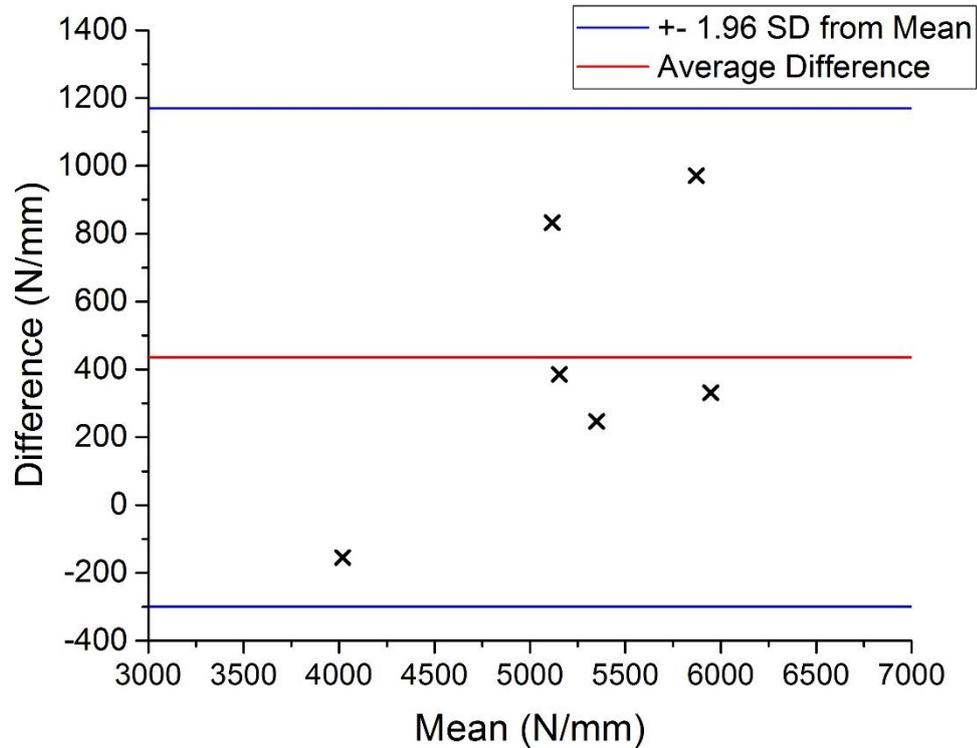
Figure 6-3, Bland-Altman plot for stiffness validation set showing agreement over the range of means in the dataset, with average mean and ±1.96 standard deviation lines representing the 95% confidence interval.

6.2.2. Yield Strain Optimisation

The following presents the results for the derived element-level yield strain values, optimised for the overall yield strain of the vertebrae by direct comparison with experimental yield strain results. The processes for calculating yield strain from experimental and finite element data are described in Chapters 3 and 4 respectively. Yield strain was compared rather than stiffness, as was used for the previous optimisation, in order to assess the ability of the models to predict plastic or yield behaviour.

The same specimens were used for calibration and validation sets as were used for the greyscale conversion factor optimisation. The bone elements within the models were assigned an elastic-perfectly plastic material model and were run under load control rather than displacement control. Validating the models for experimentally relevant loads was

important for the fatigue modelling, where different load values were used for each specimen in the experimental study, so was also used in the FE models. A script was written to implement the optimised yield strain and Young's modulus values to calculate yield stress, by calculating element specific modulus multiplied by yield strain, as this is the input value required in Abaqus.

The results are shown in Figure 6-4 as a direct comparison between experimental yield strain and predicted FE yield strain, alongside the equivalent Bland-Altman plot shown in Figures 5 and 6. Compared to the stiffness optimisation, poor agreement was seen between experimental and computational yield strain and CCC for the validation set was 0.15. In the calibration set, in all cases the models underestimate yield strain. This is because when a higher element yield strain value is applied in the optimisation script, one or more of the vertebrae no longer fail, meaning the yield properties cannot be found. Therefore the best-case scenario was with an element input yield strain of 0.047. Mean error in the calibration set was 14.25% and for the validation set the error was 23.76%. The Bland-Altman plots show the spread of data above and below the mean in both sets with errors of up to 20% in the worst case in the calibration set and up to 42% in the validation set.
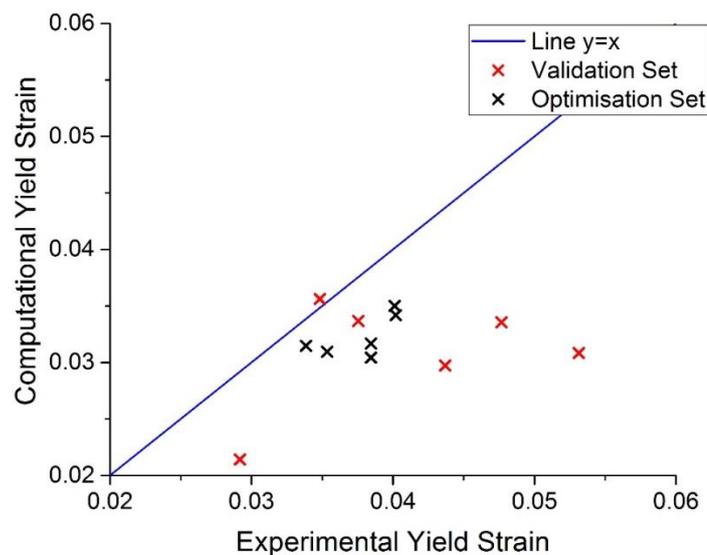
Figure 6-4, Experimental stiffness against FE predicted yield strain for the optimisation and validation sets of vertebrae, with line y=x showing perfect agreement. Optimisation set CCC = 0.138; validation set CCC=0.15.
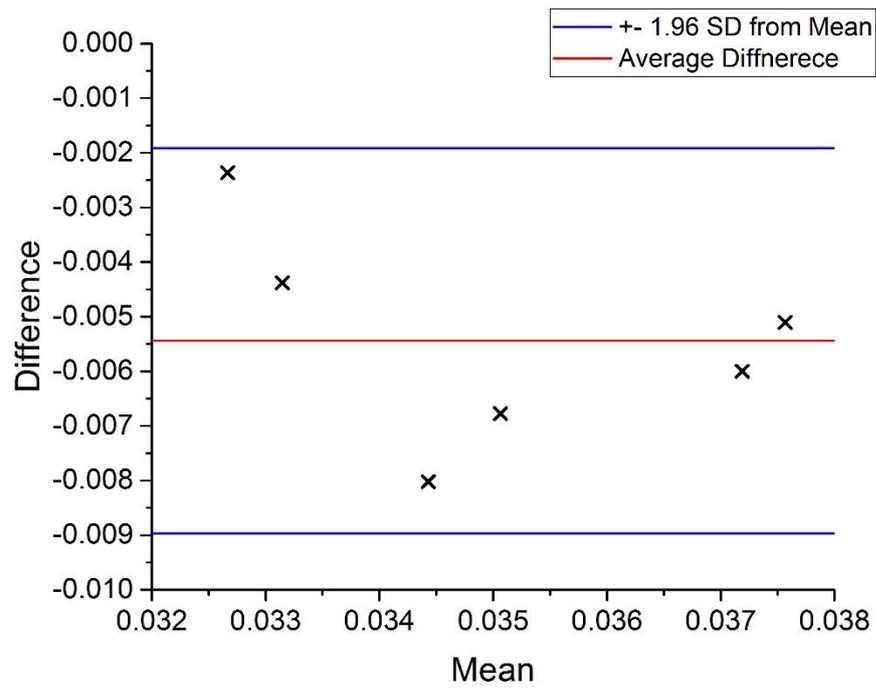
Figure 6-5, Bland-Altman plot for yield strain optimisation set showing agreement over the range of means in the dataset, with average mean and ±1.96 standard deviation lines representing the 95% confidence interval.
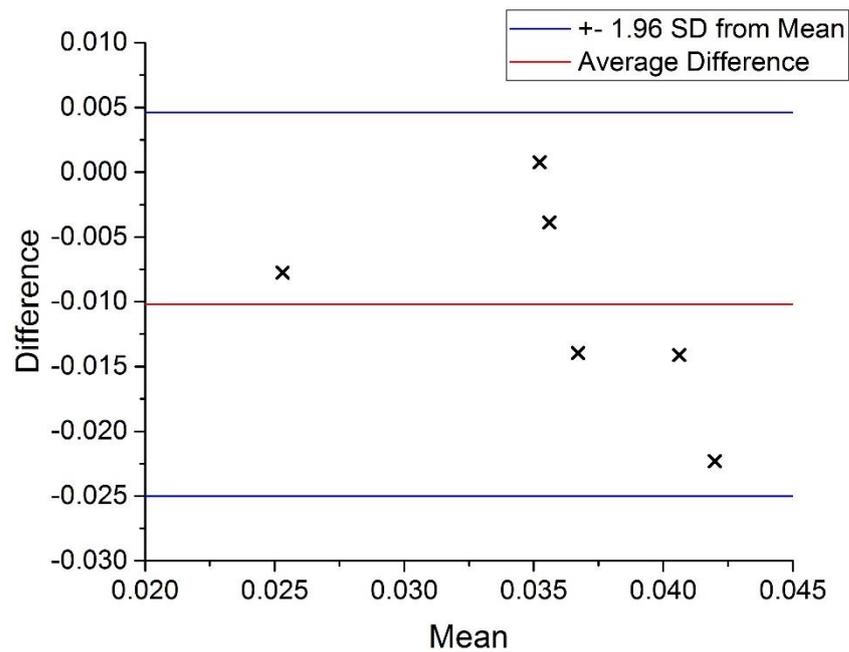
Figure 6-6, Bland-Altman plot for yield strain validation set showing agreement over the range of means in the dataset, with average mean and ±1.96 standard deviation lines representing the 95% confidence interval.

Typical experimental and comparative FE load-displacement responses modelled using the optimised yield strain for two vertebrae loaded to 9.5kN are shown in Figure 6-7. Figure 6-7A shows a response where the yield strain is underestimated by the FE model, as was seen in the majority of cases where the approximate experimental yield displacement is 2.0 mm and the equivalent FE is 1.5 mm. Figure 6-7B shows an example where the load-displacement curve is better predicted, where the approximate experimental yield displacement is 2.0 mm and the equivalent FE is 2.0 mm. Due to the large variation between specimens, and some not seeing failure behaviour with values that would improve results for other specimens, these results could not be improved using this model.

Optimising a single yield strain value across all specimens was found to be challenging, however the value found, 0.047, was suitable to be taken forward into the development of the fatigue modelling. This was compared to values found in the literature determined from different types of trabecular bone: approximately 0.01 and 0.02 (Kopperdahl and Keaveny, 1998) found from bovine tibial bone; approximately 0.005 (Nagaraja et al., 2005) looking at micro-damage in bovine trabeculae; 0.1 for whole porcine vertebrae (C. A. Hanlon, University of Leeds, 2012) and 0.16 for porcine lumbar trabecular bone (Teo et al., 2006). It can be seen that the 0.047 value found in this study sits within the literature range and in cases where it was greater than the literature values were for isolated trabecular bone specimens rather than for whole vertebrae where the denser vertebral shell and processes provide more support for the specimen, increasing yield properties. The value found in the current study was less than that for whole porcine vertebrae tested in a similar fashion, which could highlight that the non-load bearing vertebrae tested in this study have a lower yield strength than the load-bearing ones. Using a single yield strain meant there was variance in the yield stress due to the different elastic modulus between elements. This varying yield stress was intended to account for some of the different behaviour seen between bone elements However, results indicate that it is likely there is a variance in yield strain between areas of bone. Assuming a constant yield strain with varying yield stress, due

to the inhomogeneous Young's modulus, was still an improvement on assuming a constant yield stress across all elements, and results were deemed suitable to take forward into fatigue models.
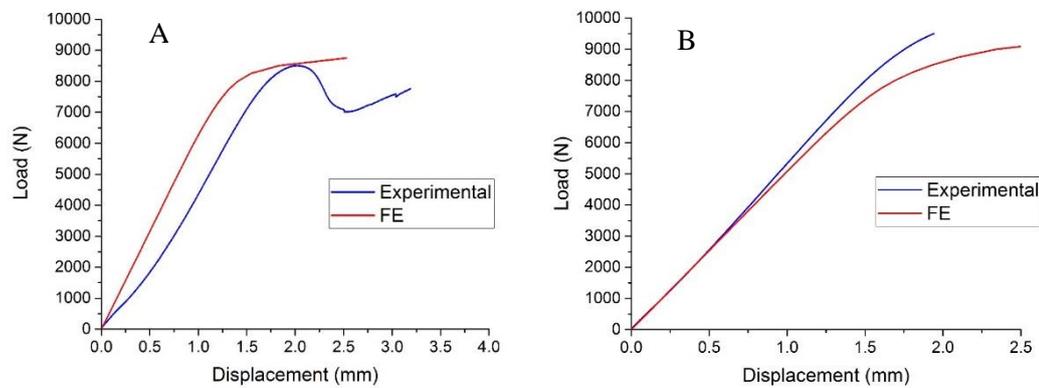
Figure 6-7, Load-displacement curves for experimental and FE models loaded to 9.5kN, the latter with an elastic-perfectly plastic material model, for A) T6CC2 where FE under-predicted yield strain and B) T7CC2 showing closer agreement.

6.3. Sensitivity Analysis for Fatigue Modelling

The following covers the results from the FE fatigue modelling, utilising the code described in the methods in Chapter 5. Specifically the bone elements in these models were assigned the density-based Young's modulus values and yield strain of 0.047, and load specific to the peak load applied to each vertebra in the fatigue experiments. Each iteration included a load and unload step, after which the material properties were updated and a new input model was created, whilst the original mesh was kept and models revert back to having no plastic strain at the beginning of each iteration. Peak displacement for each step was recorded and each iteration had an associated Abaqus output file.

Initial indications from running the fatigue modelling script using the published material property reduction equations showed that a variety of outcomes could occur. This included in some cases vertebrae 'failing' (ie reaching a state where the model could no longer solve) very quickly and in others vertebrae exhibiting some initial changes but then reaching a plateau in displacement where no further plastic strain occurred. An example of this

response is shown in Figure 6-8, where displacement did not increase after four iterations. Vertebrae models are shown without PMMA endcaps, as no plastic strain was seen in these regions.
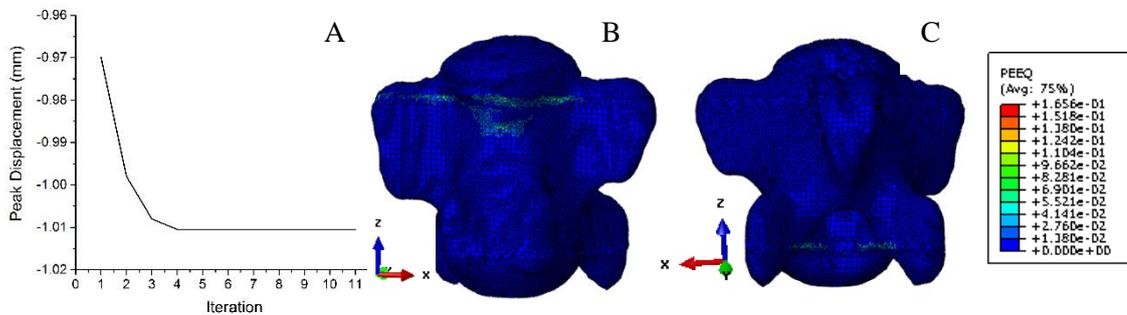
Figure 6-8, FE response of example vertebra T12CC2 using iterative material property reduction showing A) Peak Displacement over 2 iterations for which the model could solve, B) Anterior view of equivalent plastic strain distribution, C) Posterior view and equivalent plastic strain contour key.

6.3.1. Modulus and Strength Reduction Equations

A number of approaches were taken to understand whether the material reduction parameters could be optimised to prevent plateauing of displacement and to improve the distribution of plastic strain to better match the response typically seen by vertebrae. These sensitivity studies involved investigating which reduction parameter, modulus or strength, had the greatest effect on displacement outcome by removing one and then the other parameter, then setting each parameter to a notionally high constant reduction of 90% whilst the other parameter remained the same. One vertebrae model was used for this, specifically a model that saw poor results with little distribution of plastic strain and displacement trends that plateaued rather than increasing. The changes made to the equations are displayed in Table 6-2, and the resulting changes to the peak displacement for each case are shown in Figure 6-9.

Table 6-2, Four combinations of reduction equations used to assess the relative effect of each parameter. Tests 1 and 2 are with no strength reduction and high fixed strength reduction respectively, and tests 3 and 4 are with no modulus reduction and high fixed modulus reduction respectively. The equations are taken from Keaveny et al. as described in Chapter 5, and describe the percentage reduction in modulus and strength with respect to plastic strain (when used as a percentage).

Test	Modulus Reduction	Strength Reduction	Test	Modulus Reduction	Strength Reduction
1	$\dfrac{111\varepsilon_p}{\varepsilon_p + 0.751}$	No reduction	3	No reduction	$20.8\varepsilon_p - 6.4$
2	$\dfrac{111\varepsilon_p}{\varepsilon_p + 0.751}$	90% reduction	4	90% reduction	$20.8\varepsilon_p - 6.4$
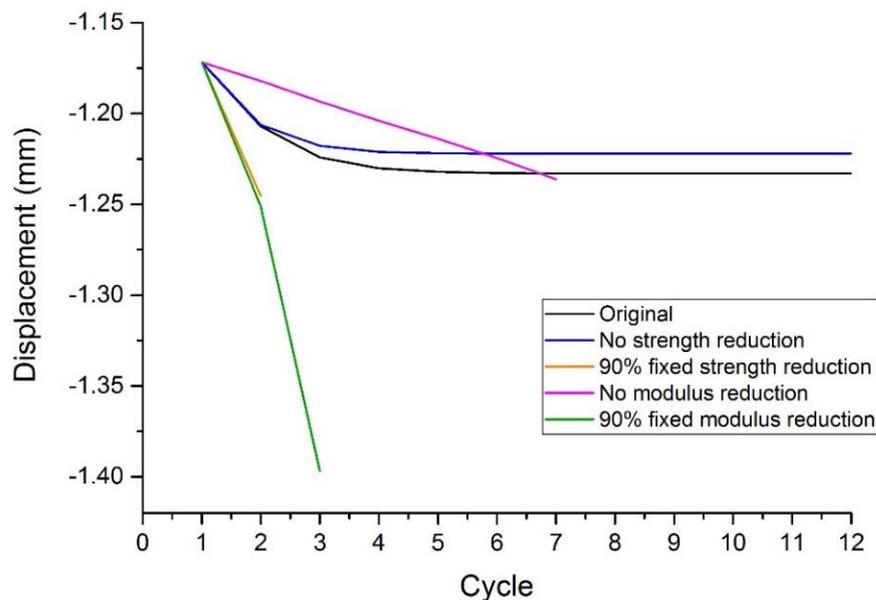
Figure 6-9, Displacement against cycles for vertebra T11CC1 for four variations of reduction equations: removal of strength or modulus parameter and fixed high strength or modulus reduction parameter, as defined in Table 6-2. Shown compared to original response.

Initially, the model was run with just modulus reduction then just strength reduction and it was seen that modulus reduction had the greatest effect on output, as when this was removed, the displacement decreased more rapidly and almost linearly, however when the strength reduction was removed the response was similar to the original. The initial displacement response was the same for both cases, however the high strength reduction

prevented the model from solving one cycle before the high modulus reduction. This is because when the modulus is lowered, elements are less likely to yield but will see much greater displacement. However, when the yield strength is lowered, the elements are more likely to yield under lower displacement, giving an overall more accelerated response with lower final displacement. This is illustrated in Figure 6-10, where it can be seen that the reduction in modulus causes the yield strain to increase and reducing yield stress reduces yield strain. As it is important to find a balance between reducing modulus to increase displacement and not allowing yield strain to become too great, it is important to keep the strength reduction parameter as well.
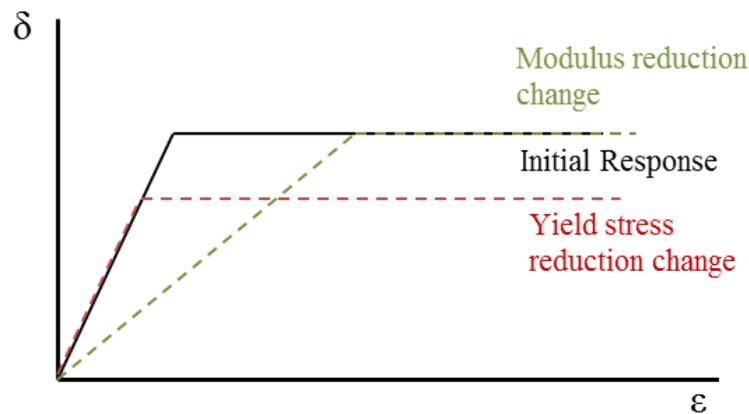
Figure 6-10, Diagram showing the elastic-perfectly plastic material response for the initial material reductions and the effect on yield stress and strain of reducing the modulus and yield stress.

To understand how to optimise the equations for the vertebrae models in this study, firstly the original equations were considered, Figure 6-11A. The reduction changes are validated by the Keaveny paper (Keaveny et al., 1999) for up to 3% plastic strain, however it was observed from the previous sensitivity study that individual elements experienced much higher plastic strains using the yield strain and density-based material properties under experimentally-relevant loads. When extended to up to 50% plastic strain, the equations can be seen to almost instantly reach the maximum reduction values set by the limits, Figure 6-11B. This may be the cause of error in the results, as it prevents elements changing

proportionally to the amount of plastic strain. To modify the equations to allow for the same

relationships to be kept but over a wider range of plastic strain values, lower values for the

plastic strain variables α and β in the following equations were considered:

$$\frac{\alpha \varepsilon_p}{\varepsilon_p + 0.751}$$

$$\beta \varepsilon_p - 6.4$$

The variable α, originally set as 111 in the modulus reduction equation, was varied between

50 and 111, and the results are shown in Figure 6-12A. The variable β, originally set as 20.8

in the strength reduction equation, was varied between 1.5 and 10, and the results are shown

in Figure 6-12B.

A   B
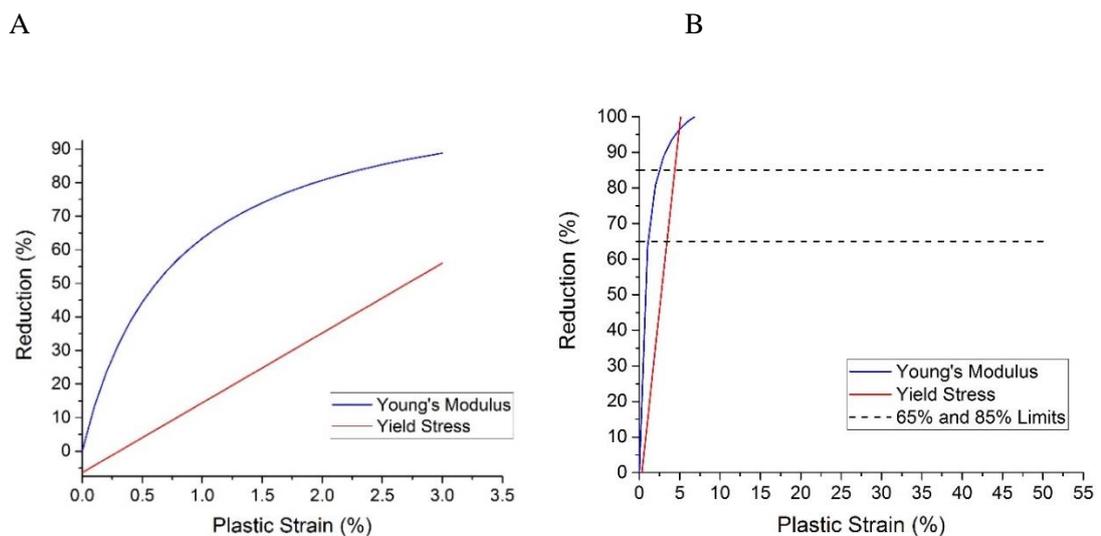
Figure 6-11, A) Original material property equations taken from the literature, showing relationship between plastic strain and percentage reduction for young's modulus and yield stress, or strength, and B) original equations extended for up to 50% plastic strain, with reduction limits indicated by dashed lines.

A

B
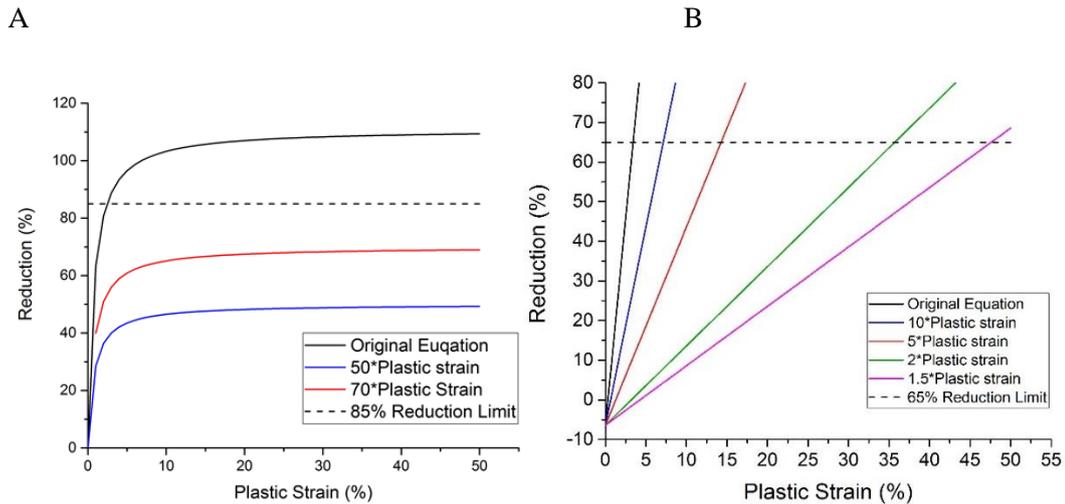
Figure 6-12, A) Reduction of Young's modulus values for plastic strain variables 50 and 70 compared to the original 111, and B) Strength reduction for varying plastic strain variables from 1.5 - 10, compared to the original 20.8. Results shown for up to 50% plastic strain.

From the above results it can be seen that in order to keep the material property results varying over a larger range of plastic strains, an α variable of between 70 and 111 and a β variable of below 2 could be more appropriate. Additionally it was noted that at very low plastic strains the strength equation becomes negative, causing the material property to increase. As this is not physically realistic, the negative term at the end of the equation was removed for this single case, however no change in response was seen.

To investigate whether these changes could improve fatigue results, firstly the modulus reduction parameter was investigated. In the same model as used for the previous sensitivity study, α variables ranging from 50-200 were investigated. The results are shown in Figure 6-13, compared with the original response. As α is increased, greater modulus reduction occurs at lower strains, causing a greater number of elements to see larger displacement. Greater displacement is seen overall in the model, which then shows yield behaviour as defined in the experimental study. At the lowest reduction, where α =50, the model saw rapid linear displacement to a point where the solution could no longer converge. This is because the elements remain stiffer but reach yield stress at a lower strain, showing a

very similar response to the case in the first sensitivity study where there was no modulus reduction, only yield stress reduction. When α was set to 70, slightly lower than the original value, a similar response to the original was seen with less initial displacement, due to less Young's modulus reduction, but more overall displacement. This is because elements that do not initially yield now go on to reach their yield point (since it is at a slightly lower strain), eventually causing slightly more displacement than the original case.
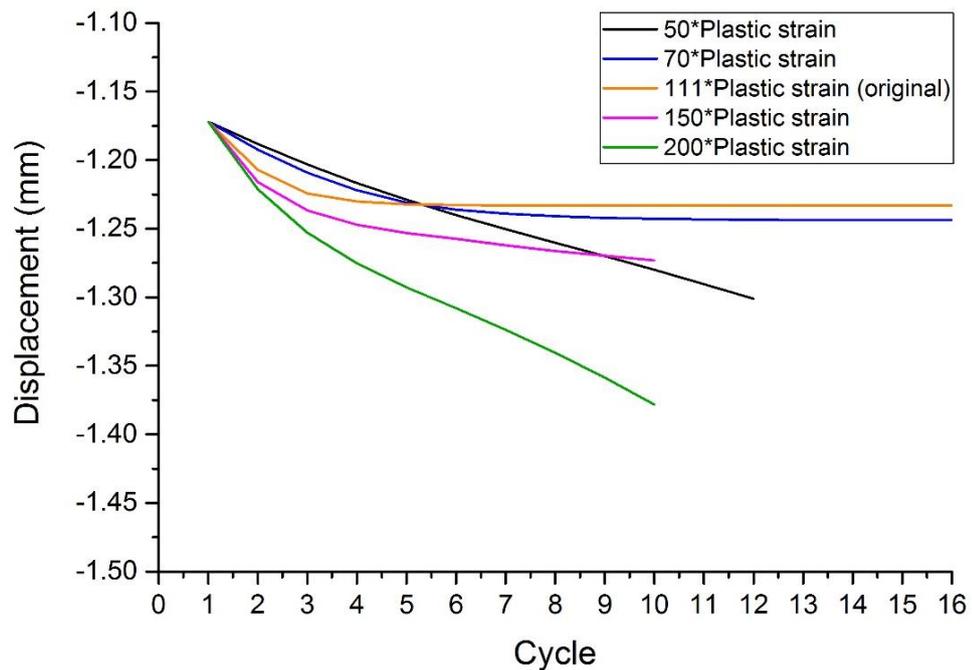
Figure 6-13, Sensitivity analysis using vertebra T11CC1 investigating the effects of changing the proportion of element Young's modulus reduction.

The results for cases using the same model whilst altering the β component are shown in Figure 6-14. Reducing the yield strength results in less displacement of the model as elements reach the yield point sooner. This is caused by elements reaching yield, and therefore entering the perfectly-plastic region, under smaller displacements. Higher values of β have not been modelled as it can be assumed the response eventually becomes that of the high fixed strength reduction in the first sensitivity analysis where the model fails to solve after two cycles.
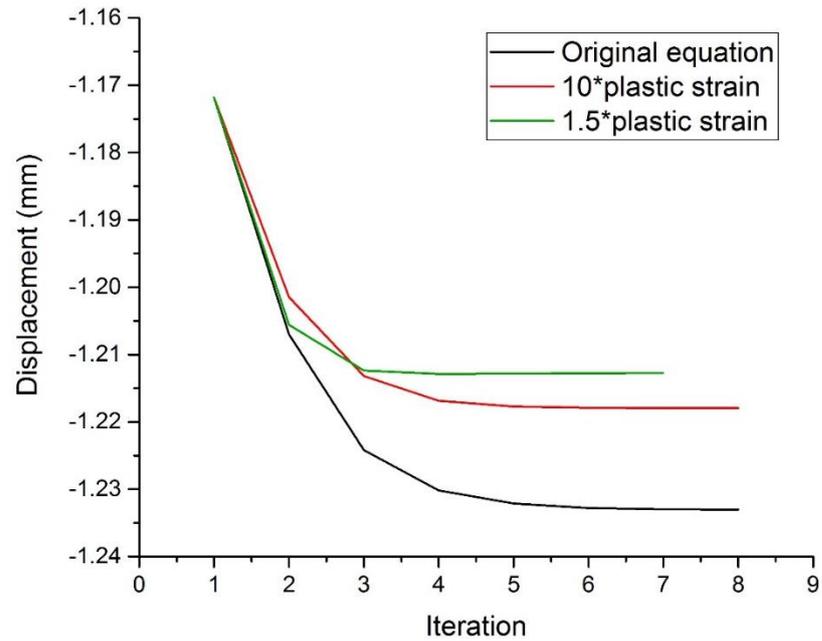
Figure 6-14, Sensitivity analysis using vertebra T11CC1 investigating the effects of changing the proportion of element yield stress reduction.

6.3.2. Modulus Reduction Cumulative Limit

To improve the model solutions and make the methods more physiologically relevant, the code was modified to include a limit on the cumulative modulus reduction. This was to prevent poorer-shaped elements experiencing very high deformations and preventing the model from solving, or having such low moduli that the elements no longer support and transfer load to the surrounding structure, causing the model to stop accumulating plastic strain in adjacent regions.

Three percentage limit values, 40, 50 and 70%, were tested on a single vertebrae model, chosen as it had a poor initial response, with results as shown in Figure 6-15. When compared to the original results, it can be seen that the addition of a limit caused the displacement to increase more linearly, rather than the sudden increase and plateau. The addition of a limit did not increase the number of cycles to failure but did allow the material reductions to continue through the iterations and for displacement to continue increasing. A 70% limit did not change the displacement response, however the 40 and 50% limit allowed

for slightly more displacement at the final cycle. There was almost no difference seen between the 40% and 50% limits, however slightly more displacement was seen in the last iteration using the 50% limit.
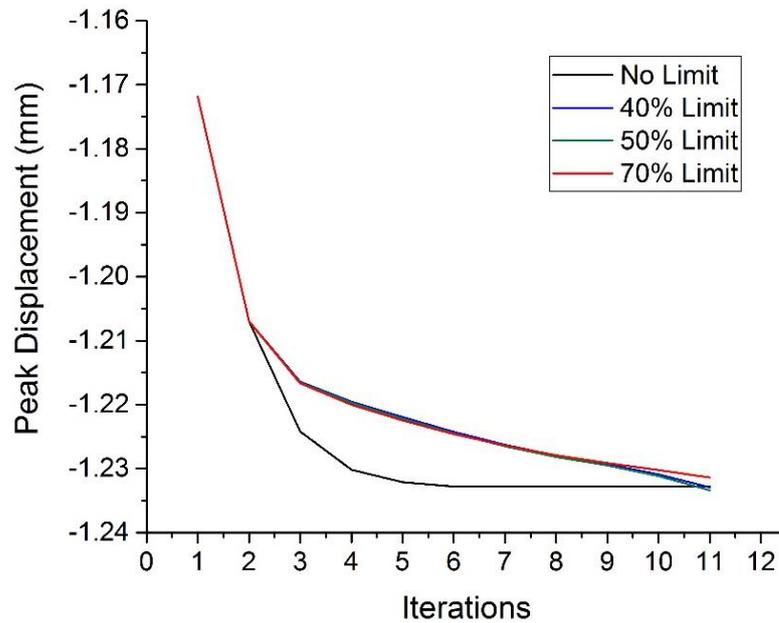
Figure 6-15, Iterations against peak displacement for different percentage limits on cumulative modulus reduction, compared against the original response with no limit.

6.3.3. Conclusions

As a result of these sensitivity studies, it was not clear how the equations might be modified to improve the results consistently for all models. Therefore, the published reduction equations were applied in their original form to investigate the response over a larger set of vertebrae. However, the inclusion of a limit on the cumulative modulus reduction over multiple cycles did appear to prevent some issues with excessive strains occurring in a small number of elements, so a cumulative limit of 50% was adopted for the subsequent modelling.

6.4. Fatigue Modelling Results

This section covers the results for specimens from each experimental load group, discussed in Chapters 3 and 4, and modelled using the fatigue simulation script and the methods described in Chapter 5.3. Models from each experimental load group were run, using the cumulative limit on modulus reduction, to gain an understanding of the spread of responses. Each vertebra has experimental data and a finite element response that could be compared. As there was large variability between specimens, comparisons were made on a case-by-case basis to attempt to assess for which cases the model has best predictability, with results from two models from each load group shown below in Figure 6-16 to Figure 6-23. The peak displacement against cycles curves were compared to experimental peak displacement trends, and the peak displacement values were compared. Equivalent plastic strain was compared to microCT scan fracture locations, which were identified and can be located by red arrows in the results images. Plastic strain contour plots from the finite element outputs were capped at 0.5 as the maximum value, shown in red, to enable comparison between vertebrae.

It was found firstly that the FE models predicted an accelerated response of the vertebrae to cyclic loading, largely underestimating the number of cycles to failure. Different levels of agreement between FE and experimental displacement trends and plastic strain distributions were seen. Two types of response were typically seen when all models that were ran were taken into account: models with large displacements and plastic strain distribution in the vertebral body failing quickly within less than ten iterations; and models with localised plastic strain distributions, typically at the cement loading plate-bone interface, not showing yield behaviour and reaching a plateau in displacement. From the examples presented, Figure 6-18, Figure 6-20, Figure 6-21 and Figure 6-23 fall into the first category, and Figure 6-16and Figure 6-17 show the latter case, with no clear plastic strain distributed through the vertebral body. Specimens in Figures 5-19 and 5-22 showed a very concentrated distribution of plastic strain in the anterior wall of the vertebrae, which in Figure 5-19

appeared to cause a protrusion of elements away from the surface as a result of the anterior tilt of the top plate. From qualitative assessment, the areas of high plastic strain appeared to relate well to fracture location in the specimens shown in Figures 6-18, 6-19 and 6-23. Displacement trends were seen to follow a similar curve in Figures 6-19, 6-20 and 6-22.

60% Load Group
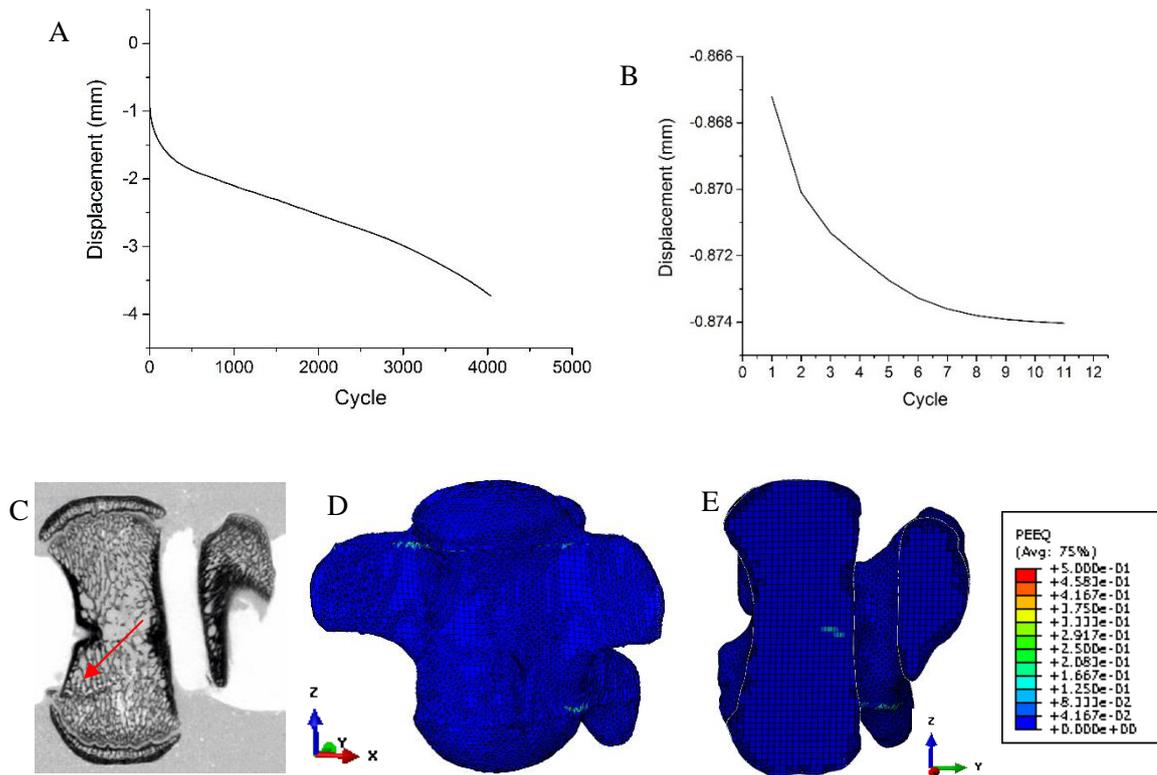
Figure 6-16, Fatigue results for T12CC1: A) Experimental and B) FE cycles against displacement; C) Post fatigue microCT; D) Anterior and E) Sagittal section of plastic strain distribution.
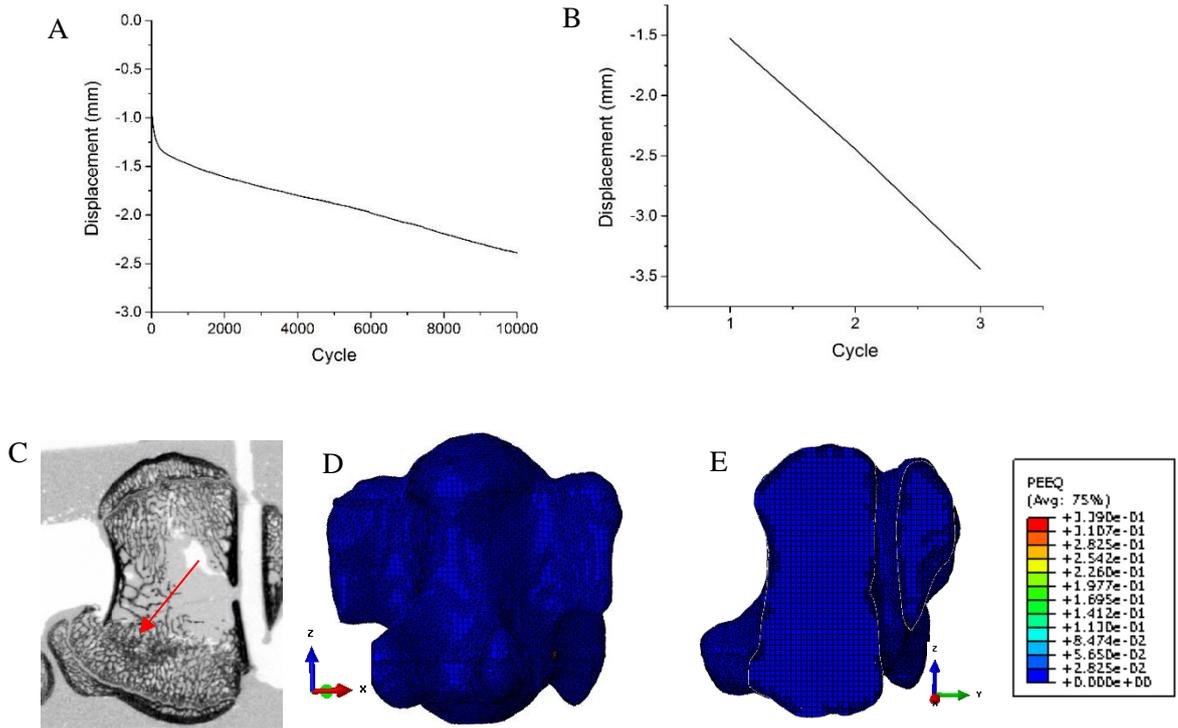
Figure 6-17, Fatigue results for T14CC2: A) Experimental and B) FE cycles against displacement; C) Post fatigue microCT; D) Anterior and E) Sagittal section of plastic strain distribution.

70% Load Group
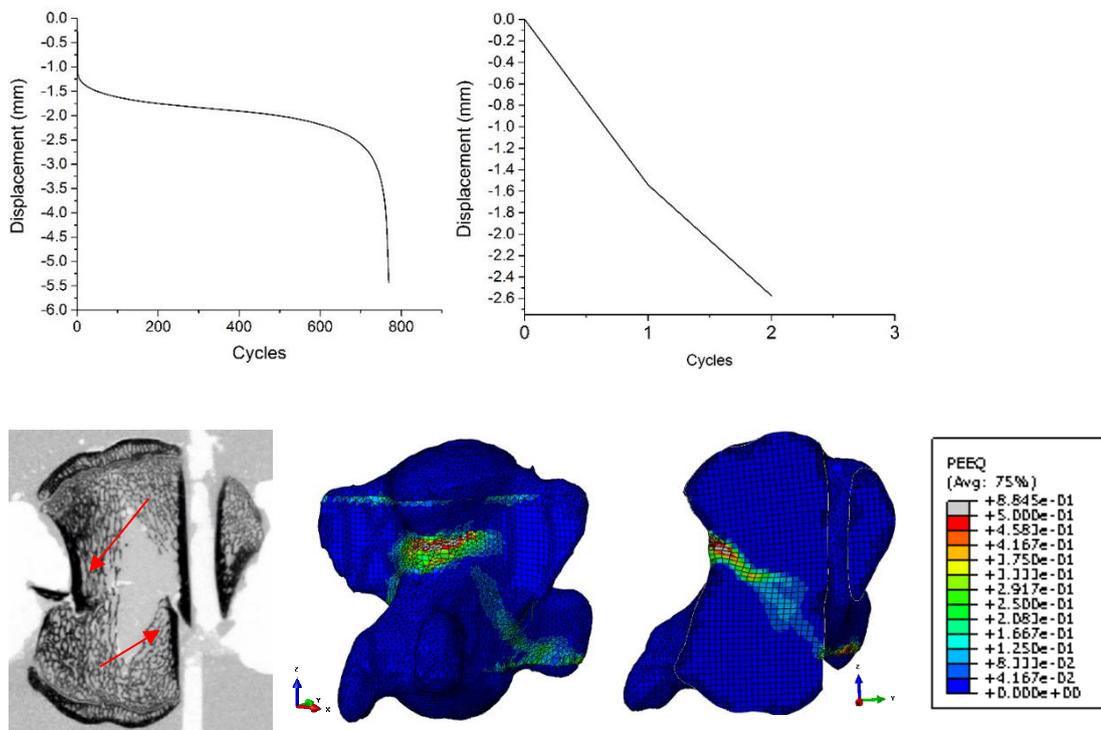
Figure 6-18, Fatigue results for T11CC4: A) Experimental and B) FE cycles against displacement; C) Post fatigue microCT; D) Anterior and E) Sagittal section of plastic strain distribution.
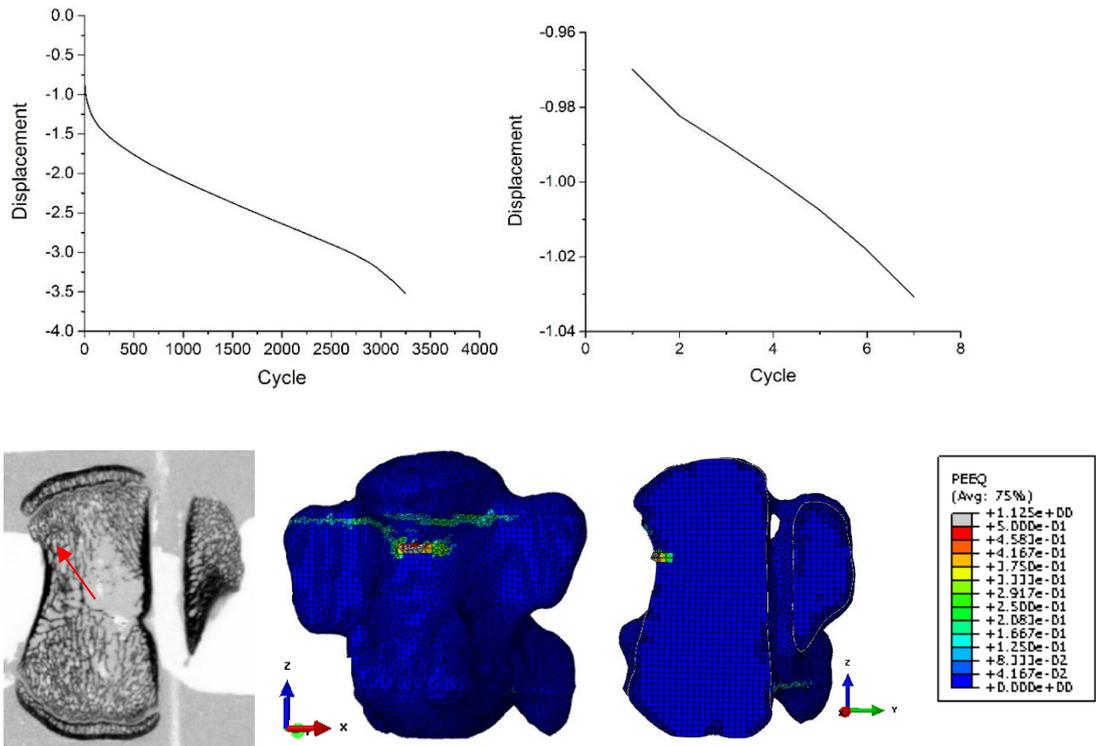
Figure 6-19, Fatigue results for T12CC2: A) Experimental and B) FE cycles against displacement; C) Post fatigue microCT; D) Anterior and E) Sagittal section of plastic strain distribution.

80% Load Group
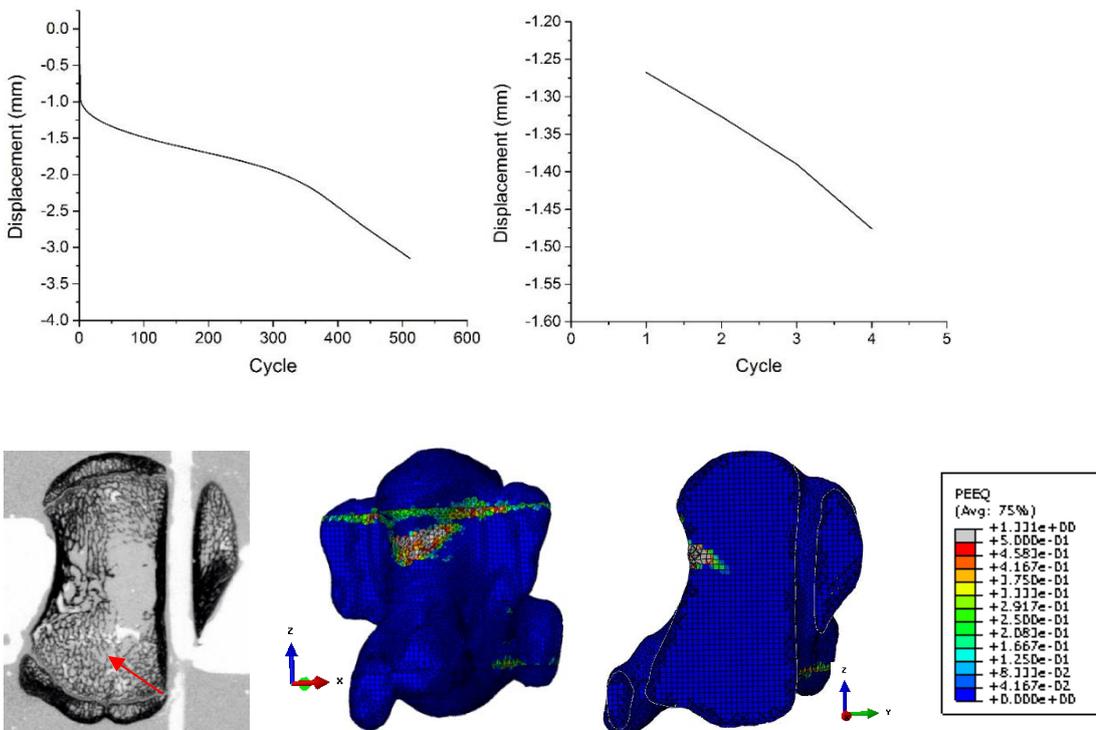
Figure 6-20, Fatigue results for T14CC3: A) Experimental and B) FE cycles against displacement; C) Post fatigue microCT; D) Anterior and E) Sagittal section of plastic strain distribution.
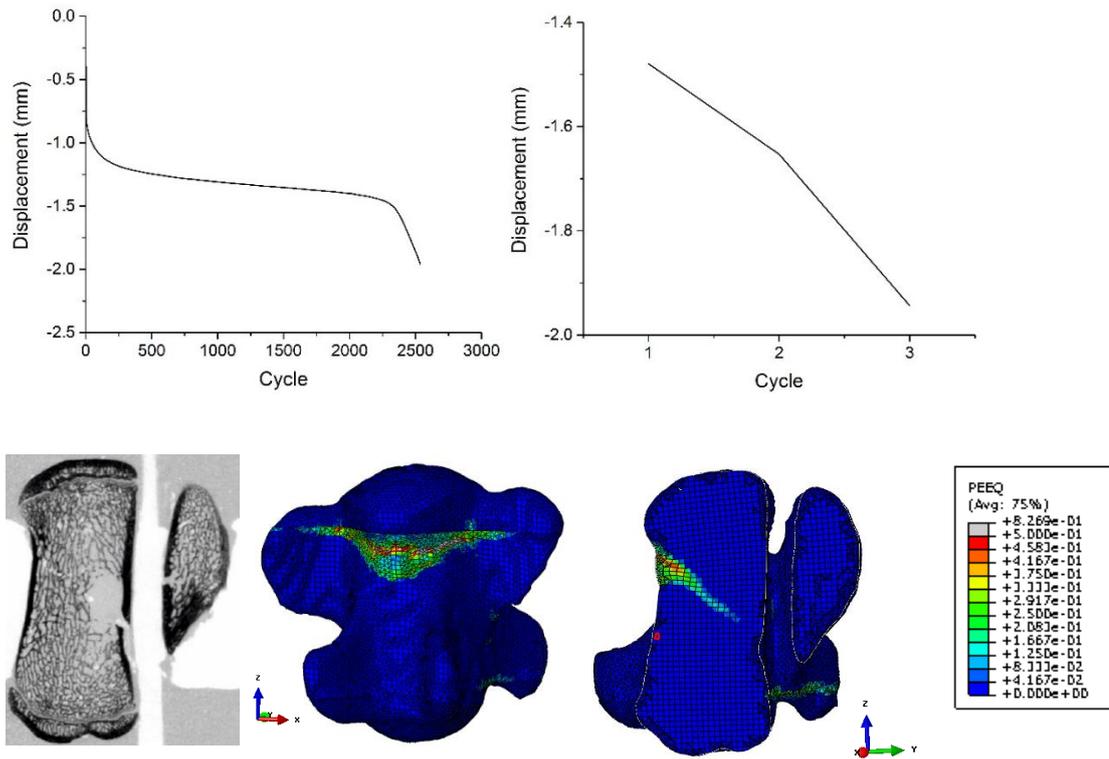
Figure 6-21 Fatigue results for T15CC2: A) Experimental and B) FE cycles against displacement; C) Post fatigue microCT; D) Anterior and E) Sagittal section of plastic strain distribution.

90% Load Group
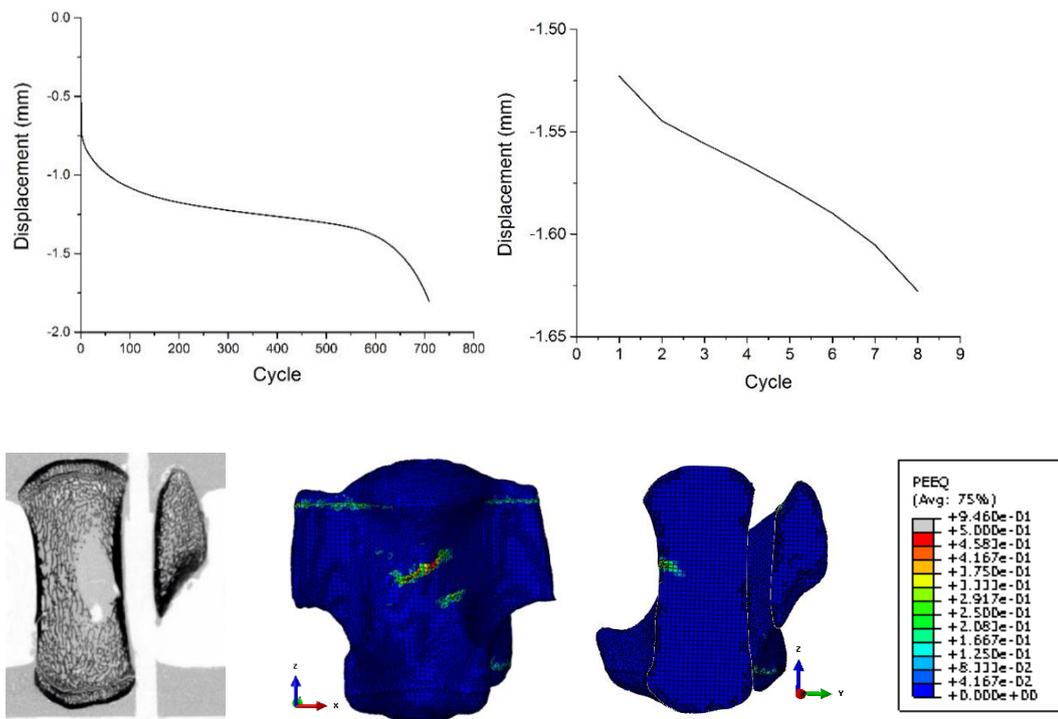
Figure 6-22, Fatigue results for T13CC2: A) Experimental and B) FE cycles against displacement; C) Post fatigue microCT; D) Anterior and E) Sagittal section of plastic strain distribution.
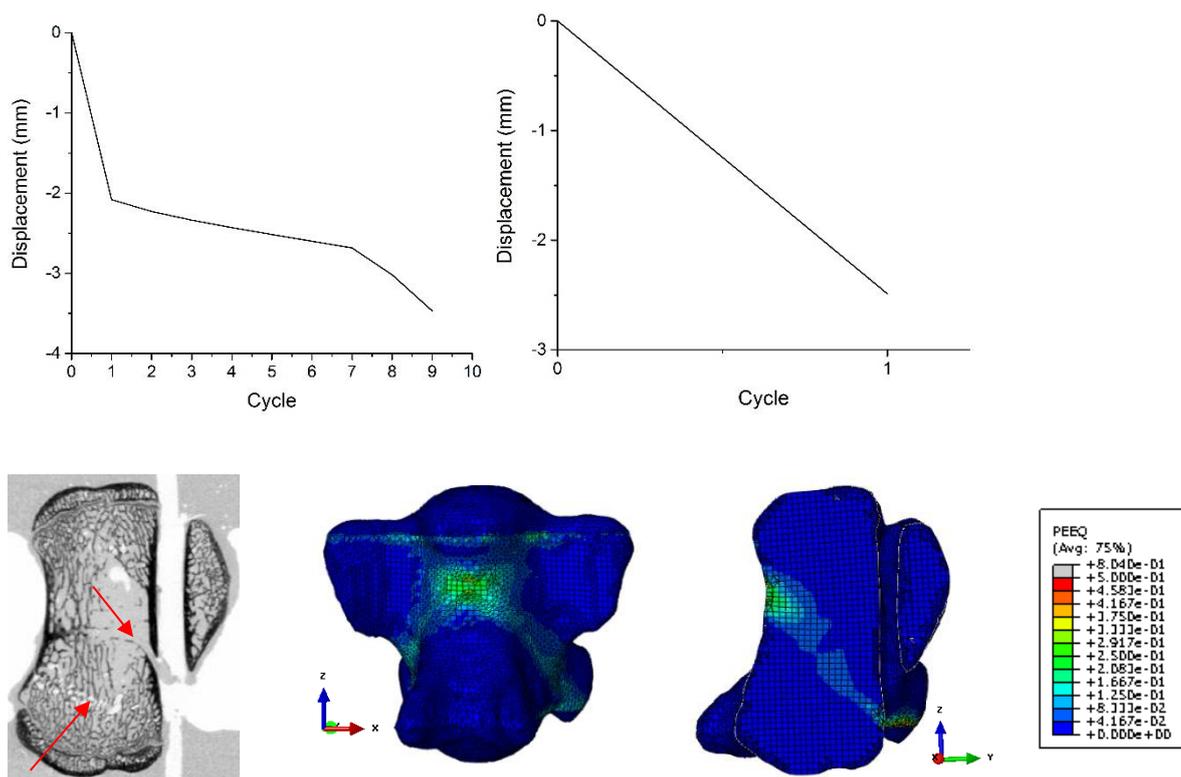
Figure 6-23, Fatigue results for T7CC3: A) Experimental and B) FE cycles against displacement; C) Post fatigue microCT; D) Anterior and E) Sagittal section of plastic strain distribution.

6.4.1. Analysis of Displacement and Plastic Strain Trends

There was no clear relationship between FE number of iterations and experimental cycles to failure, due to the inconsistency between the point at which the models 'failed', as this is the point at which they could no longer solve. This could be caused by failure of a single element not solving or by excessive displacement across the whole vertebral body. Therefore comparisons between experimental and computational results were focussed on plastic strain locations and amount of displacement. An example of the typical displacement distribution seen in one of the models is shown in Figure 6-24. Allowing for anterior rotation of the top cement plate means that in all cases this type of response is seen under load, with a greater anterior displacement. This represents what was observed experimentally, where most displacement and fractures were anteriorly located and caused varying amounts of anterior downwards tilt of the top cement loading plate.
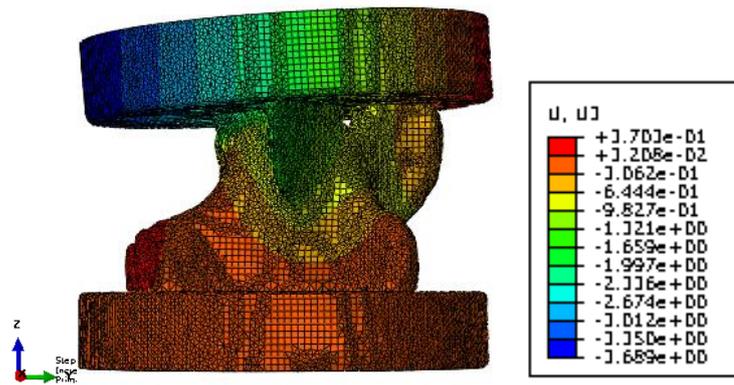
Figure 6-24, Typical displacement T15CC2, showing tilt of top PMMA plate. Peak axial displacement is shown in blue, and least, or zero, displacement in red.

Results vary between plastic strain indicated within the vertebral body and plastic strain only occurring at the cement-bone interface, due to the constraints of the boundary conditions. In a number of cases similar levels of displacement were seen between the experimental yield point and FE results, typically when plastic strain was predicted in the vertebral body. To assess this correlation, experimental displacement at the point of yield was compared directly to the displacement of the models at the second iteration. The second iteration was chosen as a consistent point which all models aside from one reached, whilst still allowing the models to undergo material property changes. In the case where only one iteration was completed, the peak displacement at this point was used. The models were split into the group with plastic strain in the vertebral body, or vertebral body and cement interface, and those with plastic strain only at the cement interface. The comparison is shown in Figure 6-25. Good correlation and was seen in cases where plastic strain was seen in the vertebral body, with an R^2 of 0.79, compared to an R^2 of 0.37 in the cases with plastic strain only at the cement interface. This prediction of high strains at the cement interface is not representative of reality and is due to model sensitivity to boundary conditions between the bone and cement materials. The main difference between these two groups both experimentally and in the models is the peak load value, which varies due to both the initial failure load of the specimen and the assigned experimental load group. The specimens which

accumulated plastic strain in the vertebral body were loaded to an average value of 7245 ± 841N and the group with only cement interface strain were loaded to an average of 5298 ± 694N. If the load required to cause failure in the main body of the vertebrae is higher than that required to cause yield at the cement interface then this response does not occur in the lower load cases where elements with high strains at the interface region prevent the model from solving before yield can occur in the vertebral body.
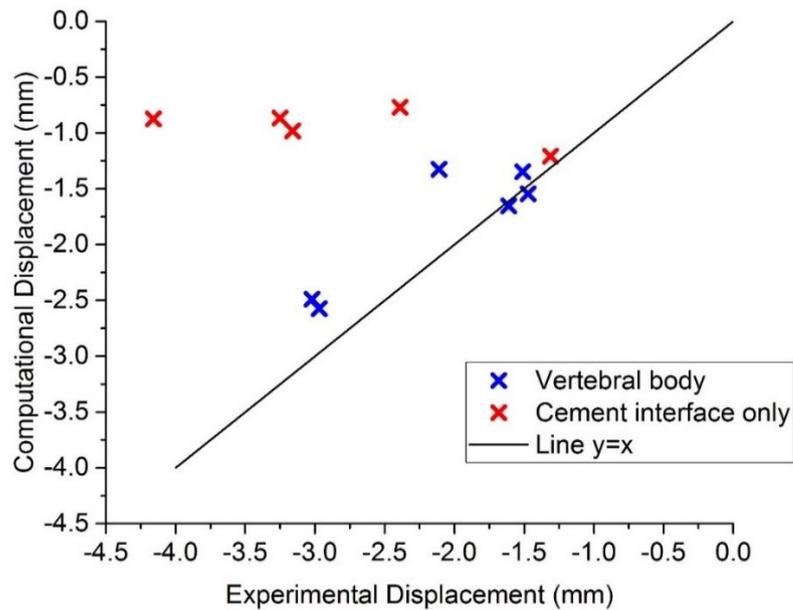
Figure 6-25, Experimental displacement at yield compared to FE displacement from cycle 2, for the group of vertebrae that saw plastic strain in the vertebral body compared to those that saw plastic strain only at the cement-bone interface. Line y=x shows perfect agreement, R^2 = 0.79 for vertebral body group and 0.37 for interface only group.

6.4.2. Summary and Discussion

Models were initially validated for a linear-elastic static loading case with density-based element Young's modulus properties for elements representing vertebral bone. These results showed good agreement within the range seen previously for other specimen-specific modelling studies using similar techniques and contributed to a comparative study by Zapata-Cornelio et. al (Zapata-Cornelio et al., 2017), which showed a concordance of 0.39 for porcine vertebrae, and 0.23 for ovine vertebrae. Wijayathunga et al. saw a root mean

square error of 12.9% between FE and experimental stiffness of human vertebrae, using a similar method to that used in the current study which saw a mean error of approximately 8.6% in the linear elastic models and approximately 24% in the non-linear models. Other studies have quoted agreement in terms of correlation, of R^2 value, for instance Liebschner et al. (Liebschner et al., 2003) who $R^2=0.81$ for a FE predicted stiffness of human vertebrae, however this was for a calibration set rather than validation.

Yield strain was then calibrated using a similar optimisation approach to determine a single value of yield strain for bone elements whilst yield stress varies with element Young's modulus to capture variance between bone densities, and therefore different areas of bone as well as different vertebrae. However the results indicated that yield strain may also vary within or between specimens as agreement from the optimisation was not as robust as was seen for the Young's modulus. Additionally, when the models were simulated over cyclic loading, in a number of cases the models could no longer solve after one or two iterations due to excessive plastic strain. It is reasonable to assume that in such cases the yield strain may be higher than in others. To assess the effect of changing the yield strain, one specimen that showed yield behaviour throughout the vertebral body within the first iteration, T7CC3, was run with three yield strain values, 0.047 (the original optimised value), 0.06 and 0.08. The results for the displacement response are shown in Figure 6-26, it can be seen that the two increases allow the model to go from instant 'failure' (i.e. no longer able to solve) to failure within three iterations and then to a point where the model does not fail.
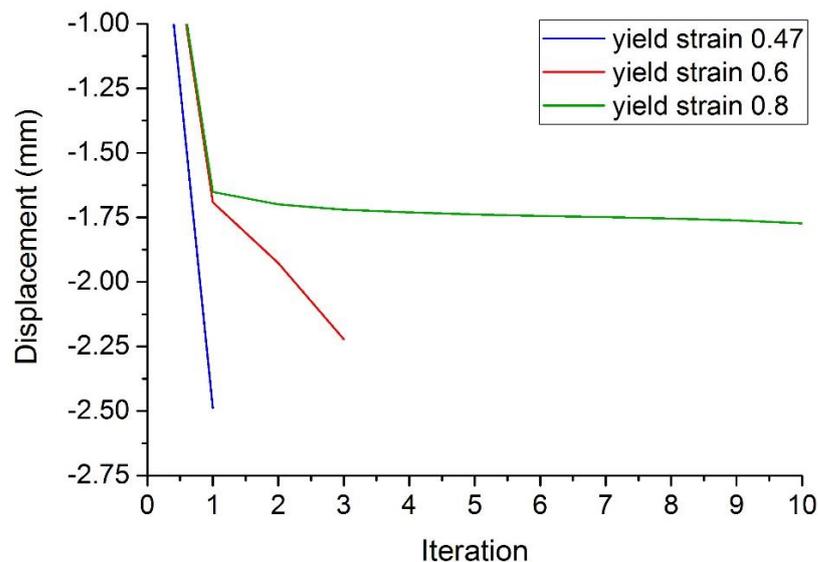
Figure 6-26, Response of vertebra T7CC3 with three different yield strain values, 0.047 (the original value from the optimisation), 0.06 and 0.08.

There is little literature on the yield strain of whole bovine vertebrae, rather than just for smaller samples of trabecular bone and bone cores. These latter have been found to be typically less than 1% yield strain, but considering such samples do not include denser cortical bone or spinal processes, the inclusion of these features would be expected to increases the yield strain (Kopperdahl and Keaveny, 1998; Nagaraja et al., 2005).

Sensitivity Analyses

The sensitivity of the models to the parameters in the reduction equations was explored in depth to assess means of tuning the material reduction process to improve the results for the vertebrae tested in this study. It was found that altering the equations can change the number of iterations before the models could no longer solve and the speed of the overall displacement accumulation; however no great improvement in the distribution of plastic strain through the vertebral body was seen. It was found that the models were also affected by the peak load, amongst other parameters. Further investigation has shown the models to be highly sensitive to boundary conditions and interaction properties between the PMMA cement loading plates and the vertebral body.

Previous studies have shown models are sensitive to boundary conditions, specifically to the location of the point load application in the static modelling case (Jones and Wilcox, 2007). To investigate the effect of variation in the loading boundary condition on displacement and plastic strain, the constraints at the point load application were explored. In the experimental testing it is assumed that load is only applied axially with no translation in the x and y directions, however there is still a possibility of translation of the upper cement plate. An example model was run with and without x and y translation constraints at the load location point, using the iterative modelling approach and the experimental load value. The difference in displacement response and plastic strain distribution can be seen in Figure 6-27. There was a clear difference between the two responses, with the constrained case displacing far less and with few elements reaching yield point. However, in the case where there was no x-y constraint, the opposite was true, with large displacements seen over two cycles and plastic strain accumulation through a large area of the vertebral body. This results shows the importance of accurately representing in vitro conditions through boundary conditions, and could be used to improve results in future work. In this study the ball is kept under the loading point, but the metal platen under the ball, although indented, may slide a small amount as well as just allowing rotation, and there may also be some bending in the loading column. Therefore it is likely that the experiments are more like the fully constrained version but not completely and it might be useful to determine a method of constraining the ball and preventing any bending in the load string in future.
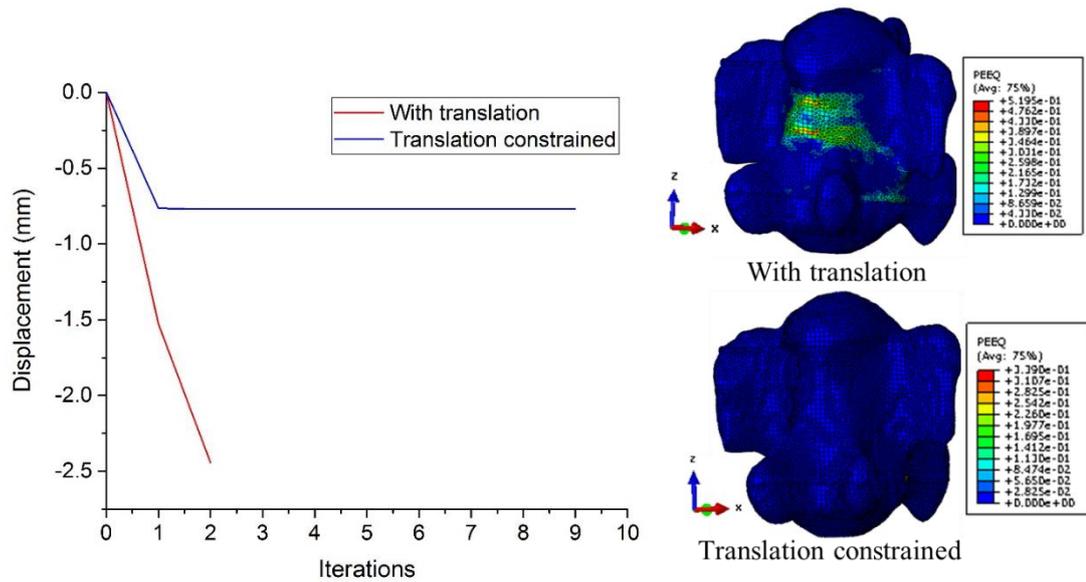
Figure 6-27, Results for a model with boundary conditions allowing translation of the model in the x and y directions at the point of load application and then with this translation constrained, as was used in the main study to best represent the experimental tests.

In a number of specimens modelled in this study large plastic strains were seen at the bone-cement interface, where a tie constraint is used between the vertebrae and PMMA loading plate. This constraint is the cause of the increased stress in these areas and, although sufficient to model a linear-elastic case, it is not the optimum method for modelling plasticity and yield. Therefore a model was run with a frictionless contact instead of the tie constraint between the vertebrae and cement on both the upper and lower interfaces to reduce the stress increase caused by over-constraint of nodes, Figure 6-28. It was found that under these conditions models could not solve in the first iteration. In the example shown in Figure 28, it can be seen that the plastic strain seen was very small and only occurred in a very small number of elements, suggesting this is not the reason for model failure, but rather the boundary condition itself. In the experiment the cement does not bond to the vertebrae so there is potential for some movement between the two surfaces, however nor is this frictionless, so a property somewhere between the two extremes is more likely to represent

reality. To investigate this condition further, the models would also have to be re-optimised for material properties as this change significantly affects the model solution results.
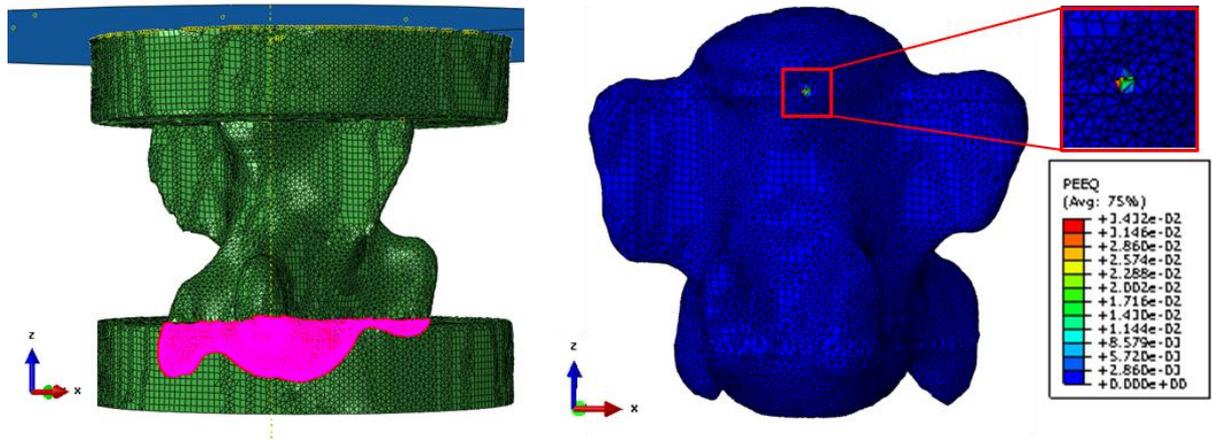
Figure 6-28, Lower bone-cement interface highlighted and changed from tie to frictionless contact, with result from a single load to 1kN, showing localised plastic strain at the interface.

6.4.2.1. Summary of Fatigue Study Results

Using the original published material property reduction equations with the addition of a limit on the cumulative reduction of Young's modulus, a set of specimen-specific vertebrae were modelled under experimentally relevant loads. It was found that the reduction method largely accelerates the response of the vertebrae compared to experimental results, in that similar levels of displacement occur and in some cases similar displacement trends, but over a much smaller number of cycles. This may be due to the fact that the fact that the original equations were determined for whole bone core specimens then applied to an element level scale. However, in cases where good plastic strain distribution was predicted, i.e. strain seen in the vertebral body rather than in a small number of poorly shaped elements at the cement interface, good agreement was seen between the experimental and FE predicted total displacement. Additionally qualitative assessment of locations of high plastic strains in these cases broadly match with the location of fractures seen in the experimental fatigue testing. There are a number of ways this procedure could be optimised to better represent the type of

vertebrae used in this study, including modifications to the reduction equations, improvement of boundary conditions and determining whether varying yield strain is necessary to more accurately capture variation between specimens. However the results are still promising and can be taken forward into studies investigating how treatments such as vertebroplasty could affect the vertebral body stiffness and how predicted fracture locations of the vertebrae are affected by vertebroplasty under fatigue loading conditions.

7.Fatigue Simulation Methods for Vertebroplasty

7.1.Introduction

The aim of the work reported in this Chapter was to apply the fatigue testing methods to vertebroplasty treatment. As discussed in Chapter 2, there is still considerable debate over the efficacy of vertebroplasty, and further investigation into the mechanical effects of the treatment could help shed light on the most appropriate use. Whilst mechanical testing is informative for the specific type of vertebrae and augmentation protocols tested, a validated finite element simulation allows for investigation into a wider variety of vertebrae and treatment parameter variations. This would facilitate investigations into different patient groups, defined by parameters such as bone mineral density (BMD), size, vertebral level, and accounting for other pathologies. Additionally a finite element model would allow for investigations into variations in cement fill, mechanical properties of the cements and cement distribution within the vertebrae. This combined with the ability to simulate longer term cases through fatigue testing can help further our understanding of vertebroplasty treatment for spinal fractures.

Therefore this chapter covers preliminary studies investigating the translation of the fatigue methodologies developed throughout this work to the application of simulating vertebroplasty. Firstly the vertebroplasty procedure developed in the laboratory for the augmentation of bovine tail vertebrae is presented. Fatigue tests of augmented vertebrae are then reported using methods described in Chapter 3, and results are compared to the non-augmented vertebrae results discussed in Chapter 4. Finally, the addition of variable yield properties to specimen–specific finite element models adapted to include cement augmentation is reported as a preliminary step towards using the iterative modelling technique with augmented vertebrae models.

7.2. In Vitro Tests

Bovine tail vertebrae were prepared, dissected into individual vertebral specimens and tested to failure in a materials testing machine (Instron 3366, UK) as described in Chapter 3. A bi-pedicular percutaneous vertebroplasty technique was then used, initially demonstrated by practicing spinal surgeons (Mr Almas Khan and Mr Vishal Borse, Leeds Teaching Hospitals NHS Trust). This part of the project was undertaken in collaboration with fellow doctoral student Gavin Day, who carried out a number of the vertebroplasty procedures and the static mechanical testing post-augmentation on specimens used in this study. The present author was involved in the development and practice of the vertebroplasty procedure and performed all subsequent fatigue testing and data analysis. A flowchart briefly describing the series of tests undertake for the augmentation methodology is shown in Figure 7-1.
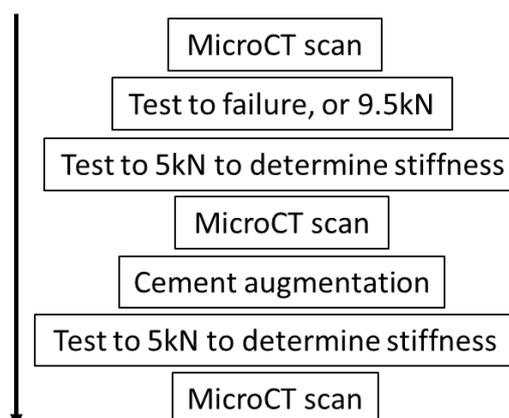
Figure 7-1, Flowchart showing sequence of tests and vertebroplasty procedure.

7.2.1. Methods

7.2.1.1. Specimen Preparation

The cement augmentation procedure was undertaken using a vertebroplasty kit comprising a cannula with a retractable inner needle. A side opening cannula was used; this redirects the cement flow laterally and reduces the chance of leakage compared to a front-opening cannula (Heini and Allred, 2002). Prior to cementing, specimens were heated in a water bath up to 37.5°C allowing fatty bone marrow within the trabeculae structure to develop

sufficiently low viscosity to be displaced by the cement, enabling cement to flow into and through the trabecular structure. A small portion of cortical shell was removed from the end of each pedicle to make it possible to insert the cannula through the trabecular bone beneath. Markings on the cannula were used to visually assess the depth and angle required for the needle to reach the central anterior region of the vertebral body. A 1:1 PMMA cement powder to liquid component ratio was used, and the powder consisted of 20wt% BaSO4 (the contrast agent barium sulphate), to ensure the cement was radiopaque on microCT scans. The needle was inserted to the required depth into each pedicle to form a channel and then removed. Subsequently a syringe with PMMA was attached to the cannula and a target volume of 3-4ml of cement was injected into each pedicle. The PMMA was backfilled into the injection channel as the needle was being removed, so as not to leave voids where the cannula had been. The procedure is shown in Figure 7-2. It was always possible to inject cement into the vertebrae. However leakage was seen in most cases, with cement passing through the vascular channels, including through the posterior channel into the neural canal. This made it difficult to assess the amount of cement successfully injected into the vertebra itself, therefore the injection process was continued until high pressure was felt on the syringe. Preliminary trials of the injection process were done on vertebrae not planned to be taken forward for further mechanical testing. These vertebrae were dissected after augmentation to assess the distribution of the cement and the integration into the trabecular structure. Images of the dissected specimens are shown in Figure 7-3, where it can be seen that cement has leaked into the spinal canal in all three examples.

Figure 7-2, A) Vertebroplasty cannula inserted into the pedicles of a bovine tail vertebra, B) Syringe with cement attached to cannula, C) Injection into the vertebra.

Figure 7-3 Photographs depicting transverse dissection of vertebrae after augmentation from three example specimens. Cement leakage into the spinal canal is visible in all cases.

7.2.1.2.   Fatigue Testing

To assess the effect of the augmentation on the fatigue behaviour of bovine tail vertebrae, a set of eleven specimens were prepared, augmented and tested under fatigue loading in the same manner as the non-augmented vertebrae described in Chapters 3 and 4. The amount of cement able to be injected into the vertebrae varied between 2.9ml and 16.7ml. For these

vertebrae, additional static tests of up to 5 kN compressive loading were conducted after the test to failure and after subsequent vertebroplasty. Due to the smaller specimen set and large variations between individual specimens, plus the additional variation caused by the augmentation and difficulties found in keeping cement fill consistent, the vertebrae were all tested at 80% of the initial load to failure. As described in Chapter 3, fatigue testing was carried out in a dynamic materials testing machine (Instron Electropuls e10000, Instron UK), and vertebrae were loaded between 50 N and the specimen-specific peak load value at a frequency of 1 Hz. Tests were run until yield behaviour was seen or until 10000 cycles had been achieved. MicroCT scans were taken of vertebrae used in this study before testing, after augmentation and after fatigue testing.

7.3. Results

MicroCT imaging was used to assess the distribution of PMMA cement after the vertebroplasty procedure. Scan images from immediately before and after cement augmentation, and after the fatigue tests are shown for three examples in Table 7-1. As image colours have been inverted for clarity, cement can be identified as very dark areas in the images, since the addition of a radiopaque agent in the PMMA meant the cement appears as a very dense substance. Additionally 3D reconstructions of the scans with the cement masked inside the vertebrae are depicted. Different cement patterns were seen and figures in Table 7-1 show examples of each type seen. The first example, T1CC1, cement was successfully injected into the vertebral body, but also leakage in the canal and through the anterior vascular channel. The second example, T2CC1, shows a case where the majority of the cement leaked into the canal, with only a small amount remaining in the vertebral body. In the third example, T2CC2, no cement leakage was observed. In the three examples below, severe fracture near the inferior cement plate was observed in the third example, whilst in the first two no visible signs of fracture on the CT scans could be seen.

Table 7-1, MicroCT image data for three example vertebrae after the initial static load, augmentation and after fatigue testing.

Specimen	After Static Test	After Augmentation	3D Reconstruction	After Fatigue
T1 CC1				
T2 CC1				
T2 CC2				
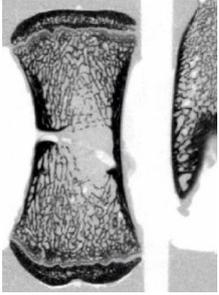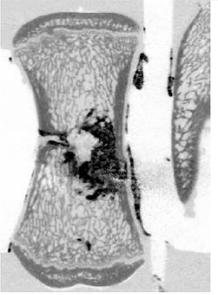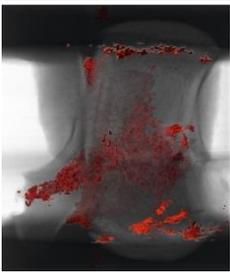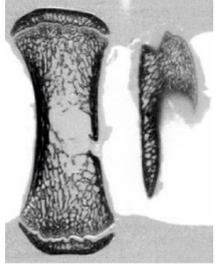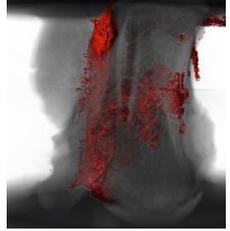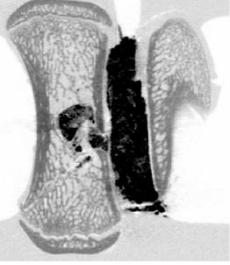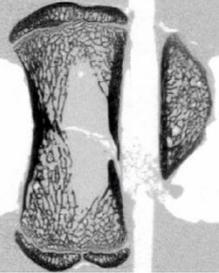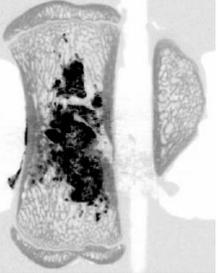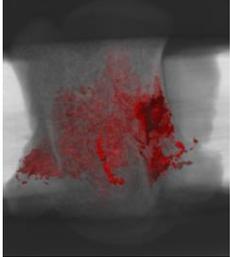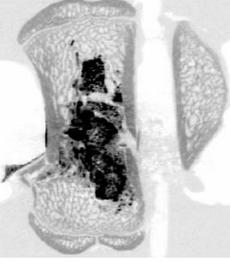
From the static test to failure, the non-destructive test undertaken immediately afterwards and the test after augmentation, see Figure 7-1, three values for elastic stiffness were calculated using the automated method described in Chapter 2. Briefly, the gradient of the load-displacement curve was found over consecutive 0.6mm sections in increments of 0.1mm, and the greatest stiffness value from these calculations was the mechanical stiffness value used. The stiffness values at each stage of testing for each specimen are shown in Figure 7-4. Since large differences in the initial change in stiffness were observed, this allows the mechanical effects of the initial test to failure and the subsequent augmentation to be assessed. In ten cases out of 11, the stiffness reduced as a result of the first test; six of these nine cases saw an increase in stiffness after augmentation, showing some evidence that

augmentation can increase the stiffness. In a number of cases the changes in stiffness after augmentation were subtle, and restoration to the value of the intact stiffness, or greater than the intact stiffness was seen in two cases.
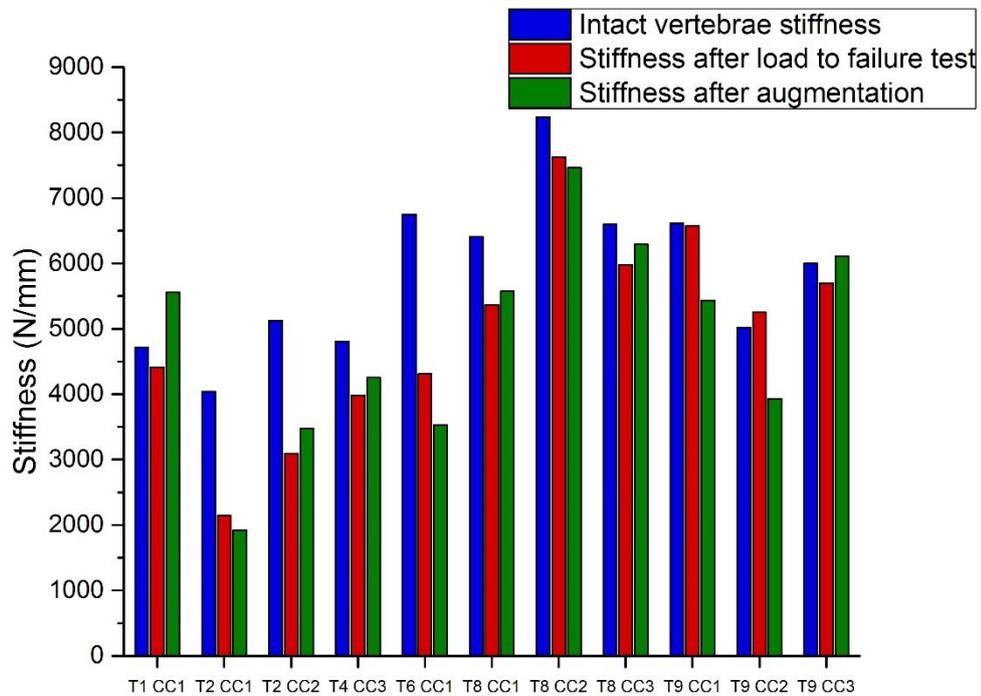
Figure 7-4, Stiffness before and after the test to failure and after the subsequent augmentation, taken from load-displacement data for each specimen.

Cycles to failure for the un-treated and augmented vertebrae in the equivalent 80% load group are shown in Figure 7-5, with box plots depicting median, 25th and 75th percentile and range. No significant difference was seen between the two groups (p>0.05). All specimens in the un-treated group tested at 80% failure load failed below 2500 cycles whereas there was a greater spread in the augmented group, with one vertebra not showing failure behaviour before 10000 cycles, identified as an outlier on the box plot. This in part is due to the greater number of specimens in the augmented group, and it can be seen that the median cycles to failure between groups is similar. Mean cycles to failure for the untreated group

was 1176±938 cycles, and for the augmented group, excluding the outlier, was 1898±2057 cycles.

Additionally the average change in stiffness for the un-treated and augmented groups is shown in Figure 7-6. These values were taken from the tenth cycle, allowing ten cycles for pre-conditioning, and the final cycle. The un-treated group stiffness decreased from 8540 ± 1437N/mm to 5374 ±1348N/mm whilst the augmented group stiffness decreased from 9686 ±1030N/mm to 7672 ± 976: a 37% decrease for the un-treated group compared to a 21% decrease for the augmented group. The mean stiffness at the end of the testing appears noticeably greater for the augmented group, however a one-way ANOVA concluded this was not statistically significant (p>0.05). Additionally it was found that the reductions in stiffness were not significant between the two groups.
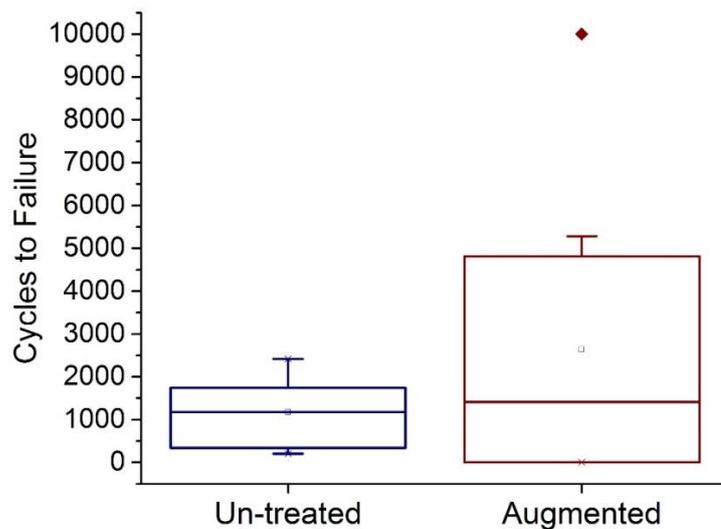
Figure 7-5, Cycles to failure for vertebrae from the un-treated group and augmented vertebrae. Specimens in both groups were loaded to 80% of their individually-determined failure loads. Box plots show median, 25th & 75th percentile and range.
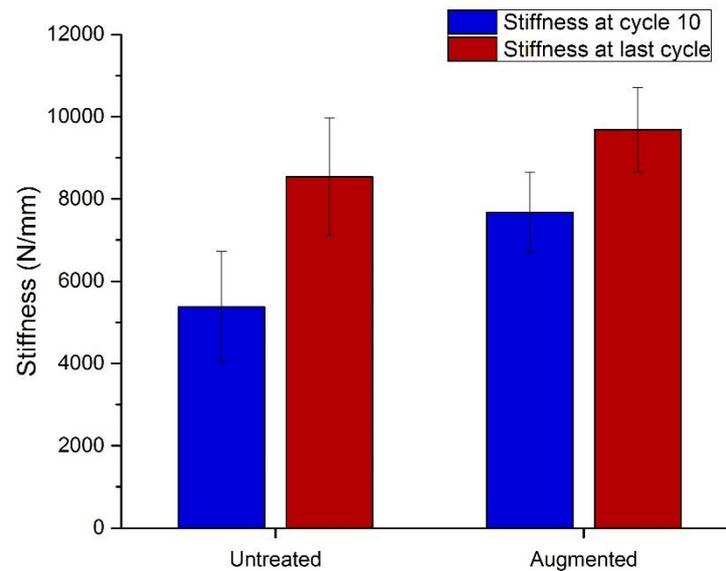
Figure 7-6 Mean stiffness values near the beginning and end of the fatigue tests for un-treated group and the augmented vertebrae, also tested at 80% of the initial yield load. Values are taken from the tenth cycle and the final cycle.

A number of possible relationships between parameters were investigated to establish whether the augmentation affected the fatigue results. The reconstructed microCT scan data was used to determine the cement fill by separately masking the bone and cement regions (see Chapter 2, section x for segmentation methods). The relationship between percentage cement fill achieved during vertebroplasty and the number of cycles to failure is shown in Figure 7-7. No correlation was seen, however there was a large variation in the amount of cement injected into the vertebrae, with very little cement injected in some cases. It can be seen that fills ranged from approximately 2 to 17%.
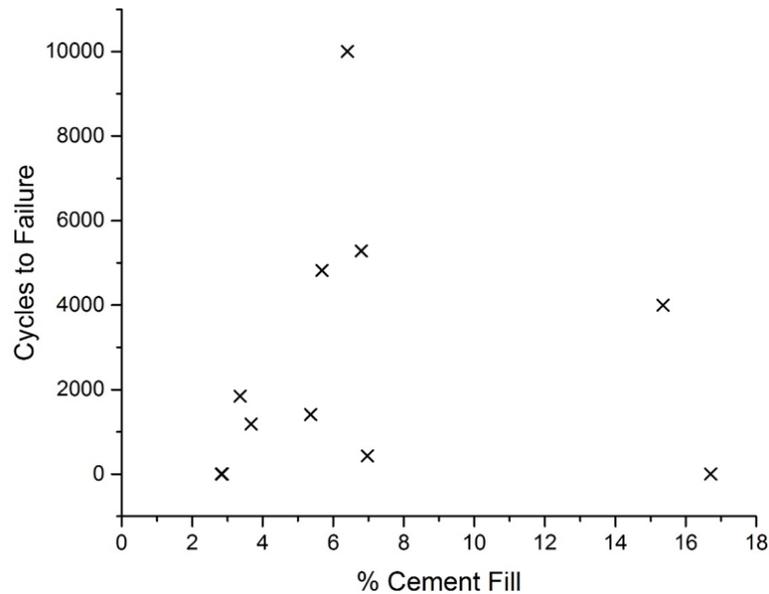
Figure 7-7, Relationship between percentage cement fill of augmented vertebrae and number of cycles to failure. No correlation can be seen between amounts of cement and fatigue performance.

To take account of the variations in vertebral geometry, the load and vertebral compression were normalised to stress and strain values. Strain was calculated by taking dividing the change in height at the end of the test to the initial specimen height from scan data and stress was determined by dividing the applied load by an approximated cross sectional area, found by dividing total vertebra volume by height, both taken from segmented microCT scan data. Stress and strain values were calculated at peak load during the cyclic testing.

The relationships between strain and number of cycles to failure, and stress against number of cycles to failure are shown in Figure 7-8 and Figure 7-9 respectively depicted in log(S)-log(N) curves. For both groups no correlation was seen between strain and number of cycles to failure, suggesting vertebrae that fail after fewer cycles do not experience higher displacements. Plotting stress against cycles to failure shows an S-N curve, typically used in engineering materials to provide fatigue life for a material over a large range loads, or stresses. When plotted on a logarithmic scale, the S-N relationship can be represented by a straight line defined by a power law equation. This was plotted on the S-N curve shown in

Figure 7-9, calculated by an automatic fitting tool in Microsoft Excel (MS Excel 2013, Microsoft Corporation, USA). Regression analysis for the resulting line of fit showed low correlation was seen for both the un-treated and augmented vertebrae groups (R^2<0.3).
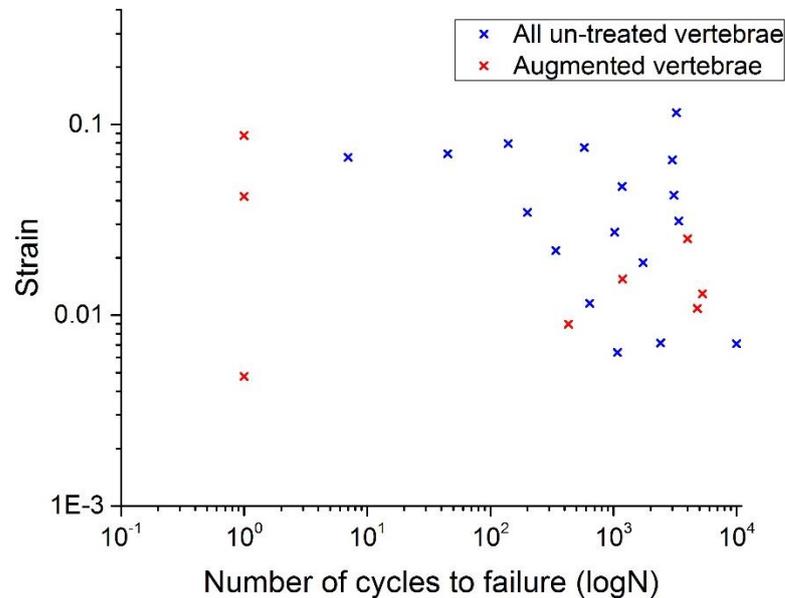
Figure 7-8, Maximum strain at peak against cycles to failure for all fatigue tested un-treated vertebrae and augmented vertebrae, plotted on a logarithmic scale.
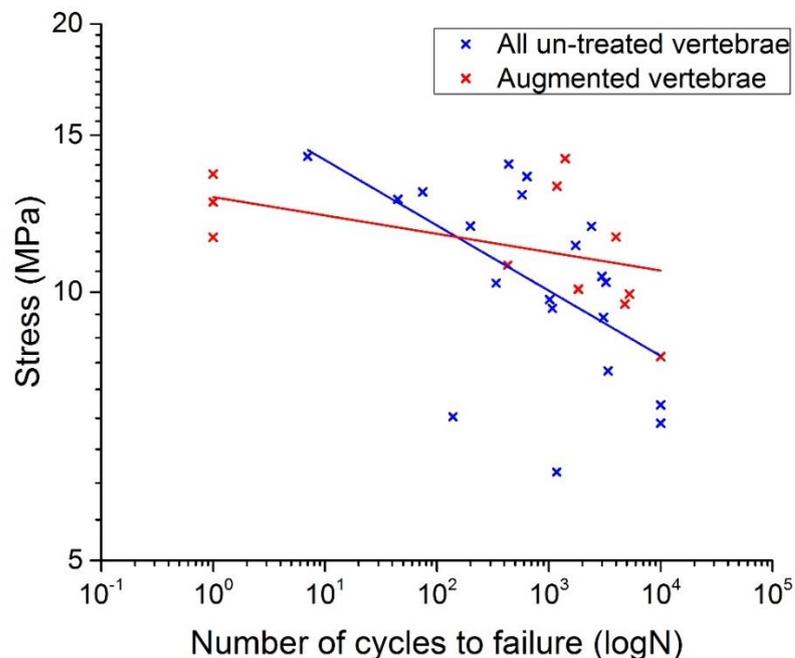
Figure 7-9, Maximum stress at peak against cycles to failure for all fatigue tested un-treated vertebrae and augmented vertebrae plotted on a logarithmic scale with a power law fit showing a correlation of R^2 < 0.31 and 0.29 for un-treated and augmented groups respectively.

7.4. Finite Element Simulation of Augmented Vertebrae

To assess the feasibility of using the developed FE fatigue methods to model augmented vertebrae, a method of modelling cement augmentation in the previously described voxel-based vertebrae models (Chapter 4) was adopted. The method was developed by PhD student Gavin Day (unpublished work, direct communication with Mr Day), adapted from a previous study that had shown proof of principle in a trabecular bone model (Sikora, 2013).

7.4.1. Methods

The method adopted gave the best agreement between FE and experimental stiffness predictions from a number of trialled methods when tested under 1mm displacement with a linear-elastic material model. The approach to modelling the vertebrae followed that described in Chapter 5, with additional steps used to segment and model the cement region within the vertebrae as follows. First, the cement was segmented using scan processing software (ScanIP V7.0, Exeter, UK), and the region was assigned homogenous material properties to represent bone cement (Young's modulus value of 2.45 GPa and Poisson's ratio of 0.3). Second, a boundary layer around the cement was defined using morphological dilate function in ScanIP. This layer was modelled with a low yield strain (0.005) to represent the region where there is a small amount of cement combined with possibly damaged trabecular bone. The models incorporated the elastic-plastic behaviour of the bone elements, using a constant yield strain of 0.047 as determined by the optimisation methods described in Chapter 4. Initially a single load of 9 kN was applied to the superior loading plate, representing the experimental load used in the static test, as the vertebrae models were created from intact scans, rather than scans after the static test as were used for the fatigue simulation models.

7.4.2. Results

None of the models that were tested were able to successfully complete a full solution, that is, to solve when the full 9kN load was applied. Models failed to solve even under far lower loads of 1kN. An example of a section view of an FE model of vertebra at the last iteration

before the solver failed to converge, with colour map representing peak equivalent plastic strain, is shown in Figure 7-10. Very large displacements and rotations of the superior cement plate were seen in all cases, and solutions were particularly poor when the cement interface layer coincided with the outer edge of the vertebral bone. Despite the low loads that could be applied prior to model failure, it can be seen that areas of plastic deformation in the anterior wall of the vertebrae are similar to regions of failure observed in some experimental specimens. Since the model could not be solved for sufficiently high loads to simulate the experimental fatigue modelling, no results could be obtained for the behaviour over multiple cycles. Re-optimising the model including the cement augmentation for new values of the greyscale density to Young's modulus conversion value and altering the yield strain value may improve these results. Additionally further investigations into the best representation of the cement-bone interface would be desirable for future work.
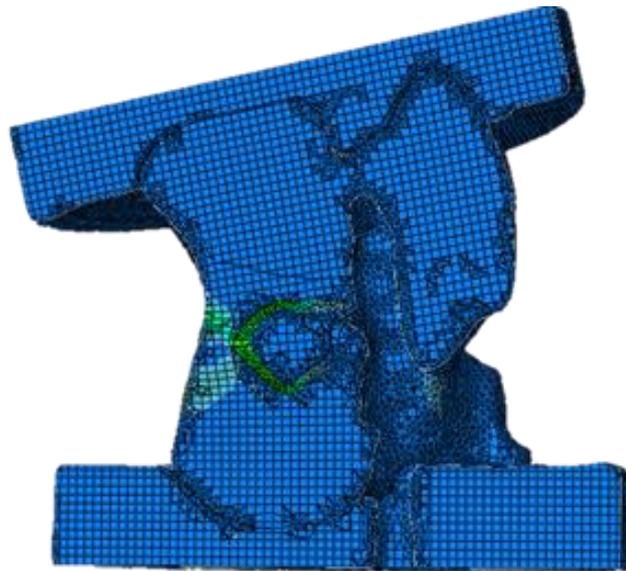
Figure 7-10, Cut through section view of an example augmented vertebrae model

7.5. Discussion

This chapter presents the methods and results for investigating the fatigue performance of bovine tail vertebrae following vertebroplasty. Additionally it reports the FE modelling and preliminary investigation into adding plastic bone material properties into an existing linear elastic model.

Cement was successfully injected into the vertebral body. However large variation was seen in the amount of cement injected, largely due to cement leakage into the neural canal and through the channel created in the opposite pedicle when the second pedicle was injected. Attempts were made to block this channel using a dowel, however as the pressure required to inject the cement was quite high, this was often insufficient to prevent cement leakage. High pressures on the syringe were required as the bovine bone is dense compared to osteoporotic human vertebral bone. Additionally the dissection methods used to isolate the vertebrae included the removal of all soft tissues, which allowed cement to leak through vascular channels in the anterior and posterior wall of the vertebral body. MicroCT scans showed that the cement distribution was consistently centrally located when considering the inferior-superior directions, however it varied much more in the anterior-posterior and medial-lateral directions. A number of *in vitro* and experimental studies have shown that variations in cement distribution can alter load transfer through augmented vertebrae, and in the case of medial-lateral variations cause more unstable loading *in vitro* (Liebschner et al., 2001; Sun and Liebschner, 2004; Molloy et al., 2005). However, the greatest increases in stiffness and strength were seen when cement spanned fully the axial distance between the two endplates which was not achieved in study in this study (Chevalier et al., 2008; Liebschner et al., 2001; Polikeit et al., 2003). Percentage cement fill ranged between 2-17%. Although this is a large range, it is still similar to *in vitro* studies on human vertebrae, such as 8-22% (Chevalier et al., 2008), 2-28% (Liebschner et al., 2001) and 5-30% (Luo et al., 2009). A systematic review of clinical vertebroplasty and kyphoplasty studies by Hulme et. al show that amount of cement injected ranged between approximately 2-8ml, in cases

where it was reported (Hulme et al., 2006). In the current study, approximately 3-16ml of cement was injected; whilst the lower end of this range is clinically relevant, this is less so at the higher end of the range where much more cement was injected due to overcompensation for visible cement leakage.

In six out of eleven cases, an increase in mechanical stiffness was seen after augmentation, but in five of these cases the increase was only 10% or less, and in the remaining five specimens, stiffness was seen to have decreased further. A reduction in stiffness after the initial static load to failure occurred in ten of the specimens, with an average decrease of - 16%. Additionally, (Liebschner et al., 2001) found that average cement fill of 14% restored stiffness to pre-vertebroplasty level, whilst higher cement fill values of approximately 30% increased stiffness by around 50%. Finally, (Luo et al., 2009) found that greater values of cement fill of 15-50% were required just to restore the stiffness to pre-stiffness levels. It is worth noting that in these studies human vertebrae were used, which have a lower bone volume than animal vertebrae (Zapata-Cornelio et al., 2017), so there is a greater disparity between the bone stiffness and cement stiffness. Therefore the cement is likely to increase the stiffness by a greater proportion of the original stiffness. It is thought that the general overall restoration in mechanical properties, typically stiffness and strength, is a good indication of patient improvement through re-established load transfer and biomechanics (Belkoff et al., 1999). It can be seen that there is no ideal level of percent cement fill to restore mechanical properties, as this is also dependant on cement distribution and properties of the vertebrae being tested. After investigating the relationship between cement fill and change in stiffness after augmentation, it was found that there was no clear correlation, and specimens which saw a decrease in stiffness after augmentation did not generally have less cement injected, Figure 7-11.
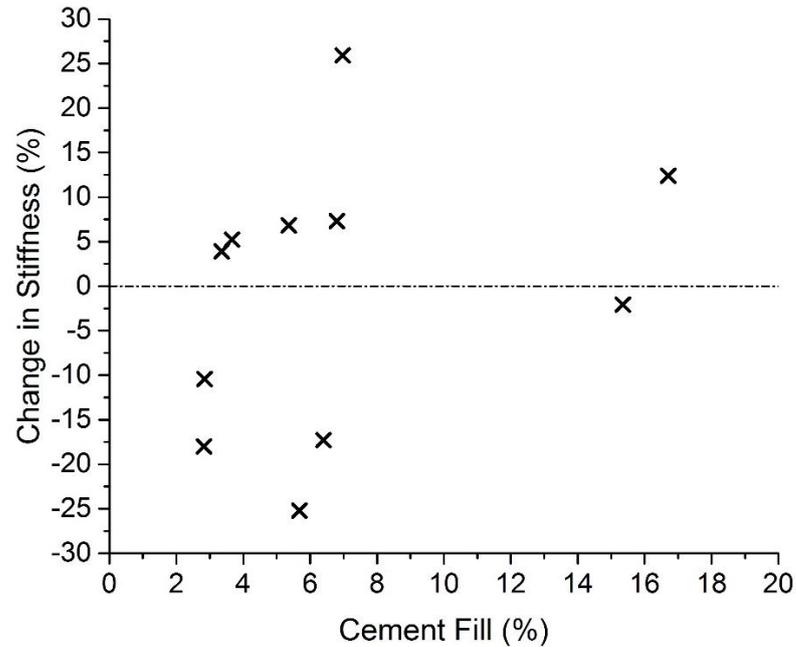
Figure 7-11, Percentage cement fill against percentage change in stiffness after augmentation. Dashed line at y=0 indicates whether specimens increased or decreased in stiffness after augmentation.

Large variations were seen in the number of cycles to failure when the augmented specimens were tested for fatigue. This was expected due to the limitations of the vertebroplasty procedure discussed above. Augmented vertebrae did appear to maintain mechanical stiffness better than untreated vertebrae over the cyclic testing. However this result was not statistically significant, and refinement of the vertebroplasty procedure and larger specimen groups might demonstrate better correlation.

To account for some of the variation between individual test vertebrae caused by anatomy, approximated stress against number of cycles, and strain against number of cycles were investigated. No correlation was seen between strain and cycles to failure. These properties were seen in the initial pre-conditioning of the vertebrae when tested to failure under static load, see Chapter 4, where it was noted that larger displacements were seen on some vertebrae, however this did not relate to the yield properties. In contrast, there was a small

correlation between stress and cycles to failure when investigated on a logarithmic scale using a power law relationship, which was very similar for both group.

From attempts made to model cement augmentation using FE methods both in this study and in the literature, it can be seen that this is challenging: few studies have tried to validate augmentated vertebrae models. (Wijayathunga et al., 2008) showed good agreement between experimental and FE predicted results when modelling human vertebrae without augmentation, however when augmentation was added the agreement was vastly inferior.

The new method developed by (Sikora, 2013) had shown promise under low static loads, so was adopted here. However, it was shown not to work with the higher loads used in this study and would therefore need further development. It is suggested that the cement-bone interface properties are optimised for higher loads, such as including a stiffening property after a certain strain is reached, to represent the compaction of the trabecular structure. This might prevent the large strains occurring which prevent the model from solving.

In conclusion, this chapter presented initial work to simulate the fatigue behaviour of vertebroplasty in both a laboratory model and in an FE model. It was seen that there is some evidence to suggest cement augmentation can help vertebrae retain mechanical stiffness during fatigue testing, however no significant increase in ability to withstand cyclic loading was observed. Additionally it was found through the adoption of current method used to simulate cement augmentation computationally, that the addition of yield properties to vertebral bone combined with high load conditions remains challenging and requires further investigation.

8. Discussion and Conclusion

This chapter presents a discussion on the methods developed and results found in the work undertaken for this thesis. Merits and limitations of the methods used are discussed, and the perceived achievements are compared back to the initial objectives set out after reviewing current literature. Finally comments are made regarding novelty and clinical relevance, and recommendations for future work are made.

8.1. Discussion of Experimental Testing

The following sections discuss the merits and limitations of the methods developed for the static and fatigue testing of bovine vertebrae. Additionally the *in vitro* vertebroplasty methods developed in this work, and the implications of cement augmentation on fatigue properties of vertebrae, are explored further.

8.1.1. Animal Model and Static Testing

A bovine tail vertebrae model was used for all experimental testing after preliminary work showed that ovine vertebrae were too strong to use as a fracture model, within the capabilities of the available materials testing machines. Additionally, previous work carried out in the research group had shown that finite element models of ovine vertebrae had a poorer agreement with experimental data than other types of bone such as porcine and human vertebrae (Zapata-Cornelio et al., 2017). Generally, the bovine vertebrae provided a suitable model for testing to yield under static load, fatigue method development, and for providing image data and mechanical properties for finite element method development. Bovine specimens also provided a suitable structure for augmentation. Despite this, a number of limitations on the use of this tissue were found, and should be considered when taking these methods forward.

In a small number of cases, the bovine vertebrae did not reach a yield point below 9.5kN. High yield strength is one of the main limitations of using animal tissue for fracture models.

It has been shown that vertebrae from the spine of a quadruped are of a higher density than that of a human spine, suggesting axial compressive forces transmitted through the quadruped spine are greater, hence the higher yield properties (Smit, 2002). In the literature it can be seen that cadaveric vertebrae are used in the majority of vertebral studies requiring a fracture model (Crawford et al., 2003a; Dall'Ara et al., 2010; Imai et al., 2006). Previous studies have shown that use of burst fracture loading, or high energy impact loading, for fracture generation can allow the use of a successful large animal vertebrae model (Tarsuslugil et al., 2014; Wang et al., 2007). This method was investigated briefly in this study, however it was found to be challenging to control, producing very low numbers of suitably fractured specimens. Despite this, the many similarities, such as general geometry and load transfer, mean that animal models are still a useful tool for investigating vertebrae; and selecting vertebrae from the tail, where loads are lower than in other regions of the spine, is likely the most suitable for fracture creation. Additionally, in cases where macroscopic yield behaviour was not seen, it is still likely that damage was caused in the form of trabecular micro-damage and macro-fractures caused by the high static load (Wang and Niebur, 2006).

Aside from fracture strength, other key differences between human and the bovine vertebrae used in this study were the higher bone density of the latter which affected the ease of which they could be augmented with cement and their dynamic loading properties; therefore fatigue results can only be compared with, and applied to, the same type of vertebrae. Availability of tissue was an important consideration for this work, where large numbers of specimens were used for method development purposes, and bovine tail vertebrae were widely available. Additionally, there are ethical considerations concerning the use of human tissue for the use of method development, where large numbers of specimens may be used trying out methodologies but not providing usable results. The use of animal tissue as a model for human vertebrae is undoubtedly a limitation of this study; however there is substantial literature evidence describing the merits and similarities of animal vertebrae, and

how they are still valuable as a way of investigating spinal biomechanics and interventions (Sheng et al., 2010). The work by Sheng et al., in comparison to similar studies at the University of Leeds, has shown that in general bovine vertebrae have a lower stiffness than porcine and ovine bone, making it the most suitable material for these tests, and the closest to human bone with regards to stiffness (Zapata-Cornelio et al., 2017).

Static testing methods already established at the University of Leeds for the compressive testing of porcine and human vertebrae were adapted for use with the bovine model (Tarsuslugil et al., 2014; Wijayathunga et al., 2008). These provide a highly controlled, repeatable method of compressive testing, which allowed for the replication of boundary conditions in the FE modelling. The main limitation of this method is the constraint of the bone at the interface between the vertebral body and the PMMA cement loading plate. There has been little investigation into the effect of this interface acting as a stress riser, and how much movement can happen between the bone and cement in this specific situation, with relatively thin cement plates around very convex bone surfaces under off-axis loading. This will be discussed further in the finite element fatigue loading section.

8.1.2. Fatigue Methods and Outcomes

A high load-low cycle fatigue test was carried out on a set of vertebrae, and although this is less physiologically relevant than a low load– high cycle fatigue testing, fractures in the latter would not be seen to the extent that they were in these studies, and other differences such as strain and stiffness reduction would not have been as apparent. It was important to get measurable results with which FE models could be directly compared, so a high load – low cycle approach was taken. Since high loads are an exaggeration of typical physiological loading, more evidence would be required to show whether results can be extrapolated to represent a low load – high cycle case. Specifically, information about whether this would show different outcomes in terms of fracture, damage and stiffness reduction would need to be investigated.

When conducting an engineering fatigue test, stress amplitude (S) against number of cycles to failure (N) is used to provide an S-N curve, describing the full range of behaviour from high stresses to the fatigue limit at low stress amplitudes, where failure is not seen. This is done by testing identical specimens across a large range of peak loads, which provides information about the response of the material at a given load. One of the limitations of this study was that the large variation between specimens meant a method to account for some of this variation had to be used. This was done by testing specimens in load groups, where the peak load was a percentage of the initial load to failure. A typical method used to account for inter-specimen variability in fatigue testing is to normalise stress against pre-fatigue Young's modulus (Haddock et al., 2004; Moore and Gibson, 2003). This method was not suitable for this study as calculating stress would not be accurate due to the differences in geometry and cross sectional area through a specimen, so this method would be more suitable to specimens of a regular shape, such as bone cores. From the tests reported in this thesis, only the lowest load group showed a significant difference in number of cycles to failure. There was also no noticeable differences in the severity of fractures between the different load groups. This means that using this data as a predictive tool for the fracture of vertebrae is challenging, and methods for reducing these large variations should be considered. This would also be useful in order to improve FE predictions. The high load method did highlight that vertebrae can withstand very large amounts of displacement and damage before reaching failure, and at 60% of the failure load, there were specimens that showed no visible sign of failure after 10000 cycles. Longer testing would be necessary to determine whether this level of loading causes enough local damage to accumulate into a full fracture.

A further limitation of this testing methodology was the change in strain rate between the initial test to failure and the fatigue test. The initial test applied a load ramped slowly at 1mm/min to produce a static failure typically within 1-3 minutes after cyclic pre-loading, whereas fatigue tests were run at 1Hz, where similar levels of displacements were applied

over just 1 second. Due to the visco-elastic properties of bone, stiffness values calculated from the fatigue test loading cycles was far greater than those found from the initial static tests. This meant that fatigue stiffness could not be directly compared to initial specimen static stiffness.

Despite large variations, it was seen that there was a general decrease in fatigue life with an increase in stress. Few other studies have tried to characterise fatigue behaviour of vertebrae, however this result does support the limited literature available for cadaveric and animal bone (Rapillard et al., 2006; Moore and Gibson, 2003; Haddock et al., 2004). These studies all found a strong S-N relationship, however these only involved testing of bone cores rather than whole vertebrae. This highlights that differences between testing bone cores rather than whole vertebrae are substantial and consideration of the whole vertebral structure is important when assessing biomechanical changes.

Brinckmann et al. (1988) conducted low cycle fatigue tests on human lumbar vertebrae at different percentages of the ultimate load and found that at loads of 60-70% ultimate load 92% of vertebrae failed before 5000 cycles were reached and 84% before 1000. In the present study it was found that 80% of vertebrae from the equivalent load groups had failed by 5000 cycles, however only 20% had failed by 1000 cycles (Brinckmann et al., 1988). This shows that even when initial yield load is accounted for, human lumbar vertebrae still have a lower fatigue strength than bovine vertebra, with a much larger proportion failing before testing reached 1000 cycles.

Finally, it was found that the effects of creep behaviour in the vertebra during fatigue loading were negligible, and this is in agreement with results from a study by (Moore et al., 2004). It is known that creep effects increase with temperature, and therefore further investigation into combined fatigue and creep effects at body temperature (37C) would be useful to confirm this result (Rimnac et al., 1993; Bowman et al., 1994).

8.1.3. Vertebroplasty

The vertebroplasty procedure developed in the laboratory for the augmentation of the bovine tail vertebra showed some success in restoring the mechanical stiffness of vertebrae previously loaded to failure. Despite this there were some important limitations to the *in vitro* vertebroplasty procedure, and it proved difficult to keep the procedure consistent between specimens.

The main limitation was the variation in cement fill, caused by cement leakage and difficulties injecting cement into the trabecular structure, which is far denser than that of osteoporotic human vertebral bone, where vertebroplasty is typically used. Additionally there was variation in the locations of the cement within the vertebrae. Whilst these limitations may play a role in the large variation in measured mechanical properties, making it more difficult to distinguish between the effects of vertebroplasty and natural variation, this variation is somewhat true to clinical situations. Other *in vitro* studies have also shown large variations in the cement fill and location (Jensen et al., 1997; Dean et al., 2000; Weikopf et al., 2008).

The use of animal vertebrae for *in vitro* vertebroplasty studies is uncommon, however the known differences between animal and human vertebrae can be used to hypothesise the differences in the vertebroplasty procedure. Animal vertebrae have a much higher density of bone than typical vertebroplasty patients, so there is less penetration of cement into the vertebral body through the trabecular structure (Tarsuslugil et al., 2013). It was noted from the microCT scans taken in the current study that bovine tail vertebrae often have a large void in the centre of the vertebral body, where there is a very sparse trabeculae structure. It is hypothesised that this is due to the lack of compressive loading through the tail of the animal. Theoretically, this should make it easier to inject a larger volume of cement into bovine tail vertebrae compared to porcine or ovine vertebrae, bringing the amount of cement fill more in line with that seen clinically.

No significant differences were seen in post-test stiffness between the untreated and augmented groups, however there was some evidence that the augmented specimens maintain their stiffness better, and some evidence of a restoration of mechanical stiffness after augmentation. This has also been reported in the literature (Liebschner et al., 2001; Luo et al., 2009). It is suggested that a larger group and improved *in vitro* vertebroplasty procedure would confirm these results, providing a better set of specimens with which to investigate fatigue. It is recommended that human vertebrae are necessary to avoid the issues highlighted in this study relating to differences in bone density and structure.

8.1.4. Summary of Experimental Testing

Despite the good level of control achieved in the experimental testing, large variations between specimens were still seen. Regardless, fatigue testing of augmented and untreated vertebrae using this methodology has provided information about the high load- low cycle fatigue properties of these two groups, specifically showing typical fracture locations for this experimental set-up. It is acknowledged that fracture locations were affected by the constraints on the vertebrae due to test equipment, however, the results for the two groups are still directly comparable. In contrast, the high levels of control in the experimental procedure should allow for effects of augmentation to be isolated from other factors. Additionally, the experimental test setup allowed for finite element models to be created with comparable boundary conditions, allowing for direct comparison of results.

Due to the animal model and loading regimes used, this work does not directly correspond to an *in vivo* situation. However, even in an ideal *in vitro* test, outcomes cannot be translated directly into a clinical output, such as *in vivo* fatigue fracture predication, as initial conditions of the vertebrae *in vivo* are unknown, such as amount of previous high cycle loading and level of ongoing bone repair. However, it does provide an insight into the fatigue behaviour of these specific vertebral specimens and how this might be altered by cement augmentation, as well as providing a fatigue testing methodology that can be used for human vertebrae specimens in the future.

One concern was the physiological relevance of testing at such high loads, however, Brinkmann et al. (1988) also conducted tests at high loads and low cycles, up to 5000, and suggested that 5000 such cycles may accumulate within two weeks of excessive loading of the spine, caused by sport or repetitive lifting. Within such a short time, repair mechanisms would not take effect, hence the relevance of these results to real life situations (Brinckmann et al., 1988).

8.2. Discussion of Finite Element Investigation

The following sections discuss the merits and potential for the finite element methods developed in this study and the identified limitations.

8.2.1. Finite Element model of Bovine Vertebrae

The finite element model from previous studies adapted for the bovine tail vertebrae tested in this work showed good agreement with experimental stiffness values. The level of agreement was comparable to published data for human, porcine and ovine vertebrae. A concordance correlation coefficient (CCC) of 0.62 was found for stiffness comparisons, which is in line with CCCs of 0.69 (Tarsuslugil et al., 2014) and >0.75 (Wilcox, 2007) for porcine vertebrae. Likewise a RMS (root mean square) error of 12.9 % was found for human vertebrae (Wijayathunga et al., 2008), whereas it was 11.3% for the current study. Results for these bovine vertebrae were superior to those for ovine vertebrae, where a CCC of 0.24 and RMS error of 21.9% were found (Zapata-Cornelio et al., 2017). This demonstrates the ability of the present model to capture variation in the mechanical bovine vertebral bone using the greyscale based element method at a down-sampled $1mm^3$ voxel resolution. Whilst this mesh resolution allowed good model agreement, a limitation of the study is that no mesh convergence study was carried out. This decision was based on evidence showing that a $1mm^3$ mesh resolution is sufficient for modelling porcine vertebrae (Jones and Wilcox, 2007). Additionally, it is expected that increasing the voxel resolution (and therefore element density), would not produce a converged solution due to the constantly changing size of voxels in relation to trabecular structures. For example, a slightly higher resolution

may result in trabecular bone being captured entirely within whole voxels, resulting in the image containing very stiff elements adjacent to much less stiff elements representing the voids between trabecular. Then a slightly higher resolution again may result in many voxels capturing edge artefacts of the trabeculae, resulting in more bone being averaged with the void in the same voxel, bringing the stiffness value down. At a resolution of $1mm^3$, trabecular architecture is not captured, so this always produces a mesh with no pure bone or pure void voxels. Additionally for this study, computational time needed to be minimised to allow use of the models in the fatigue studies, typically one iteration of the code, representing one cycle, in an elastic-perfectly plastic model takes approximately 1.5 hours.

Finally, (Zapata-Cornelio et al., 2017), the publication containing contributions from this work, showed by comparison of greyscale to modulus conversion values for different species that the variation seen in these parameters is caused by something not captured either by the microCT scans or by the FE models. This could be the hydration state of the tissue, contributions of cartilaginous growth plates or information regarding trabecular architecture lost through the down-sampling process, such as trabecular orientation. Whilst the present models are sufficient for the investigations and method development in this work, better accuracy could be achieved by accounting for some of these variations.

8.2.2. Modelling Yield Behaviour

A single value for element yield strain, 0.047, was found using the optimisation methods initially used for greyscale conversion factor. This allowed plasticity to be added into the material model of the vertebra whilst still capturing the variation in properties between bone elements, as the element modulus varied with image density, and hence yield strain resulted in varying yield stresses from one element to another. This optimised yield strain gave FE predicted results of specimen-level yield properties within a 95% confidence interval. Despite this, there were limitations with this method. Large variations in specimen-level yield strain could not be captured by FE models, which, even with the element-level differences in properties, showed a much more narrow range of specimen-level yield strains.

It is likely that this variation cannot be captured by one single yield strain value. Varying yield strain as well as the current variations in element yield stress and Young's modulus may improve results, however investigating the variation of so many parameters simultaneously would be challenging.

(Imai et al., 2006) created FE models of human lumbar vertebrae, modelling yield behaviour by having element Young's modulus and strength vary with ash density, using relationships derived from vertebral and femoral bone samples by Kayak et Al (1994). This method gave good correlation for both yield load and fracture load, however the authors did not show concordance, or agreement, of the models with experimental data (Imai et al., 2006; Keyak et al., 1994). Although producing promising results for yield load and fracture prediction, yield strain was not compared. Crawford et al. (2003) also modelled human vertebrae using a voxel based FE model with material properties as a function of bone density. Compressive strength was derived as a function of vertebrae height and stiffness, so a different yield stress value was calculated for each specimen. This approach was effective, but again was only assessed using regression analysis rather than concordance (Crawford et al., 2003a). It is important to measure level of agreement between FE and experimental results using concordance (i.e. the one-to-one agreement), rather than just a general correlation, for validation of the model (Jones and Wilcox, 2008).

8.2.3. Iterative Modelling of Fatigue Loading

The iterative approach to modelling material property reduction over a number of cycles showed relative success in predicting specimen displacements and plastic strain distributions when models that showed plastic strain distribution away from the cement plates was seen. A strong correlation (R^2=0.79) was seen between experimental displacement at yield and FE displacement at the second loading iteration. However a number of limitations were found with this method. Firstly, the equations derived from the literature were not optimum for the relatively large numbers of cycles endured by the vertebrae in the experimental fatigue tests. Rather, they were derived initially for human bone core samples tested at high strains. There

is little literature evidence available for relationships describing material property changes over a number of loading cycles, so the study by Keaveny et. al provided a good basis with which to develop the FE fatigue methods (Keaveny et al., 1999).

It is known that models of vertebrae loaded experimentally in compression are sensitive to boundary conditions (Jones and Wilcox, 2007). Previously when modelling a linear-elastic case, good results were obtained between FE and experimental testing by ensuring careful control of experimental tests and accurate representation of testing conditions in the models. However, when plasticity was included in the vertebrae model, more issues were seen with boundary conditions and constraints, in some cases to the point where models could no longer solve due to the excessive element distortions in areas affected by the constraints of the model. Previous studies have primarily focused on the stiffness behaviour under static loads, so the effect of the interface conditions were less crucial. At high loads and with progressive fatigue behaviour in the specimens, it became apparent that the interface was important and more consideration needs to be given in future studies as to how this can be controlled experimentally to provide a known interface, for example completely fixed via a more permanent bond. This has highlighted the need to reassess the mesh quality or boundary conditions when yield properties are included in the models.

The effect of bone remodelling was not considered during the fatigue testing. This still remains very challenging in terms of FE modelling, and it is known that osteoporosis is an imbalance of the bone remodelling process, therefore remodelling is much slower in osteoporotic spines. Additionally cement augmentation can cause differences in load transfer (Liebschner et al., 2001) which may have some stress shielding effects. Finally one of the main purposes of the FE modelling was to achieve correlation with the experimental *in vitro* results which of course do not include remodelling.

8.3. Key Achievements and Conclusions

8.3.1. Review of Aims and Objectives

Methods of investigating and modelling the mechanics of the spine are essential to better our understanding of existing and future treatments for spinal pathologies. A review of the current literature showed extensive work has been done in this field over the last two decades to provide a deeper understanding of the mechanisms behind vertebroplasty treatment. Despite this, there is still controversy over the efficacy of vertebroplasty and its best use. Investigations utilising *in vitro* and *in silico* models have provided some further understanding towards the changes in the biomechanics of the spine after vertebroplasty, however these typically have considered simple static loading cases only. With the growing elderly population and increase in life expectancy it is becoming more important to optimise vertebroplasty, which is mainly currently used in elderly patients. Therefore the aim of this work was to develop methods to investigate the mechanics of vertebroplasty under dynamic testing with the objective of characterising the fatigue properties of vertebrae with and without cement augmentation.

The following reiterates the objectives set out after reviewing the current literature, and assesses the extent to which they have been achieved:

- **Develop a method of creating reproducible, physiologically relevant fractures *in vitro*:**

A method was adapted from previous studies (Tarsuslugil et al., 2014; Wijayathunga et al., 2008) which allowed vertebrae to be prepared and tested in compression until yield. This method was highly repeatable, and variation seen within the results was a result of differences between biological specimens. Efforts were made to keep these differences to a minimum by only taking vertebrae from the first three levels of the bovine tail sections, and by removing all soft tissues so any variance was due to specimen-specific geometry and bone properties.

- **Create a set of specimens that can be fractured and augmented using vertebroplasty techniques:**

Specimens were created and loaded to yield point in a repeatable manner. These were then augmented using PMMA cement to simulate vertebroplasty treatment, utilising clinical techniques demonstrated by spinal surgeons. MicroCT scan images showed the extent and limitations of the cement augmentation.

- **Define a protocol for fatigue testing augmented vertebrae *in vitro*:**

A fatigue testing method was developed firstly using non-augmented vertebrae, by cyclically testing specimens in four groups at different levels of the specimen-specific initial yield load. This method accounted for some of the natural variation between specimens by normalising the peak fatigue load against the initial failure load.

- **Develop methods to model the fatigue behaviour of bone using FE:**

Published equations were adapted into a customisable script that runs with the FE software to iteratively change the material properties of the vertebral bone elements as a function of the plastic strain. This successfully modelled changes in vertebrae over a number of load cycles.

- **Validate results of FE analysis by direct comparison with experimental results:**

Direct comparisons of FE displacements and plastic strain distributions with experimental cyclic loading data and microCT scans were made. The FE models showed an accelerated level of plastic strain accumulation in comparison with the experimental tests, however the models showed very good agreement with the overall level of displacement in the vertebrae, and good indication of plastic strain distribution in cases where there was damage away from the cement endplates.

8.3.2. Novelty and Clinical Relevance

Novel methods were developed for the *in vitro* fatigue simulation of bovine tail vertebrae and the translation of these methods to finite element models. Specifically, previously developed methods from the University of Leeds were applied to bovine bone, allowing for insight into, and comparison of greyscale based FE models, which was then published (Zapata-Cornelio et al., 2017). Additionally, no evidence was found for previous use of bovine vertebrae as a model for vertebroplasty treatment.

A set of specimens were used for the calibration and validation of a single yield strain value to represent bovine tail vertebrae, and an automated method for calculating specimen yield strain was created through a custom script. A novel, customisable script was written for the implementation of material property interrogation and manipulation on an element level. This is a tool that can be used for a number of fatigue modelling or iterative based modelling studies in the future, providing complete control over material property changes.

Clinical relevance:

Insight into the biomechanics of vertebrae is incredibly important in order to understand how interventions can affect the patient. Specifically, vertebroplasty treatment is known to affect the loading of the spine due to the much higher mechanical stiffness of the bone cement compared to the typically osteoporotic bone. Additionally there is still considerable debate over the efficacy of vertebroplasty. Whilst this topic has been covered extensively in the literature with regards to static loading, there is far less information concerning how the fatigue behaviour of the spine changes with intervention. This work has developed a methodology that can be used to assess vertebroplasty under fatigue loading to determine how the biomechanics of the spine change under more complex loading conditions than a simple static load, and to assess whether this can provide an indication towards the best use of vertebroplasty treatment.

8.3.3. Recommendations for Future Work

From assessing the limitations and results of this work the following recommendations are made for future work:

- Due to limitations found with the use of both ovine and bovine vertebrae, and similar limitations with porcine bone documented previously (Tarsislugil et al, 2014) it is recommended that fatigue testing is repeated with human vertebrae. This should allow for a more robust fracture model, due to the lower strength of human specimens compared to animal vertebrae. Additionally this would provide a better insight into the effects of vertebroplasty on fatigue properties of vertebrae, as the mechanical properties and the difference in stiffness between bone and cement would be more true to *in vivo* conditions. This is especially relevant because the cadaveric tissue available is likely to be from older humans and therefore osteoporotic and even less stiff.

- Investigations into reducing cement leakage during the in vitro vertebroplasty procedure for bovine tail vertebrae are recommended. It is known that variations in cement volume effect restoration of cement and stiffness (Wilcox, 2004), so better control over this procedure would reduce variations in the testing results. This may be achieved by using a more viscous cement mixture. In this study a 1:1 liquid to powder component was used to provide good injectability and longer working times but is important to find a balance between injectability and potential cement leakage. This would be easier in human specimens as the cement is easier to inject into the less dense bone.

- It would be insightful to complete higher cycle fatigue tests by using lower, more realistic loads. This would only be appropriate with osteoporotic vertebrae, as lower loads may not result in any failure in a healthy animal model. Additionally, it would

be recommended to study a control set without any initial fracture. This would provide baseline data with which results from augmented specimens could be compared to assess the ability of the treatment to restore mechanical properties to those of an un-fractured case. The methods used in this study required measurement of the initial yield strength to calculate test load; however it has been shown elsewhere that ultimate strength can be predicted from stiffness or BMD measurements (Hansson et al., 1987; Brinckmann et al., 1988) .

- Further investigation into the best yield behaviour properties for the FE models should be carried out for improved validation of the elastic-plastic vertebrae models. An elastic-perfectly plastic material model was assumed, whereas in reality there is generally a progressive drop off seen in the stress-strain behaviour, rather than the assumed linear stress. It is also likely that an increase in stiffness is eventually seen under large displacements due to compaction of the trabecular structure. Exploration of the underlying factors affecting the yield properties of vertebrae may provide an insight into ways to group the specimens with similar properties together to validate for groups with less inter-specimen variation. Additionally, further work to find the best way to model the interface between the cement loading plate and the vertebral body would be beneficial, as the current method of using a tie condition appears to over-constrain the model, and assuming frictionless contact appears to unsuitable for non-linear models, despite showing promise for linear-elastic cases. It is likely that the true contact between the two surfaces is somewhere between these two extremes, and implementing a constraint to represent this will likely improve results.

8.3.4. Overall Summary and Conclusion

This thesis presents novel methodologies to assess the fatigue behaviour of vertebrae using an *in vitro* animal model, demonstrating the behaviour under various levels of cyclic

loading. Vertebrae augmented with PMMA cement were fatigue tested and directly compared to non-augmented vertebrae. Additionally, a highly tuneable script to be used with finite element software was developed and used to investigate the ability of published equations describing material property changes in trabecular bone to represent the experimentally tested vertebrae. The methodologies developed in this work could provide a useful tool for the investigation of fatigue behaviour in alternative applications within the medical field where it is advantageous to use implicit finite element methods. Specifically, where changes in material properties for given conditions are known and plastic deformation behaviour over longer periods of time is of interest. However, with the current methodologies these applications are limited to those where it is acceptable to assume the relationship defining the material changes is the same at every cycle, and does not account for changes in the bulk material that may occur over time such as more severe changes in stiffness due to structural changes or large deformations.

The numerical model describes the level of displacement seen in the vertebrae well, and provides a good indication of likely fracture locations in high load cases. Whilst there are a number of recommended enhancements to the simulation of the vertebroplasty procedure, this combined experimental-numerical modelling approach offers useful insight into the dynamic response of damaged vertebrae both in the untreated state and after vertebroplasty and will in the longer term enable more informed clinical decisions to be taken.

9. References

Abeloff, D. 1982. *Medical art: graphics for use.* Williams & Wilkins.

Adams, M.A. and Dolan, P. 2011. Biomechanics of vertebral compression fractures and clinical application. *Archives of orthopaedic and trauma surgery.* **131**(12), pp.1703-1710.

Aquarius, R. et al. 2014. Prophylactic vertebroplasty can decrease the fracture risk of adjacent vertebrae: An< i> in vitro</i> cadaveric study. *Medical engineering & physics.* **36**(7), pp.944-948.

Belkoff, S. et al. 1999. An in vitro biomechanical evaluation of bone cements used in percutaneous vertebroplasty. *Bone.* **25**(2), pp.23S-26S.

Berenson, J. et al. 2011. Balloon kyphoplasty versus non-surgical fracture management for treatment of painful vertebral body compression fractures in patients with cancer: a multicentre, randomised controlled trial. *The lancet oncology.* **12**(3), pp.225-235.

Betts, J.G. 2013. *Anatomy and physiology.* Houston, Texas: OpenStax College, Rice University.

Bowman, S.M. et al. 1994. Compressive creep behavior of bovine trabecular bone. *Journal of biomechanics.* **27**(3), pp.301-305.

Brinckmann, P. et al. 1988. Fatigue fracture of human lumbar vertebrae. *Clinical Biomechanics.* **3**, pp.i-S23.

Brinckmann, P. et al. 1989. Prediction of the compressive strength of human lumbar vertebrae. *Clinical Biomechanics.* **4**, pp.1-27.

Brown, K.R. et al. 2014. Comparative finite-element analysis: a single computational modelling method can estimate the mechanical properties of porcine and human vertebrae. *Journal of The Royal Society Interface.* **11**(95), p20140186.

Buchbinder, R. et al. 2009. A randomized trial of vertebroplasty for painful osteoporotic vertebral fractures. *New England Journal of Medicine.* **361**(6), pp.557-568.

Charosky, S. et al. 2014. Instability and instrumentation failures after a PSO: a finite element analysis. *European Spine Journal.* **23**(11), pp.2340-2349.

Cheng, X.G. et al. 1997. Prediction of vertebral strength in vitro by spinal bone densitometry and calcaneal ultrasound. *Journal of Bone and Mineral Research.* **12**(10), pp.1721-1728.

Chevalier, Y. et al. 2008. A patient-specific finite element methodology to predict damage accumulation in vertebral bodies under axial compression, sagittal flexion and combined loads. *Computer methods in biomechanics and biomedical engineering.* **11**(5), pp.477-487.

Chevalier, Y. et al. 2009. The role of cortical shell and trabecular fabric in finite element analysis of the human vertebral body. *Journal of biomechanical engineering.* **131**(11), p111003.

Chiang, C.-K. et al. 2009. Prophylactic vertebroplasty may reduce the risk of adjacent intact vertebra from fatigue injury: an ex vivo biomechanical study. *Spine.* **34**(4), pp.356-364.

Cotterill, P.C. et al. 1986. An anatomical comparison of the human and bovine thoracolumbar spine. *Journal of Orthopaedic Research.* **4**(3), pp.298-303.

Crawford, R.P. et al. 2003a. Finite element models predict in vitro vertebral body compressive strength better than quantitative computed tomography. *Bone.* **33**(4), pp.744-750.

Crawford, R.P. et al. 2003b. Quantitative computed tomography-based finite element models of the human lumbar vertebral body: effect of element size on stiffness, damage, and fracture strength predictions. *Journal of biomechanical engineering.* **125**(4), pp.434-438.

Cummings, S.R. and Melton, L.J. 2002. Epidemiology and outcomes of osteoporotic fractures. *The Lancet.* **359**(9319), pp.1761-1767.

Dall'Ara, E. et al. 2010. A nonlinear finite element model validation study based on a novel experimental technique for inducing anterior wedge-shape fractures in human vertebral bodies< i> in vitro</i>. *Journal of Biomechanics.* **43**(12), pp.2374-2380.

Dall'Ara, E. et al. 2012. QCT-based finite element models predict human vertebral strength in vitro significantly better than simulated DEXA. *Osteoporosis International.* **23**(2), pp.563-572.

Dean, J.R. et al. 2000. The Strengthening Effect of Percutaneous Vertebroplasty. *Clinical Radiology.* **55**(6), pp.471-476.

Denis, F. 1983. The three column spine and its significance in the classification of acute thoracolumbar spinal injuries. *Spine.* **8**(8), pp.817-831.

Denis, F. 1984. Spinal instability as defined by the three-column spine concept in acute spinal trauma. *Clinical orthopaedics and related research.* **189**, pp.65-76.

Dickey, B. et al. 2012. < i> In silico</i> evaluation of stress distribution after vertebral body augmentation with conventional acrylics, composites and glass polyalkenoate cements. *Journal of the mechanical behavior of biomedical materials.* **5**(1), pp.283-290.

Dougherty, G. 2010. *Image analysis in medical imaging: Recent advances in selected examples.*

Ebbesen, E.N. et al. 1999. Lumbar vertebral body compressive strength evaluated by dual-energy X-ray absorptiometry, quantitative computed tomography, and ashing. *Bone.* **25**(6), pp.713-724.

Ebraheim, N.A. et al. 2004. Functional anatomy of the lumbar spine. *Seminars in Pain Medicine.* **2**(3), pp.131-137.

Erdem, I. et al. 2013. Simulation of the behaviour of the L1 vertebra for different material properties and loading conditions. *Computer methods in biomechanics and biomedical engineering.* **16**(7), pp.736-746.

Erkan, S. et al. 2010. Biomechanical comparison of transpedicular versus extrapedicular vertebroplasty using polymethylmethacrylate. *Journal of spinal disorders & techniques.* **23**(3), pp.180-185.

Eswaran, S.K. et al. 2006. Cortical and trabecular load sharing in the human vertebral body. *Journal of Bone and Mineral Research.* **21**(2), pp.307-314.

Fyhrie, D. and Schaffler, M. 1994. Failure mechanisms in human vertebral cancellous bone. *Bone.* **15**(1), pp.105-109.

Gallagher, S. et al. 2007. A comparison of fatigue failure responses of old versus middle-aged lumbar motion segments in simulated flexed lifting. *Spine.* **32**(17), pp.1832-1839.

Garfin, S.R. et al. 2001. New technologies in spine: kyphoplasty and vertebroplasty for the treatment of painful osteoporotic compression fractures. *spine.* **26**(14), pp.1511-1515.

Garo, A. et al. 2011. Calibration of the mechanical properties in a finite element model of a lumbar vertebra under dynamic compression up to failure. *Medical & Biological Engineering & Computing.* **49**(12), pp.1371-1379.

Grote, H. et al. 1995. Intervertebral variation in trabecular microarchitecture throughout the normal spine in relation to age. *Bone.* **16**(3), pp.301-308.

Haddock, S.M. et al. 2004. Similarity in the fatigue behavior of trabecular bone across site and species. *Journal of biomechanics.* **37**(2), pp.181-187.

Han, K.-S. et al. 2013. Lumbar spinal loads vary with body height and weight. *Medical engineering & physics.* **35**(7), pp.969-977.

Hanlon, C.A. 2012. *Modelling the Longer Term Effects of Spinal Burst Fracture Repair using Vertebroplasty.* Doctor of Philosophy thesis, University of Leeds.

Hansson, T. et al. 1987. Mechanical behavior of the human lumbar spine. II. Fatigue strength during dynamic compressive loading. *Journal of Orthopaedic Research.* **5**(4), pp.479-487.

Harrison, N.M. and McHugh, P.E. 2010. Comparison of trabecular bone behavior in core and whole bone samples using high-resolution modeling of a vertebral body. *Biomechanics and modeling in mechanobiology.* **9**(4), pp.469-480.

Heini, P.F. and Allred, C.D. 2002. The use of a side-opening injection cannula in vertebroplasty: a technical note. *Spine.* **27**(1), pp.105-109.

Heini, P.F. et al. 2001. Augmentation of mechanical properties in osteoporotic vertebral bones–a biomechanical investigation of vertebroplasty efficacy with different bone cements. *European Spine Journal.* **10**(2), pp.164-171.

Helgason B. et al. 2013. Influence of cement stiffness and bone morphology on the compressive properties of bone–cement composites in simulated vertebroplasty. *Journal of Biomedical Materials Research Part B: Applied Biomaterials.* **101B**(2), pp.364-374.

Higgins, K.B. et al. 2006. Biomechanical Alterations in Intact Osteoporotic Spine Due to Synthetic Augmentation: Finite Element Investigation. *Journal of Biomechanical Engineering.* **129**(4), pp.575-585.

Hitchon, P.W. et al. 2001. Comparison of the biomechanics of hydroxyapatite and polymethylmethacrylate vertebroplasty in a cadaveric spinal compression fracture model. *Journal of Neurosurgery: Spine.* **95**(2), pp.215-220.

Holdsworth, F. 1963. OF THE SPINE.

Holsgrove, T.P. et al. 2015. Advanced Multi-Axis Spine Testing: Clinical Relevance and Research Recommendations. *International Journal of Spine Surgery.* **9**, p34.

Hosseini, H.S. et al. 2014. Experimental Validation of Finite Element Analysis of Human Vertebral Collapse Under Large Compressive Strains. *Journal of biomechanical engineering.* **136**(4), p041006.

Huber, G. et al. 2010. High cycle fatigue behaviour of functional spinal units. *Industrial health.* **48**(5), pp.550-556.

Hulme, P.A. et al. 2006. Vertebroplasty and kyphoplasty: a systematic review of 69 clinical studies. *Spine.* **31**(17), pp.1983-2001.

Imai, K. et al. 2006. Nonlinear finite element model predicts vertebral bone strength and fracture site. *Spine.* **31**(16), pp.1789-1794.

Jensen, M.E. et al. 1997. Percutaneous polymethylmethacrylate vertebroplasty in the treatment of osteoporotic vertebral body compression fractures: technical aspects. *American Journal of Neuroradiology.* **18**(10), pp.1897-1904.

Jones, A.C. and Wilcox, R.K. 2007. Assessment of factors influencing finite element vertebral model predictions. *Journal of biomechanical engineering.* **129**(6), pp.898-903.

Jones, A.C. and Wilcox, R.K. 2008. Finite element analysis of the spine: towards a framework of verification, validation and sensitivity analysis. *Medical engineering & physics.* **30**(10), pp.1287-1304.

Kallmes, D.F. et al. 2009. A randomized trial of vertebroplasty for osteoporotic spinal fractures. *New England Journal of Medicine.* **361**(6), pp.569-579.

Kayanja, M.M. et al. 2004. Distribution of anterior cortical shear strain after a thoracic wedge compression fracture. *The Spine Journal.* **4**(1), pp.76-87.

Keaveny, T.M. and Hayes, W.C. 1993. A 20-year perspective on the mechanical properties of trabecular bone. *Journal of biomechanical engineering.* **115**(4B), pp.534-542.

Keaveny, T.M. et al. 1999. Mechanical behavior of human trabecular bone after overloading. *Journal of Orthopaedic Research.* **17**(3), pp.346-353.

Kennedy, O.D. et al. 2009. Variation of trabecular microarchitectural parameters in cranial, caudal and mid-vertebral regions of the ovine L3 vertebra. *Journal of anatomy.* **214**(5), pp.729-735.

Keyak, J. et al. 1994. Correlations between orthogonal mechanical properties and density of trabecular bone: use of different densitometric measures. *Journal of biomedical materials research.* **28**(11), pp.1329-1336.

Kinzl, M. et al. 2012. The effect of standard and low-modulus cement augmentation on the stiffness, strength, and endplate pressure distribution in vertebroplasty. *European Spine Journal.* **21**(5), pp.920-929.

Klazen, C.A. et al. 2010. Vertebroplasty versus conservative treatment in acute osteoporotic vertebral compression fractures (Vertos II): an open-label randomised trial. *The Lancet.* **376**(9746), pp.1085-1092.

Kolb, J.P. et al. 2013. Does the cement stiffness affect fatigue fracture strength of vertebrae after cement augmentation in osteoporotic patients? *European Spine Journal.* **22**(7), pp.1650-1656.

Kopperdahl, D.L. and Keaveny, T.M. 1998. Yield strain behavior of trabecular bone. *Journal of biomechanics.* **31**(7), pp.601-608.

Kopperdahl, D.L. et al. 2002. Quantitative computed tomography estimates of the mechanical properties of human vertebral trabecular bone. *Journal of orthopaedic research.* **20**(4), pp.801-805.

Kothe, R. et al. 2004. Biomechanical analysis of transpedicular screw fixation in the subaxial cervical spine. *Spine.* **29**(17), pp.1869-1875.

Kowalski, R.J. et al. 2005. Biomechanics of the spine. *Neurosurgery Quarterly.* **15**(1), pp.42-59.

Lambers, F.M. et al. 2013. Microdamage Caused by Fatigue Loading in Human Cancellous Bone: Relationship to Reductions in Bone Biomechanical Performance. *Plos One.* **8**(12), pe83662.

Leventon, M.E. et al. 2000. Statistical shape influence in geodesic active contours. In: *Computer Vision and Pattern Recognition, 2000. Proceedings. IEEE Conference on*: IEEE, pp.316-323.

Li, D. et al. 2014. Novel, fast and efficient image‑based 3D modeling method and its application in fracture risk evaluation. *Experimental and Therapeutic Medicine.* **7**(6), pp.1583-1590.

Liang, Y. et al. 2014. Biomechanical effects of bone cement volume on the endplates of augmented vertebral body: a three-dimensional finite element analysis. *Chinese medical journal.* **127**(1), pp.79-84.

Liebschner, M.A. et al. 2003. Finite element modeling of the human thoracolumbar spine. *Spine.* **28**(6), pp.559-565.

Liebschner, M.A. et al. 2001. Effects of bone cement volume and distribution on vertebral stiffness after vertebroplasty. *Spine.* **26**(14), pp.1547-1554.

Lin, L.I.K. 1989. A Concordance Correlation Coefficient to Evaluate Reproducibility. *Biometrics.* **45**(1), pp.255-268.

Liu, Y.K. et al. 1983. Fatigue response of lumbar intervertebral joints under axial cyclic loading. *Spine.* **8**(8), pp.857-865.

Lu, Y. et al. 2014. Finite element analyses of human vertebral bodies embedded in polymethylmethalcrylate or loaded via the hyperelastic intervertebral disc models provide equivalent predictions of experimental strength. *Journal of Biomechanics.*

Luo, J. et al. 2009. Vertebroplasty: only small cement volumes are required to normalize stress distributions on the vertebral bodies. *Spine.* **34**(26), pp.2865-2873.

Magerl, F. et al. 1994. A comprehensive classification of thoracic and lumbar injuries. *European Spine Journal.* **3**(4), pp.184-201.

Matsuura, Y. et al. 2014. Specimen-Specific Nonlinear Finite Element Modeling to Predict Vertebrae Fracture Loads After Vertebroplasty. *Spine.* **39**(22), pp.E1291-E1296.

Melton, L.r. et al. 1997. Fractures attributable to osteoporosis: report from the National Osteoporosis Foundation. *Journal of Bone and Mineral Research.* **12**(1), pp.16-23.

Mengoni, M., opti4Abq, a generic python code to run Abaqus in an optimisation loop. 2017.

Mengoni, M. et al. 2015. Derivation of inter-lamellar behaviour of the intervertebral disc annulus. *journal of the mechanical behavior of biomedical materials.* **48**, pp.164-172.

Mengoni, M. et al. 2016. Subject-specific multi-validation of a finite element model of ovine cervical functional spinal units. *Journal of Biomechanics.* **49**(2), pp.259-266.

Mirzaei, M. et al. 2009. On prediction of the strength levels and failure patterns of human vertebrae using quantitative computed tomography (QCT)-based finite element method. *Journal of Biomechanics.* **42**(11), pp.1584-1591.

Molloy, S. et al. 2005. Effect of cement volume and placement on mechanical-property restoration resulting from vertebroplasty. *American journal of neuroradiology.* **26**(2), pp.401-404.

Moore, T. et al. 2004. Creep does not contribute to fatigue in bovine trabecular bone. *Journal of biomechanical engineering.* **126**(3), pp.321-329.

Moore, T.L. and Gibson, L.J. 2003. Fatigue of bovine trabecular bone. *Journal of biomechanical engineering.* **125**(6), pp.761-768.

Mosekilde, L. 1988. Age-related changes in vertebral trabecular bone architecture—assessed by a new method. *Bone.* **9**(4), pp.247-250.

Müller, R. and Rüegsegger, P. 1997. Micro-tomographic imaging for the nondestructive evaluation of trabecular bone architecture. *Studies in health technology and informatics.* pp.61-80.

Nachemson, A. 1966. The load on lumbar disks in different positions of the body. *Clinical orthopaedics and related research.* **45**, pp.107-122.

Nagaraja, S. et al. 2005. Trabecular bone microdamage and microstructural stresses under uniaxial compression. *Journal of biomechanics.* **38**(4), pp.707-716.

Niosi, C.A. and Oxland, T.R. 2004. Degenerative mechanics of the lumbar spine. *The Spine Journal.* **4**(6, Supplement), pp.S202-S208.

Oakland, R.J. et al. 2009. Preliminary biomechanical evaluation of prophylactic vertebral reinforcement adjacent to vertebroplasty under cyclic loading. *The Spine Journal.* **9**(2), pp.174-181.

Pahr, D.H. and Zysset, P.K. 2009a. A comparison of enhanced continuum FE with micro FE models of human vertebral bodies. *Journal of Biomechanics.* **42**(4), pp.455-462.

Pahr, D.H. and Zysset, P.K. 2009b. From high-resolution CT data to finite element models: development of an integrated modular framework. *Computer methods in biomechanics and biomedical engineering.* **12**(1), pp.45-57.

Palastanga, N. and Soames, R. 2011. *Anatomy and Human Movement, Structure and function with PAGEBURST Access, 6: Anatomy and Human Movement.* Elsevier Health Sciences.

Panjabi, M.M. et al. 1994. Mechanical behavior of the human lumbar and lumbosacral spine as shown by three-dimensional load-displacement curves. *JBJS.* **76**(3), pp.413-424.

Panjabi, M.M. and White III, A.A. 1980. Basic biomechanics of the spine. *Neurosurgery.* **7**(1), pp.76-93.

Pernelle, K. et al. 2017. Microscale mechanical and mineral heterogeneity of human cortical bone governs osteoclast activity. *Bone.* **94**, pp.42-49.

Polikeit, A. et al. 2003. The effect of cement augmentation on the load transfer in an osteoporotic functional spinal unit: finite-element analysis. *Spine.* **28**(10), pp.991-996.

Pollintine, P. et al. 2009. Bone creep can cause progressive vertebral deformity. *Bone.* **45**(3), pp.466-472.

Purcell, P. et al. 2014. A parametric finite element analysis of the compacted bone-cement interface following balloon kyphoplasty. *Proceedings of the Institution of Mechanical Engineers Part H-Journal of Engineering in Medicine.* **228**(1), pp.89-97.

Rapillard, L. et al. 2006. Compressive fatigue behavior of human vertebral trabecular bone. *Journal of Biomechanics.* **39**(11), pp.2133-2139.

Rho, J.-Y. et al. 1998. Mechanical properties and the hierarchical structure of bone. *Medical Engineering & Physics.* **20**(2), pp.92-102.

Riggs, B.L. 1991. Overview of osteoporosis. *Western journal of medicine.* **154**(1), p63.

Riggs, B.L. et al. 1998. A unitary model for involutional osteoporosis: estrogen deficiency causes both type I and type II osteoporosis in postmenopausal women and

contributes to bone loss in aging men. *Journal of bone and mineral research.* **13**(5), pp.763-773.

Rimnac, C. et al. 1993. The effect of temperature, stress and microstructure on the creep of compact bovine bone. *Journal of biomechanics.* **26**(3), pp.219-221.

Rodriguez, A.G. et al. 2012. Morphology of the human vertebral endplate. *Journal of Orthopaedic Research.* **30**(2), pp.280-287.

Rohlmann, A. et al. 2014. Activities of Everyday Life with High Spinal Loads. *Plos One.* **9**(5), pe98510.

Rohlmann, A. et al. 2006. Analysis of the influence of disc degeneration on the mechanical behaviour of a lumbar motion segment using the finite element method. *Journal of biomechanics.* **39**(13), pp.2484-2490.

Rousing, R. et al. 2009. Percutaneous vertebroplasty compared to conservative treatment in patients with painful acute or subacute osteoporotic vertebral fractures: three-months follow-up in a clinical randomized study. *Spine.* **34**(13), pp.1349-1354.

Rüger, M. and Schmoelz, W. 2009. Vertebroplasty with high-viscosity polymethylmethacrylate cement facilitates vertebral body restoration in vitro. *Spine.* **34**(24), pp.2619-2625.

Sato, K. et al. 1999. In vivo intradiscal pressure measurement in healthy individuals and in patients with ongoing back problems. *Spine.* **24**(23), p2468.

Schmidt, H. et al. 2010. Response analysis of the lumbar spine during regular daily activities—a finite element analysis. *Journal of biomechanics.* **43**(10), pp.1849-1856.

Serhan, H.A. et al. 2007. Biomechanics of the posterior lumbar articulating elements. *Neurosurgical focus.* **22**(1), pp.1-6.

Sheng, S.R. et al. 2010. Anatomy of large animal spines and its comparison to the human spine: a systematic review. *European Spine Journal.* **19**(1), pp.46-56.

Shim, V. et al. 2005. Characterisation of the dynamic compressive mechanical properties of cancellous bone from the human cervical spine. *International Journal of Impact Engineering.* **32**(1-4), pp.525-540.

Sikora, S.N.F. 2013. *Experimental and computational study of the behaviour of trabecular bone-cement interfaces.* PhD thesis, University of Leeds.

Silva, M.J. et al. 1998. Computed tomography-based finite element analysis predicts failure loads and fracture patterns for vertebral sections. *Journal of Orthopaedic Research.* **16**(3), pp.300-308.

Smit, T.H. 2002. The use of a quadruped as an in vivo model for the study of the spine–biomechanical considerations. *European Spine Journal.* **11**(2), pp.137-144.

Sun, K. and Liebschner, M.A. 2004. Evolution of vertebroplasty: a biomechanical perspective. *Annals of biomedical engineering.* **32**(1), pp.77-91.

Tabensky, A.D. et al. 1996. Bone mass, areal, and volumetric bone density are equally accurate, sensitive, and specific surrogates of the breaking strength of the vertebral body: an in vitro study. *Journal of Bone and Mineral Research.* **11**(12), pp.1981-1988.

Tarsuslugil, S.M. et al. 2013. Development of calcium phosphate cement for the augmentation of traumatically fractured porcine specimens using vertebroplasty. *Journal of Biomechanics.* **46**(4), pp.711-715.

Tarsuslugil, S.M. et al. 2014. Experimental and Computational Approach Investigating Burst Fracture Augmentation Using PMMA and Calcium Phosphate Cements. *Annals of biomedical engineering.* **42**(4), pp.751-762.

Teo, J.C.M. et al. 2006. Relationship between CT intensity, micro-architecture and mechanical properties of porcine vertebral cancellous bone. *Clinical Biomechanics.* **21**(3), pp.235-244.

Trout, A.T. et al. 2006. New fractures after vertebroplasty: adjacent fractures occur significantly sooner. *American Journal of Neuroradiology.* **27**(1), pp.217-223.

Troyer, K.L. and Puttlitz, C.M. 2011. Human cervical spine ligaments exhibit fully nonlinear viscoelastic behavior. *Acta Biomaterialia.* **7**(2), pp.700-709.

Tsouknidas, A. et al. 2013. The effect of kyphoplasty parameters on the dynamic load transfer within the lumbar spine considering the response of a bio-realistic spine segment. *Clinical Biomechanics.* **28**(9), pp.949-955.

Unnikrishnan, G.U. et al. 2013. Effect of Specimen-Specific Anisotropic Material Properties in Quantitative Computed Tomography-Based Finite Element Analysis of the Vertebra. *Journal of biomechanical engineering.* **135**(10), p101007.

Urban, J.P. and Roberts, S. 2003. Degeneration of the intervertebral disc. *Arthritis Res Ther.* **5**(3), p120.

Verhulp, E. et al. 2006. Comparison of micro-level and continuum-level voxel models of the proximal femur. *Journal of Biomechanics.* **39**(16), pp.2951-2957.

Wang, X.-Y. et al. 2007. The Load-Sharing Classification of Thoracolumbar Fractures: An In Vitro Biomechanical Validation. *Spine.* **32**(11), pp.1214-1219.

Wang, X.-Y. et al. 2008. Biomechanical effect of the extent of vertebral body fracture on the thoracolumbar spine with pedicle screw fixation: An< i> in vitro</i> study. *Journal of Clinical Neuroscience.* **15**(3), pp.286-290.

Wang, X. and Niebur, G.L. 2006. Microdamage propagation in trabecular bone due to changes in loading mode. *Journal of biomechanics.* **39**(5), pp.781-790.

Wardlaw, D. et al. 2009. Efficacy and safety of balloon kyphoplasty compared with non-surgical care for vertebral compression fracture (FREE): a randomised controlled trial. *The Lancet.* **373**(9668), pp.1016-1024.

Weikopf, M. et al. 2008. Intravertebral pressure during vertebroplasty and balloon kyphoplasty: an in vitro study. *Spine.* **33**(2), pp.178-182.

Whitesides Jr, T.E. 1977. Traumatic kyphosis of the thoracolumbar spine. *Clinical orthopaedics and related research.* **128**, pp.78-92.

Wijayathunga, V. et al. 2008. Development of specimen-specific finite element models of human vertebrae for the analysis of vertebroplasty. *Proceedings of the Institution of Mechanical Engineers, Part H: Journal of Engineering in Medicine.* **222**(2), pp.221-228.

Wijayathunga, V.N. et al. 2013. Vertebroplasty: Patient and treatment variations studied through parametric computational models. *Clinical Biomechanics.* **28**(8), pp.860-865.

Wilcox, R. 2004. The biomechanics of vertebroplasty: a review. *Proceedings of the Institution of Mechanical Engineers, Part H: Journal of Engineering in Medicine.* **218**(1), pp.1-10.

Wilcox, R. 2006. The biomechanical effect of vertebroplasty on the adjacent vertebral body: a finite element study. *Proceedings of the Institution of Mechanical Engineers, Part H: Journal of Engineering in Medicine.* **220**(4), pp.565-572.

Wilcox, R.K. 2007. The influence of material property and morphological parameters on specimen-specific finite element models of porcine vertebral bodies. *Journal of Biomechanics.* **40**(3), pp.669-673.

Wilke, H.-J. et al. 2011. Biomechanical in vitro evaluation of the complete porcine spine in comparison with data of the human spine. *European Spine Journal.* **20**(11), pp.1859-1868.

Wilke, H.-J. et al. 1997a. Are sheep spines a valid biomechanical model for human spines? *Spine.* **22**(20), pp.2365-2374.

Wilke, H.-J. et al. 2006. Biomechanical evaluation of vertebroplasty and kyphoplasty with polymethyl methacrylate or calcium phosphate cement under cyclic loading. *Spine.* **31**(25), pp.2934-2941.

Wilke, H.-J. et al. 1998. Testing criteria for spinal implants: recommendations for the standardization of in vitro stability testing of spinal implants. *European spine journal.* **7**(2), pp.148-154.

Wilke, H.J. et al. 1997b. Anatomy of the sheep spine and its comparison to the human spine. *The Anatomical Record.* **247**(4), pp.542-555.

Wilke, H.J. et al. 1999. New in vivo measurements of pressures in the intervertebral disc in daily life. *Spine.* **24**(8), pp.755-762.

Woodburne and Burkel. 1988. *Essentials of Human Anatomy* 8th ed. United Kingdom.

Wu, Z.-x. et al. 2007. Staged-Injection Procedure to Prevent Cement Leakage During Vertebroplasty: An In Vitro Study. *Spine*. **32**(22), pp.2437-2442.

Xu, G. et al. 2014. Biomechanical effects of vertebroplasty on thoracolumbar burst fracture with transpedicular fixation: A finite element model analysis. *Orthopaedics & Traumatology-Surgery & Research*. **100**(4), pp.379-383.

Yeni, Y.N. et al. 2005. Effect of microcomputed tomography voxel size on the finite element model accuracy for human cancellous bone. *Journal of biomechanical engineering*. **127**(1), pp.1-8.

Zapata-Cornelio, F.Y. et al. 2017. Methodology to Produce Specimen-Specific Models of Vertebrae: Application to Different Species. *Annals of Biomedical Engineering*.

Zeng, Z.L. et al. 2013. Formative mechanism of intracanal fracture fragments in thoracolumbar burst fractures: a finite element study. *Chinese Medical Journal*. **126**(15), pp.2852-2858.